

Artificial Intelligence Based Non-linear PID Speed and Current Control of
Brushless DC Motor for Electric Vehicle Drive. (The Case of Bajaj Qute)

Minyamer Gelawe Wase



A Thesis Submitted to
The Department of Electrical Power and Control Engineering
School of Electrical Engineering and Computing

Presented in Partial Fulfillment of the Requirement for the Master of Science
Degree in Electrical Power and Control Engineering (Power Electronics)

Office of Graduate Studies
Adama Science and Technology University

July, 2020
Adama, Ethiopia

Artificial Intelligence Based Non-linear PID Speed and Current Control of
Brushless DC Motor for Electric Vehicle Drive. (The Case of Bajaj Qute)

Minyamer Gelawe Wase

Advisor:

Prof. Gang Gyoo Jin



A Thesis Submitted to

The Department of Electrical Power and Control Engineering

School of Electrical Engineering and Computing

Presented in Partial Fulfillment of the Requirement for the Master of Science

Degree in Electrical Power and Control Engineering (Power Electronics)

Office of Graduate Studies


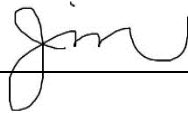
Adama Science and Technology University

July, 2020

Adama, Ethiopia

APPROVAL OF BOARD OF EXAMINERS

We, the undersigned, members of the Board of Examiners of the final open defense by Minyamer Gelawe Wase have read and evaluated his thesis entitled “Artificial Intelligence Based Non-linear PID Speed and Current Control of Brushless DC Motor for Electric Vehicle Drive. (The Case of Bajaj Qute)” and examined the candidate. This is, therefore, to certify that the thesis has been accepted in partial fulfillment of the requirement of the Degree of Masters in Power Electronics.

Name	Signature	Date
Name of Student		
Advisor		
External Examiner		
Internal Examiner		
Chair Person		
Head of Department		
School Dean		
Postgraduate Dean		

DECLARATION

I hereby declare that this MSc thesis is my original work and has not been presented for a degree in any other university, and all sources of material used for this thesis have been duly acknowledged.

Name: Minyamer Gelawe Wase

Signature:  _____

This MSc thesis has been submitted for examination with my approval as a thesis advisor.

Name: Prof. Gang Gyoo Jin

Signature:  _____

Date of submission: July 16, 2020


ADVISOR APPROVAL SHEET

To: Department of Electrical Power and Control Engineering (EPCE)

This is to certify that the thesis entitled “Artificial Intelligence Based Non-linear PID Speed and Current Control of Brushless DC Motor for Electric Vehicle Drive. (The Case of Bajaj Qute)” submitted in partial fulfillment of the requirements of the Master of Science Degree in Electrical Power and Control Engineering, postgraduate in Power Electronics, and has been carried out by Minyamer Gelawe Wase Id No. PGR/18206/11 under my supervision. Therefore, I recommend that the student has fulfilled the requirements and hereby he can submit the thesis to the department.

Prof. Gang Gyoo Jin

Name of Advisor



Signature

July 16, 2020

Date

ACKNOWLEDGMENT

First and dearest I would like to thank my supervisor **Prof. Gang Gyoo Jin** for his supervision, friendly attitude, and sharing of many good ideas. Regardless of his often high workload, he always makes time to answer questions as well as giving encouraging advice. You are highly appreciated!

I am also very grateful to **Dr. Tefera Terefe Yetayew** for lots of advice and helping in preparing the thesis documentation, but also for good ideas and discussions regarding everything from implementations of the system in Simulink in general.

I would moreover like to thank **Mr. Million Gerado Geda (MSc.)** for his patience, helpful attitude, and sharing of his work regarding the implementation of the nonlinear Simulink modeling.

Furthermore, I would also like to thank the EPCE department head **Mr. Hinsermu Alemayehu Garbaabaa (MSc.)** and laboratory staff members for encouraging, making open computer labs for discussion when I have a meeting with my advisor, for a very friendly working environment, and for making me feel very welcome during my thesis work.

Finally, I would like to thank my whole family. Especially words cannot express how grateful I am to my father and friends for their love, encouragement, and all of the sacrifices that they have made on my behalf.

ABSTRACT

*Fast depletion of fossil fuels, environmental pollution, and global atmospheric challenges are the major driving forces to explore alternative environmental friendly energy sources. In line with this, fossil fuel driven vehicles contribute a significant share in environmental pollution. Electric vehicles (EV) are alternative solutions. However, energy efficiency and utilization are the major issues in EV. According to the current research status, BLDC motor drives have better efficiency out of different electric drives even though it has relatively high torque ripple. Energy efficient and better dynamic performance features of BLDCM drive for EV application can be achieved by using appropriate control techniques. In this regard, a neural network (NN) based nonlinear PID (NPID) speed controller, genetic algorithm (GA) based PI current controller, and pulse-width-modulated (PWM) based inverter drive of BLDCM for the propulsion of EV **Bajaj Qute** are implemented for this work. To achieve this, vehicle dynamics, BLDCM, and inverter models are done mathematically. Also, for implementation purpose the corresponding models are done using MATLAB software tool. Different cascade control architectures (like ZN-PID speed and PI current, GA-PID speed and PI current, GA-NPID speed and PI current, and NN-NPID speed and GA-PI current) for the specified application are implemented and performance evaluations are done. Accordingly, NN-NPID speed controller has a settling time of 0.0275sec, 0% overshoot, and 0% steady-state error under a constant load of 20Nm condition and per 1500rpm rated speed. On the other hand, the GA-NPID speed controller has better performance than ZN-PID and GA-PID controllers, and it has a settling time of 0.03sec and 0% overshoot. However, due to a sudden load change of 30Nm, it has a +0.7% steady-state error which is twice that of the NN-NPID controller result (0.3%). Furthermore, GA-PI current controller results settling time of 0.02sec and 0% overshoot. Besides, ZN-PI current controller is performed and it has a settling time of 0.09sec and +50% overshoot which is less performance than the GA-PI controller. In addition, the performance of PWM based inverter drive showed 6% torque ripple compared to relay based inverter drive with 20% torque ripple. In general, the performance evaluations of the implemented different cascade controllers revealed that NN-NPID speed and GA-PI current cascade controller along with PWM based inverter drive for the specified application outperformed other controllers.*

Key words: *Bajaj Qute, BLDCM, NN-NPID and GA-PI cascade controller, and PWM*

TABLE OF CONTENTS

DECLARATION	i
ACKNOWLEDGMENT	iii
ABSTRACT	iv
LIST OF TABLES	x
LIST OF FIGURES	xi
LIST OF ACRONYMS	xiv
LIST OF SYMBOLS	xv
CHAPTER 1	1
1. INTRODUCTION	1
1.1. Background	1
1.2. Statement of the Problem	3
1.3. Research Questions	4
1.4. Objectives of the Study	5
1.4.1. General Objective	5
1.4.2. Specific Objectives	5
1.5. Scope of the Study.....	5
1.6. Limitations of the Study	5
1.7. Motivation of the Study.....	5
1.8. Significance of the Study	6
1.9. Thesis Organization.....	6
CHAPTER 2	7
2. LITERATURE REVIEW	7
2.1. Chapter Overview	7
2.2. Electric Vehicles	7
2.3. Electric Motor Varieties	9

2.3.1.	Brushed DC Motor.....	9
2.3.2.	Brushless DC Motor	10
2.3.3.	AC Induction Motor (IM)	10
2.3.4.	Permanent Magnet Synchronous Motor (PMSM).....	11
2.3.5.	Stepper Motor and Switched Reluctance (SR) Motor	11
2.3.6.	Performance Comparison of Various Motor Types.....	12
2.4.	Related Works on Brushless DC Motor Drive.....	15
2.4.1.	Variable Voltage Source (VVS) Based BLDC Motor Drive.....	16
2.4.2.	Relay Based BLDC Motor Drive.....	16
2.4.3.	Field Oriented Control (FOC) of BLDC Motor Drive.....	17
2.5.	Related Works on Cascade Control System of BLDCM	19
CHAPTER 3.....		22
3.	METHODOLOGY	22
3.1.	Introduction	22
3.2.	Materials.....	22
3.3.	Methods.....	22
3.4.	The Proposed Block Diagram of BLDC Motor Drive	24
3.5.	Analysis of Bajaj Qute Electric Vehicle Dynamics	24
3.5.1.	Driving Force and Power of Bajaj Qute Electric Vehicle	25
3.5.1.1.	Rolling Resistance Force.....	26
3.5.1.2.	Hill-Climbing (Gradient) Resistance Force	27
3.5.1.3.	Aerodynamic Drag Force	27
3.5.1.4.	The Effect of Bajaj Speed on the Power Requirement.....	28
3.5.1.5.	Motor Rated Power and Peak Power Matching	29
3.5.1.6.	The Effect of Gradient Angle on the Power and Speed of Vehicle	29
3.5.2.	Electric Vehicle (Bajaj Qute) Specification.....	30
3.5.3.	Reducer and Gear Specifications	30

3.5.4.	Traction Motor	31
3.5.4.1.	Selection of Traction Motor	31
3.5.4.2.	Traction Motor Specification	32
3.5.5.	Battery Specifications	34
3.5.5.1.	Matching Power Battery Parameters	34
3.5.6.	Selection of Power Semiconductor Device	35
3.6.	Modeling of BLDCM Drive for Electric Vehicle Propulsion.....	35
3.6.1.	Mathematical Modeling of Brushless DC Motor	36
3.6.1.1.	Rotor Position Hall Sensors Modeling.....	38
3.6.1.2.	Modeling of Ideal Back-EMF	39
3.6.1.3.	Dynamics Modeling of BLDC Motor	40
3.6.2.	Modeling of Armature and Dynamics Transfer Functions of BLDCM	40
3.6.2.1.	Armature Transfer Function.....	40
3.6.2.2.	Motor Dynamics Transfer Function	41
3.6.3.	Modeling of Three Phase Inverter Transfer Function	41
3.6.4.	Modeling of Current Feedback Sensor Transfer Function	42
3.6.5.	Modeling of Speed Feedback Sensor Transfer Function.....	42
3.7.	Cascade Control System for BLDCM Drive.....	42
3.7.1.	Nonlinear PID Controller for BLDC Motor Speed Control	43
3.7.1.1.	Implementation of Nonlinear Gain using Fuzzy Logic.....	44
3.7.2.	PI Controller for BLDC Motor Current Control.....	48
3.7.3.	Implementation of BLDCM Cascade Control System using GA.....	48
3.7.3.1.	Parameter Tuning of Cascade NPID and PI Controller	52
3.7.4.	NN-NPID Speed and GA-PI Current Cascade Control of BLDCM	54
3.7.5.	ZN Based PID Speed and PI Current Controllers of BLDCM	61
3.7.5.1.	Tuning of PID Controller Using ZN Based Relay Control.....	61
3.7.5.2.	Design of PI Current Controller of BLDCM using ZN Tuning	62

3.7.5.3.	Design of PID Speed Controller of BLDCM using ZN Tuning	65
3.7.6.	GA Tuning of Cascade PID and PI Controller	68
3.8.	The Proposed BLDC Motor Drive Setup	71
3.8.1.	Lithium-Ion Battery Source	71
3.8.2.	Three Phase Inverter BLDC Motor Drive	71
3.8.3.	The Proposed Cascade Control System	72
3.8.4.	BLDCM Rotor Position Sensor Signal Decoder Implementation	72
3.8.5.	Reference Current Generation	74
3.8.6.	Pulse Width Modulation (PWM) Based BLDCM Drive	74
3.8.7.	Relay Based BLDCM Drive	75
CHAPTER 4.....	77
4.	RESULTS AND DISCUSSIONS	77
4.1.	The Proposed BLDCM Control and Drive System Result	77
4.1.1.	The Proposed Cascade Control System Results of BLDCM.....	77
4.1.1.1.	NN Based NPID Speed Controller Result of BLDCM.....	77
4.1.1.2.	GA-PI Current Controller Result of BLDCM.....	78
4.1.2.	PWM Based Nonlinear BLDCM Drive Output Results	79
4.1.2.1.	BLDCM Stator Current Result.....	79
4.1.2.2.	BLDCM Three Phase Trapezoidal Back-EMF Result.....	79
4.1.2.3.	BLDCM Electromagnetic Torque Result.....	81
4.1.2.4.	Three Phase Inverter Output Voltage of BLDCM	81
4.1.2.5.	Vehicle Speed vs Battery State of Charge	83
4.2.	Discussion of Results	84
4.2.1.	Discussion of BLDCM Cascade Control System Result.....	84
4.2.1.1.	Speed Dynamic Performance of BLDCM	84
4.2.1.2.	Current Dynamic Performance of BLDCM	90
4.2.2.	Discussion of BLDC Motor Drive Results	92

4.2.2.1. PWM Based BLDCM Drive Results Discussion	92
4.2.2.2. Discussion of Relay Based BLDCM Drive Result	93
CHAPTER 5.....	95
5. CONCLUSIONS AND RECOMMENDATIONS	95
5.1. Conclusions	95
5.2. Recommendations	96
References.....	97
Appendixes	106
Appendix A: Appendixes related to analysis of data.....	106
Appendix B: Appendixes related to system modeling.....	108
Appendix C: Related to the linear BLDC motor MATLAB/Simulink model.....	117
Appendix D: Related to the nonlinear BLDC motor Simulink model.....	118
Appendix E: Appendixes related to data collection.....	125

LIST OF TABLES

Table 2.1 Different models of electric vehicles and their motors	8
Table 2.2 Comparison between brushed DC and brushless DC motors.....	13
Table 2.3 Comparison between AC induction and BLDC motors	14
Table 2.4 Dynamic performance analysis of BLDC motor.....	20
Table 3.1 Coefficient of frictions for different types of surfaces	26
Table 3.2 Bajaj quite electric vehicle and driving motor specifications.....	30
Table 3.3 Gear box specifications	31
Table 3.4 Performance comparison between BLDC and PMSM motors.....	32
Table 3.5 Parameter specifications of BLDC motor used in this study	33
Table 3.6 Parameter specifications of Lithium-ion battery	34
Table 3.7 Hall effect signals and inverter switches status of the BLDC motor	38
Table 3.8 Parameter settings of the genetic algorithm optimization	52
Table 3.9 The GA optimized parameters of the cascade NPID and PI controllers	53
Table 3.10 ZN-PID parameters according to the ultimate point	62
Table 3.11 Parameter settings of the genetic algorithm optimization	69
Table 3.12 The GA optimized parameters of the cascade PID and PI controllers	70
Table 3.13 Truth table of hall sensor decoder	72
Table 4.1 Speed controller comparison of performance parameter results	86
Table 4.2 Speed controller performance parameter results under 30Nm load	89
Table 4.3 Current controller comparison of performance parameter results.....	90

LIST OF FIGURES

Figure 2.1 Motor classification.....	9
Figure 2.2 Brushed DC motor	10
Figure 2.3 Brushless DC motor	10
Figure 2.4 Induction motor	11
Figure 2.5 Permanent magnet synchronous motor	11
Figure 2.6 Stepper motor and Switched reluctance (SR) motor.....	12
Figure 2.7 Performance comparison of different electric motors.....	15
Figure 2.8 The three phase BLDC motor drive	15
Figure 2.9 Variable voltage source based BLDC motor drive	16
Figure 2.10 Relay based BLDC motor drive	17
Figure 2.11 Relay based BLDC motor drive for each phase.....	17
Figure 2.12 FOC based on direct torque control of BLDC motor.....	18
Figure 2.13 Graphical comparison of different BLDC motor drives	18
Figure 3.1 Block diagram of the research methodology	23
Figure 3.2 Block diagram of the proposed drive control system.....	24
Figure 3.3 Pure electric vehicle power system structure	25
Figure 3.4 Forces acting on the moving four wheel bajaj vehicle platform.....	26
Figure 3.5 Driving power vs speed of the bajaj vehicle	28
Figure 3.6 Torque versus speed characteristics of the BLDC motor.....	29
Figure 3.7 Driving power vs gradient angle of the vehicle	29
Figure 3.8 Reducer (gearbox) and shaft	31
Figure 3.9 Stator connected three phase circuit diagram of BLDC motor winding.....	36
Figure 3.10 Back-EMF and rotor position hall sensor modeling	40
Figure 3.11 The proposed cascade control system block diagram of BLDC motor	43
Figure 3.12 A NPID controller structure	43
Figure 3.13 Shapes of $K(e)$ versus e for different Y_s	44
Figure 3.14 Implementation of nonlinear gain using fuzzy logic for NPID controller	45
Figure 3.15 Fuzzy logic structure block diagram	45
Figure 3.16 The input membership function of the fuzzy logic	46
Figure 3.17 The fuzzy logic system rule view.....	47
Figure 3.18 The surface view of the output in three 3D (left) and 2D (right).....	47
Figure 3.19 MATLAB/Simulink implementation of the nonlinear gain.....	47

Figure 3.20 Flow chat of genetic algorithm optimization	49
Figure 3.21 Block diagram of GA implementation in cascade control of BLDC motor	50
Figure 3.22 Fitness values vs generation for object function	52
Figure 3.23 GA based NPID speed controller result of BLDC motor	53
Figure 3.24 GA based PI current controller result of BLDC motor	54
Figure 3.25 The proposed cascade control system	55
Figure 3.26 Neural network structure used in this thesis	56
Figure 3.27 Flow chart of the neural network training	56
Figure 3.28 Generating the input and output data from the GA-based control system.....	57
Figure 3.29 Validation of the mean squared error.....	58
Figure 3.30 Regression plots of the training, validation, and test sets	59
Figure 3.31 The Simulink block of the trained neural network structure.....	59
Figure 3.32 Neural network based NPID speed control system of the BLDC motor	60
Figure 3.33 NN based NPID speed controller of the BLDC motor output result	60
Figure 3.34 Block diagram for ultimate point estimation	61
Figure 3.35 Reduced block diagram of the internal loop of the main block diagram	62
Figure 3.36 Internal current controller of the BLDC motor block diagram	63
Figure 3.37 Simulink model of BLDC motor internal loop using a relay controller	63
Figure 3.38 Output armature current based on relay current controller	63
Figure 3.39 The MATLAB/Simulink model of internal current loop using PI controller ..	65
Figure 3.40 BLDC motor output current result using ZN-PI current controller	65
Figure 3.41 MATLAB/Simulink model of BLDC motor relay based speed controller.....	66
Figure 3.42 Output motor speed result based on relay controller	66
Figure 3.43 BLDC motor speed result using ZN-PID speed controller	67
Figure 3.44 Current result of linear PID-PI cascade control system.....	68
Figure 3.45 Fitness values vs generation for object function	69
Figure 3.46 GA-PID controller speed result.....	70
Figure 3.47 Three phase inverter and energy flow for BLDC motor	71
Figure 3.48 MATLAB/Simulink model of hall sensor signal decoder	73
Figure 3.49 Three phase hall sensor and its decoded signal.....	73
Figure 3.50 Three phase reference current signal.....	74
Figure 3.51 The proposed PWM based BLDC motor drive Simulink diagram	75
Figure 3.52 Triangular carrier voltage signal	75
Figure 3.53 Relay based BLDC motor inverter drive	76

Figure 4.1 The proposed speed control result of the BLDC motor	78
Figure 4.2 The proposed current control result of the linear BLDC motor drive system ...	78
Figure 4.3 Three phase BLDC motor stator current result	79
Figure 4.4 BLDC motor three phase back-EMF result	80
Figure 4.5 BLDC motor three phase trapezoidal back-EMF zoomed out result.....	80
Figure 4.6 BLDC motor electromagnetic torque result.....	81
Figure 4.7 Three phase inverter output voltage.....	82
Figure 4.8 The power output of BLDC motor under the nonlinear drive system	82
Figure 4.9 Vehicle speed vs percentage of battery state of charge.....	83
Figure 4.10 SOC versus mileage in kilometer at 70km/hr constant speed.....	84
Figure 4.11 BLDC motor speed result using different controllers	85
Figure 4.12 BLDC motor speed zoomed result using different controllers	85
Figure 4.13 BLDC motor speed result using different controllers for setpoint change	87
Figure 4.14 Graphical representation of speed dynamic performance parameters result ...	87
Figure 4.15 BLDC motor speed result using different controllers at 30Nm	88
Figure 4.16 Steady state error graphical representations of speed controllers	89
Figure 4.17 BLDC motor current zoomed result using different controllers	90
Figure 4.18 BLDC motor current result using different controllers for setpoint change ...	91
Figure 4.19 Graphical representation of current controllers parameter result.....	91
Figure 4.20 The zoomed out result of the stator current under PWM based drive	92
Figure 4.21 The result of electromagnetic torque under PWM based drive.....	92
Figure 4.22 The result of the stator current under relay based drive.....	93
Figure 4.23 The result of electromagnetic torque under relay based drive	93
Figure 4.24 Percentage of torque ripple graphical representations	94

LIST OF ACRONYMS

AC	Alternating Current
ANFIS	Adaptive Neuro-Fuzzy Inference System
BJT	Bipolar Junction Transistor
BLDCM	Brushless Direct Current Motor
DC	Direct Current
DSP	Digital Signal Processor
EMF	Electromotive Force
EMI	Electromagnetic Induction
EV	Electric Vehicle
FOC	Field Oriented Control
GA	Genetic Algorithm
HVIGBT	High Voltage Insulated Gate Bipolar Transistor
IAE	Integral Absolute Error
IGBT	Insulated Gate Bipolar Transistor
IM	Induction Motor
MOSFET	Metallic Oxide Semiconductor Field Effect Transistor
NN	Neural Network
NPID	Nonlinear Proportional Integral Derivative
PD	Proportional Derivative
PI	Proportional Integral
PID	Proportional Integral Derivative
PMSM	Permanent Magnet Synchronous Motor
PSO	Particle Swarm Optimization
PWM	Pulse Width Modulation
RK4	Rang Kutta Fourth Order
SOC	State of Charge
SP	Set Point
SR	Switched Reluctance
SRM	Switched Reluctance Motor
SVM	Space Vector Modulation
VVS	Variable Voltage Source
ZN	Ziegler Nicholas

LIST OF SYMBOLS

A	Frontal area of the car
B	Friction coefficient
C_r	The coefficient of rolling resistance
$e_{a,b,c}$	Induced EMF in phase a, b &c
$f_{as,bs,cs}(\theta_r)$	Rotor position function
g	Gravitational acceleration
$I_{a,b,c}$	The phases current
J	The rotor moment of inertia
K_b	Back EMF constant
K_i	Value of the line to line inverter gain
K_f	Current filter feedback gain
K_t	Electromagnetic torque constant
L_a	Armature inductance
M	Gross mass of the bajaj qute vehicle
$P_{\text{total driving power}}$	Total driving power of the vehicle
P	The number of poles
P_m	Input power of the motor controller
S	Endurance mileage
R_a	Stator resistance
T_e	Electromagnetic torque
T_f	Current filter time delay
T_l	Load torque
T_i	Delay time of the inverter switches
V_{cm}	The maximum control voltage
V_c	Carrier voltage
V_{dc}	The DC link voltage
W_{road}	Energy needed for mileage S
θ_r	Rotor position
ω_m	Motor speed

CHAPTER 1

1. INTRODUCTION

1.1. Background

The advent of the internal combustion engine has significantly influenced human life. As the main propulsion technology used in vehicles, the internal combustion engine has become an integral part of modern life. However, as internal combustion engine vehicles increase in number, they constitute one of the largest sources of air pollution and greenhouse gas emissions. Automotive industries are targeting sustainable transportation in the future for reducing air pollution. Hence electric and hybrid vehicles are going to be popular due to their energy saving, sustainability, and less carbon emission [1].

Scientists, engineers, and vehicle manufacturers have attempted to design and improve electric vehicles (EV) for about a century. The first electric car produced in 1839 by Rodert Anderson. In 1870 David Salomon developed an electric car with a light electric motor. The batteries were heavy, at the time, therefore performance was poor [2]. But, nowadays with an improvement in battery technology EV have better performance. Gasoline bajajs are the type of vehicles but not cars and they are classified as three-wheel and four-wheel bajaj vehicles [L1]. Bajaj Auto came into existence in India as Bachraj Trading Co. Ltd. on November 29, 1945. The company got a license to manufacture the two and three-wheeler vehicles locally in 1959. Currently, the company distributes its product in 16 countries including our country, Ethiopia.

Bajajs have been commonly used for the transportation industry in Ethiopia especially in regional state cities. Until fourteen years ago, public transport was limited to minibuses and buses. Hence, three-wheel vehicle taxis, made in India, first come to Ethiopia in 2005 [L1]. They become very popular as a convenient method of transportation in the cities. But three-wheel bajaj vehicles are not good for safety, comfort as well as less fuel efficiency.

The company could introduce four-wheeler bajaj vehicles specifically in cities in the next ten and fifteen years it could replace the three-wheeler bajaj. It provides better safety, comfort, and better fuel efficiency when compared to three-wheelers [L1]. Although these four wheeler bajaj vehicles have better fuel efficiency, they are not co-friendly to the environment, so these types of gasoline bajaj vehicles should be replaced by electric ones

[3]. EV is more advantageous over internal combustion engine automobiles, including a significant reduction of air pollution and gas emissions. Electric energy stored in the battery used by EV to drive the motor and the power can be rejuvenated with electricity generation using renewable energy. The electric motor plays a significant role in any electric vehicle. The most suitable motor among various electric motors for EV is BLDC motor because it has many advantages over brushed DC motor and induction motor [4]. These are:

- Less maintenance,
- Low electric noise,
- Low inertia which improves dynamic response,
- Better speed versus torque characteristics,
- Long operating life,
- High efficiency,
- High reliability, high power density, low cost, and lower weight.

BLDC motors are synchronous motors. The three phase configuration of the motor is commonly used in high and medium power applications. BLDC motor control depends on the position of the rotor [5]. The inverter switching and instability of the system due to the complicated design of the speed and current regulator increases the complexity of the BLDC motor drive. Battery power optimization in EV is essential. For the fast braking operation and controlling the torque in the vehicle, precise model and simulation of BLDC motor drive especially speed control is required. Several techniques and algorithms have been proposed by researchers for the BLDC motor speed controller [5] [6]. Among them are PI, PID, fuzzy and adaptive fuzzy PID controllers have been widely used for speed control of BLDC motor.

The BLDC motor has a highly nonlinear characteristic because the rotor made of permanent magnet leads to magnetic saturation. This makes the developed torque nonlinear. It has a nonlinear relationship between the winding current and rotor speed. As a result, the linear PID controller may have difficulty in speed control. On the other hand, the nonlinear PID control gives accurate results for speed control of BLDC motor. However, it could produce high starting current which can be dangerous for the motor and control circuitry. The cascaded NPID speed and PI current control configuration achieves better dynamic performance, gives better setpoint tracking, disturbance regulation, and reduced starting current overshoot.

BLDC motor has high torque ripple compared with other motors. Torque ripple makes the vehicle vibrate and reduces the life span of the vehicle. Torque ripple is due to stator current harmonics. Due to electronic commutation, the stator current has harmonics and torque is proportional to the stator current. To reduce this effect to some extent BLDC motor requires better inverter switching techniques. There are different types of BLDC motor inverter switching commutation techniques. The variable voltage source drive is the one and the simplest BLDC motor drive technique. This driving scheme used in the case of variable voltage source power supply and the application without considering current harmonics.

The other one is relay based inverter drive. The inverter switch depends on the difference between the stator current and reference current. The motor current harmonics depend on the bandwidth of the relay and usually, it is high to reduce the inverter loss. Field orientated control (FOC) is another inverter drive technique and it has fewer current harmonics than a relay-based drive. FOC works based on space vector modulation (SVM), clark, and park transformation [6]. As a result, it is very difficult to implement practically. The last one and the proposed scheme is PWM based inverter drive and it has fewer current harmonics than others and it is easy to implement practically. It needs only the controlled signal and the carrier signal with at least the frequency twice the controlled signal frequency.

In this research work, the comparison of ZN-PID speed and PI current, GA-PID speed and PI current, GA-NPID speed and PI current, and NN-NPID speed and GA based PI current cascade controllers for BLDC motor control is performed. The result shows NN-NPID speed and GA-PI current cascade controller gives better speed and current dynamic performance than the others. Besides, PWM based BLDC motor inverter drive is compared with a relay-based inverter drive. As the result, PWM based inverter drive gives lower current harmonics. The electric bajaj qute vehicle dynamics mathematical modeling is performed. Also, the mathematical model and the principle of a three-phase star-connected BLDC motor drive with ideal trapezoidal back-EMF waveform is discussed. The linear and nonlinear model of BLDC motor drive for the application of electric vehicle bajaj qute is designed and simulated using MATLAB software.

1.2. Statement of the Problem

The reduction of greenhouse gases is mandatory to create a better environment. Since the pollution levels are rising at an alarmingly high rate. The usage of fossil fuels for transportation is a major cause of pollution and the emission of harmful gases into the

atmosphere. In line with this, the depletion of fossil fuel is increasing at a high rate and its cost is also increasing. To reduce certainly the above mentioned problems fossil fuel-based vehicles must be replaced by electric vehicles. However, energy efficiency and utilization issues are the major issues that need research for sustainability apart from reducing the environmental pollution role of electric vehicles. The motor is the main part of EV which needs an efficient and appropriate closed-loop motor drive control system. According to the current research status regarding the efficiency of electric drives, BLDC motor drives are considered as drives with better efficiency out of the many different electric drives. However, it has high torque ripple compared with other electric motors. The source of torque ripple is current distortion. Torque ripple can be solved by reducing the stator current harmonics, that is, by designing suitable inverter switching technique in the BLDC motor drive.

Due to the permanent magnet of the BLDC motor in the rotor, the magnetic saturation is present and making the developed torque nonlinear. As a result, a precise speed control system is complex due to nonlinear coupling between winding currents and rotor speed. Since the BLDC motor has a high starting current, this may lead to heating of the motor stator windings and the burning of the motor and its drive. The speed and current dynamic performance characteristics of the motor are essential in the case of an electric vehicle. To overcome the above mentioned problems an intelligence based speed control scheme along with the current regulator is required in the BLDC motor drive. In this research work, the NN-NPID speed and GA-PI current cascade controller and PWM inverter switching technique are proposed and developed. The proposed control and drive systems are implemented and simulated by using MATLAB software.

1.3. Research Questions

This work intends to answer the following basic research questions.

- How to determine the maximum load of an electric bajaj vehicle?
- How to select the BLDC motor rating and specifications?
- How to model and optimize the current and speed controllers of the system?
- How to reduce the current harmonics (torque ripple)?
- How to drive a BLDC motor with better speed dynamic performance?
- How to model the entire system with MATLAB/Simulink?

1.4. Objectives of the Study

1.4.1. General Objective

The general objective of the research thesis is to improve the speed and current dynamic performance of brushless DC motor for electric vehicle bajaj quite propulsion.

1.4.2. Specific Objectives

The specific objectives of this research thesis are:

- To design the maximum load of electric vehicle four-wheel bajaj.
- To select the appropriate BLDC motor for electric vehicle four-wheel bajaj.
- To design AI-based speed and current controllers for BLDC motor drive.
- To reduce torque ripple and current harmonics distortion of BLDC motor.
- To simulate the system by using MATLAB software to check performance.

1.5. Scope of the Study

The thesis focuses on the mathematical modeling and simulation design of both the vehicle (bajaj quite) dynamics and brushless DC motor. Simulation of intelligence based speed and current control of brushless DC motor using MATLAB/Simulink for the propulsion of electric vehicle (bajaj quite) application are implemented. The performance of BLDC motor drive techniques in case of both speed and current controllers and inverter driving techniques are developed and discussed.

1.6. Limitations of the Study

The thesis is limited to the simulation of the system using MATLAB/Simulink by showing how the different components of the system interact with each other. This is because the implementation of a real system is difficult to procure the components. Along with it takes the additional time and cost incurred in making the actual prototype implementation.

1.7. Motivation of the Study

Currently, many countries have an agreement to replace the gasoline based vehicles into the electric vehicle due to environmental pollution and the cost of fossil fuel. A plenty of related researches have been conducted especially in the area of electric drive control, battery optimization, and making fast charger. The future will have a huge market in the area of electric vehicles and it is important to be professional in electric vehicle propulsion design, modeling, and control.

Due to its better torque-speed characteristics, smaller and compact size, higher efficiency, wide speed range and longer operational life, the popularity of the brushless DC permanent magnet motors is increasing rapidly in the speed servo applications. The ratio of torque generated to the size of the motor is higher, in the applications where space and weight are critical factors like in EV application BLDC motor has been recommended. BLDC motor has been increasingly used in transportations, field of process control systems, computer application areas, aerospace engineering, medical equipment, industrial automation and robotics equipment, and instrumentation control system areas.

1.8. Significance of the Study

Energy wastage and air pollution are the major issues in the world as well as in our country. So, the world is shifting the energy source usage from non-renewable sources that will not be available after a few decades to the renewable energy source. Renewable energy sources are eco-friendly with the environment. Currently, these types of energy sources are accepted in many countries due to the above-mentioned problems. Especially, for ASTU Center of Transportation and Vehicle Engineering (CTVE) and E-Bajaj center of excellences are very important because of the members are trying to design and develop their electric vehicle for Ethiopian market.

1.9. Thesis Organization

This thesis organizes into five chapters.

Chapter 1: Presents introduction of the research work, statement of the problems, objectives, research questions, significance, scope, and limitation of the research.

Chapter 2: Includes a literature review on the background of BLDC motor drive and different control mechanisms to the application of electric vehicles.

Chapter 3: Describes the methodology followed in this research thesis.

Chapter 4: Presents the proposed results and discussions.

Chapter 5: Discusses the conclusions and recommendations.

CHAPTER 2

2. LITERATURE REVIEW

2.1. Chapter Overview

In this chapter different electric vehicle models with their traction motors are reviewed. The performance evaluation of a brushless DC motor is compared with those of other electric motor types. The worldwide application areas of BLDC motors, the existing controlling mechanism, the driving techniques, and other related applications of BLDC motor are discussed. Closely related works especially in speed and current regulators along with their merits and demerits are reviewed and discussed. The drive train of the BLDC motor closely related works also reviewed and disused.

2.2. Electric Vehicles

The electric motor drive used in an EV cannot be compared with drives used in industrial applications because an EV motor drive needs to face different circumstances like frequent start/stop, usage in different environments. To satisfy the need for an electric vehicle, the electric motor drive must have high torque generating capacity, high acceleration, and a high power density [7].

Since an EV need to run on any harsh environments, it must have high torque when operating at slow speeds with high efficiency as well [8]. Also, the efficiency must be high concerning the regenerative braking capacity since the battery needs to be charged as well when dealing with harsh environments. The torque being generated also depends on the speed at which the EV is generated. The maximum available torque at a time in an EV depends inversely on the operational speed.

Some of the EV models by different manufacturers are listed in Table 2.1 along with the electric motor used. Since each company uses a different electric motor drive for its propulsion system accordingly. It can be seen from Table 2.1 that BLDC and induction motors are the most popular from the manufacture's point of view.

Table 2.1 Different models of electric vehicles and their motors [7] [8] [L2]

No	EV name	Manufacturer company	Capacity of passenger	Electric motor	Country
1	Berlingo	PSA Peugeot-Citroen	5	DC	France
2	Nissan leaf	Nissan	5	BLDC	Japan
3	Mitsubishi-MiEV	Mitsubishi	4	BLDC	Japan
4	BYD E6	BYD Auto	5	BLDC	China
5	Morgan Pulse E	Morgan Motors	2	BLDC	UK
6	Toyota RAVA 4	Toyota	4	BLDC	Japan
7	Tesla	Tesla Motors	5	BLDC/IM	USA
8	BMW/X5	BMW	4	IM	Germany
9	Renault	Renault/Kangoo	4	IM	France
10	Chevrolet	Chevrolet/Silverado	4	IM	USA
11	Nissan/Tino	Nissan	4	PMSM	Japan
12	Honda/Insight	Honda Motors	4	PMSM	Japan
13	Toyota/Prius	Toyota	4	PMSM	Japan
14	Holden	Holden/ECOMmodore	4	SR	Australia

To select an appropriate motor that can mostly fulfill the EV motor technology requirements, an overall comparison of electric motors is needed based on EV requirements. The most important requirements of the EV motors are [9]:

- High speed and torque dynamic response;
- High torque at low speeds especially when climbing hill;
- High torque/power to size ratio;
- Under wide speed range power is constant;
- Accurate electronic controllability of the motor;
- Robustness and reliability of the motor and its drive;
- Low current harmonics and torque ripple of the motor;
- High efficiency of the motor and the gear transformation;
- Size and weight of the motor with the load requirement of the vehicle;
- Initial and maintenance cost of the motor and controller;

All electric motors cannot fulfill all of the above listed electric vehicle requirements and characteristics. The following section discusses the various electric motors with their structure as well as parameters performance comparison.

2.3. Electric Motor Varieties

Varieties of electric motors are classified and differentiated by structure and power sources as shown in Figure 2.1. Generally, the motors are categorized into three types: DC motor, AC motor, and other types of motors [10]. Hence BLDC motor categorized under other types because the motor has the characteristics of the DC and AC motor types.

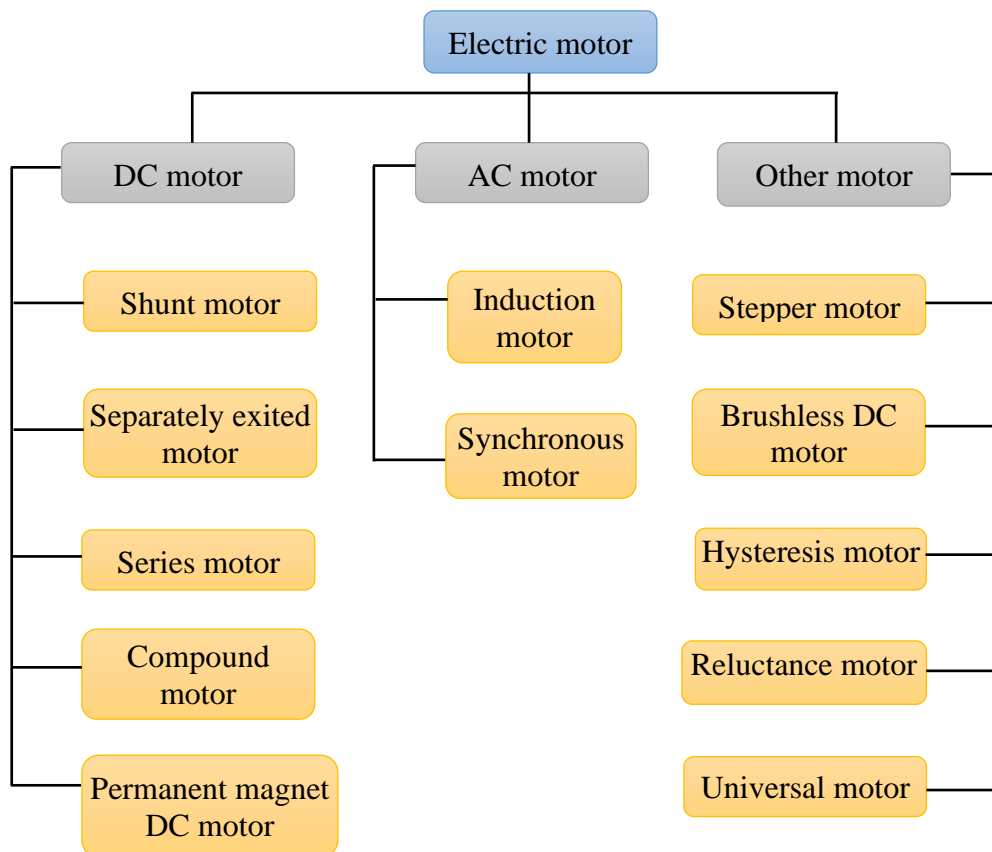


Figure 2.1 Motor classification

2.3.1. Brushed DC Motor

A brushed DC motor consists of a commutator and brushes that convert a DC current in an armature coil to an AC current, as shown in Figure 2.2. As current flows through the commutator of the armature windings, the electromagnetic field repels the nearby magnets with the same polarity and causes the winding to turn to the attracting magnets of opposite polarity [11].

As the armature turns, the commutator reverses the current in the armature coil to repel the nearby magnets, thus causing the motor to turn continuously. The fact that this motor can be driven by DC voltages and currents makes it very attractive for low-cost applications [12].

However, the arcing produced by the armature coils on the brush-commutator surface generates heat, wear, and EMI, and is a major drawback.

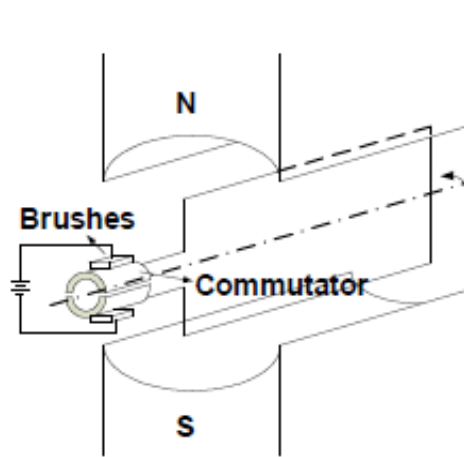


Figure 2.2 Brushed DC motor [11]

2.3.2. Brushless DC Motor

A BLDC motor accomplishes commutation electronically using rotor position feedback to determine when to switch the current [11]. The structure is shown in Figure 2.3. Feedback usually entails an attached hall sensor. The stator windings work in conjunction with permanent magnets on the rotor to generate a nearly uniform flux density in the air gap. This permits the stator coils to be driven by a constant DC voltage, which simply switches from one stator coil to the next to generate an AC voltage waveform with a trapezoidal shape [12].

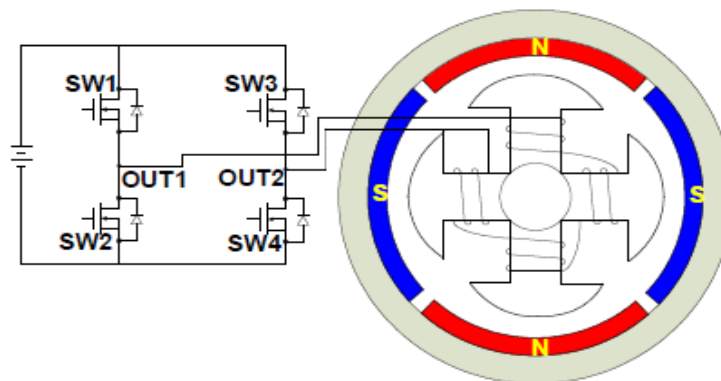


Figure 2.3 Brushless DC motor [11]

2.3.3. AC Induction Motor (IM)

A sinusoidal AC current runs through the stator to create a rotating variable magnetic field that induces a current in the rotor [11]. This induced current circulates in the bars of the rotor to generate a magnetic field. These two magnetic fields run at different frequencies (usually ω_s greater than ω_r) and to generate torque. Figure 2.4 shows the structure of an IM.

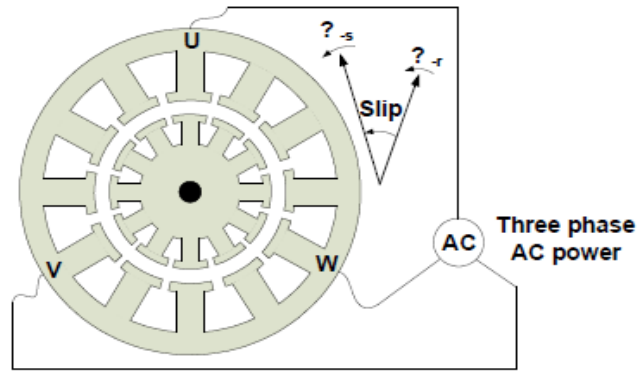


Figure 2.4 Induction motor [11]

2.3.4. Permanent Magnet Synchronous Motor (PMSM)

The PMSM motor shares some similarities with the BLDC motor, but it is driven by a sinusoidal signal to achieve lower torque ripple [11]. The sinusoidal distribution of the multi-phase stator windings generates a sinusoidal flux density in the air gap. However, newer designs can achieve this sinusoidal flux density with concentrated stator windings and a modified rotor structure [12].

Rotor magnet position can significantly alter the electrical properties. Mounting the rotor magnets on the surface results in lower torque ripple, while burying the magnets inside the rotor structure increases saliency, which increases the reluctance torque of the motor. The structure of the PMSM is shown in Figure 2.5.

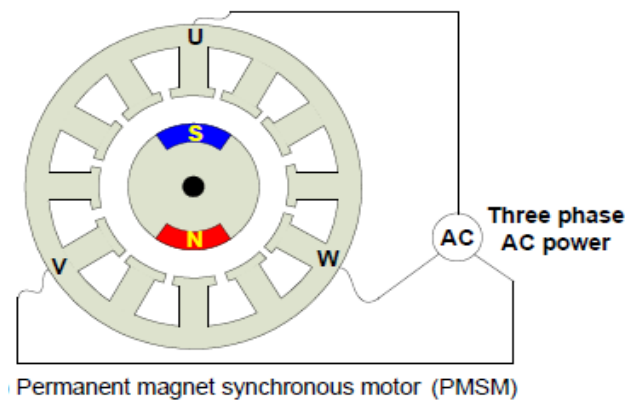


Figure 2.5 Permanent magnet synchronous motor [11]

2.3.5. Stepper Motor and Switched Reluctance (SR) Motor

Both stepper and SR motors have similar physical structures [11]. The stator consists of concentrated winding coils while the rotor is made of soft iron laminates without coils. It has a doubly salient structure as shown in Figure 2.6. When the current switches from one

set of stator coils to the next, the magnetic attraction between rotor and stator teeth induces enough torque to rotate the rotor to the next stable position. The rotation speed and distance are determined by the frequency of current pulse and number of pulses respectively. Since each step results in a small displacement, it is typically limited to low speed position control applications [12].

There is no reactive torque in an SR motor because the rotor cannot generate its magnetic field. Instead, both rotor and stator poles have protrusions so that the flux length is a function of angular position, which gives rise to saliency torque. This is the only torque-producing mechanism in an SR motor, which tends to result in high torque ripple. However, due to their simple design, SR motor is very economical to build and is perhaps the most robust motor available.

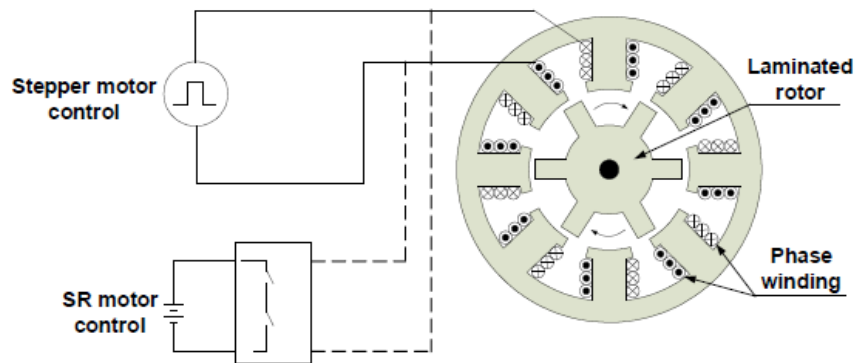


Figure 2.6 Stepper motor and Switched reluctance (SR) motor [11]

2.3.6. Performance Comparison of Various Motor Types

A basic comparison of various machine parameters of a BLDC motor with DC and IM motors and have highlighted the advantages of BLDC motor over the other types. The comparison describes how it can be widely accepted compared to the other types for the use in EV as well as for most of the other applications. And also, the comparison shows how BLDC motor has the capacity to replace all the other types owing to its wide range of merits and its capability to be applied to almost all applications where a motor is required with just a small drive system.

Table 2.2 and Table 2.3 summarizes the advantages of the BLDC motor when compared against DC and IM motors [7] [13] [14].

Table 2.2 Comparison between brushed DC and brushless DC motors

Feature	BLDC motor	Brushed DC motor	Actual advantages
Commutation	Electronic commutation based on rotor position information	Mechanical brushes commutator	Electronic switches replace the mechanical devices.
Efficiency	High	Moderate	The voltage drop on an electronic device is smaller than that on brushes.
Maintenance	Little/None	Periodic	No brushes/commutator maintenance.
Thermal performance	Better	Poor	Only the armature windings generate heat, which is the stator and is connected to the outside case of the BLDC. The case dissipates heat better than a rotor located inside of brushed DC motor.
Output power/ Frame size (ratio)	High	Moderate/Low	Modern permanent magnet and no rotor losses.
Speed/Torque characteristics	Flat	Moderately flat	No brush friction to reduce useful torque.
Dynamic response	Fast	Slow	Lower rotor inertia because of permanent magnets.
Speed range	High	Low	No mechanical limitation imposed by brushes or commutators.
Electric noise	Low	High	No arcs from brushes to generate noise, causing EMI problems.
Lifetime	Long	Short	No brushes and commutators.

Table 2.3 Comparison between AC induction and BLDC motors

Feature	BLDC motor	AC induction motor (IM)	Actual advantage
Speed/Torque characteristics	Flat	Nonlinear - lower torque at lower speeds	Permanent magnet design with rotor position feedback gives BLDC higher starting and low-speed torque.
Output power/ Frame size (ratio)	High	Moderate	Both stator and rotor have windings for induction motor.
Dynamic response	Fast	Low	Lower rotor inertia because of the permanent magnet.
Slip between stator and rotor frequency	No	Yes; rotor runs at a lower frequency than stator by slip frequency and slip increases with the load on the motor.	BLDC is a synchronous motor; the induction motor is an asynchronous motor.
Torque ripple	High	Less	Due to electronic commutation, BLDC motor has a high torque ripple than the induction motor.

A graphical comparison amongst various electric motors used in an EV has been made based on certain parameters like power density, cost of motors and their controller, dynamic response, efficiency, operation life, and the torque versus speed characteristics [15] [16]. Figure 2.7 shows the general graphical comparison of different electric motors.

Except for the controller and its cost, BLDC motor is the most efficient motor. Induction and SR motor both having almost similar efficiency but the least efficient being is the DC motor. The BLDC motor has a high cost and followed by the DC and SR motor, and the least is IM. Considering the power density, the BLDC motor leads and followed by IM and SR motor. Here once again the BLDC motor and IM have better operation life than the others. Hence due to the wearing and sparking of brushes, DC motor is the least in case of operation life [17]. The result shows BLDC motor has good performance parameters than other types.

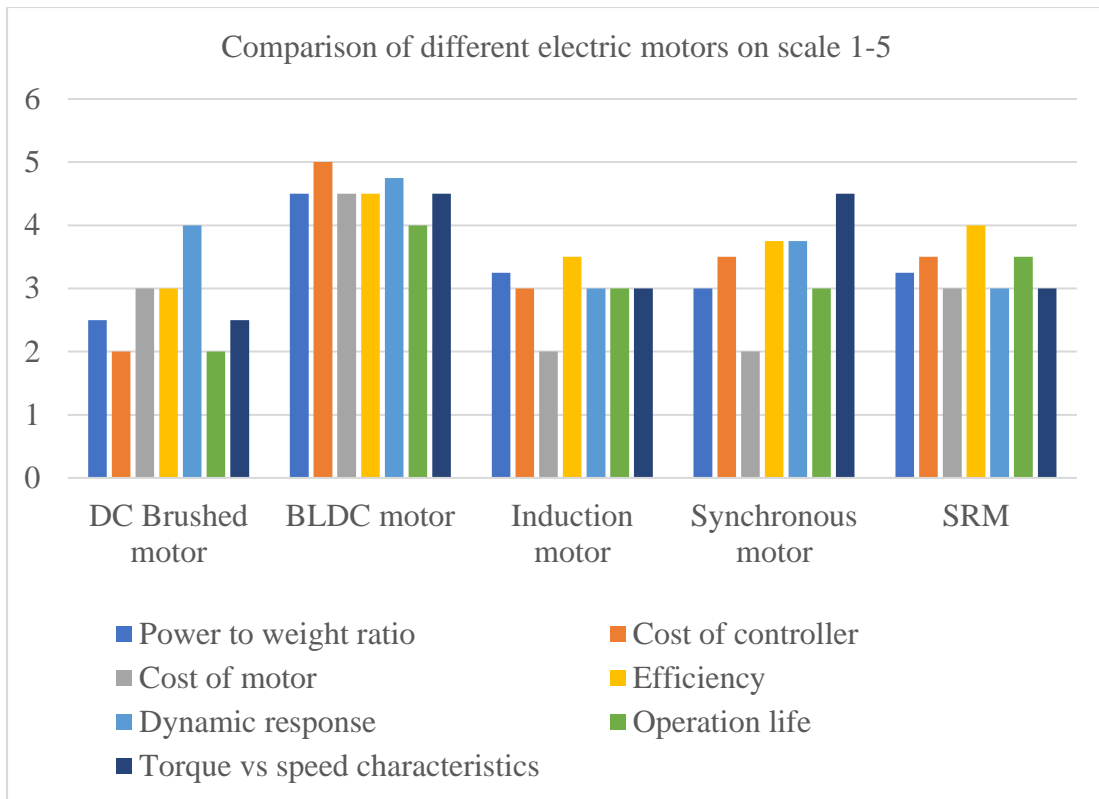


Figure 2.7 Performance comparison of different electric motors

2.4. Related Works on Brushless DC Motor Drive

Trapezoidal based BLDC motor has two type of drives. These are by using hall effect sensors and sensor less detection of rotor position. The main components of BLDC motor drives are the power source, inverter, and motor driver [18]. The common schematic diagram of three phase BLDC motor and its drive is depicted in Figure 2.8. The driver consists of speed and current controllers, and inverter switching commutation schemes. Parameters controller and commutation schemes are always depending on the requirement of specific applications.

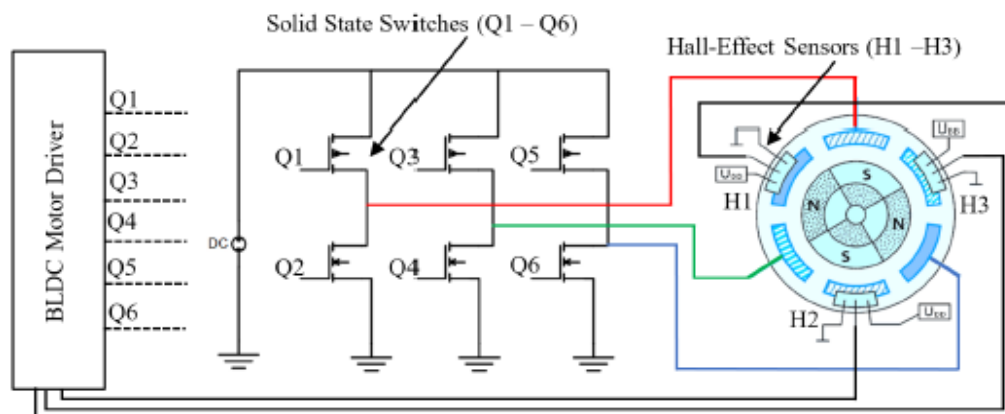


Figure 2.8 The three phase BLDC motor drive [18]

Based on the hall effect rotor position detection drive, there are different drives commonly used in the BLDC motor drive. Among them are summarized in the following sections.

2.4.1. Variable Voltage Source (VVS) Based BLDC Motor Drive

VVS based inverter commutation of BLDC motor drive is applicable in the case of a variable voltage source is used and, in the application, without considering the effect of current harmonics [19]. This scheme can be used for both sinusoidal and trapezoidal back-EMF BLDC motor drive types. The inverter commutation signals are generated directly from the hall decoded signals. The signal from the speed controller output determines the input voltage to the three phase inverter as shown in Figure 2.9. The inverter switches will be controlled depending on the rotor position sensor decoded signals [20]. This inverter scheme has high current harmonics (30%) than other techniques reported in the literature [21]. This leads to high torque ripple in the motor and it is not advisable to use in EV motor drive.

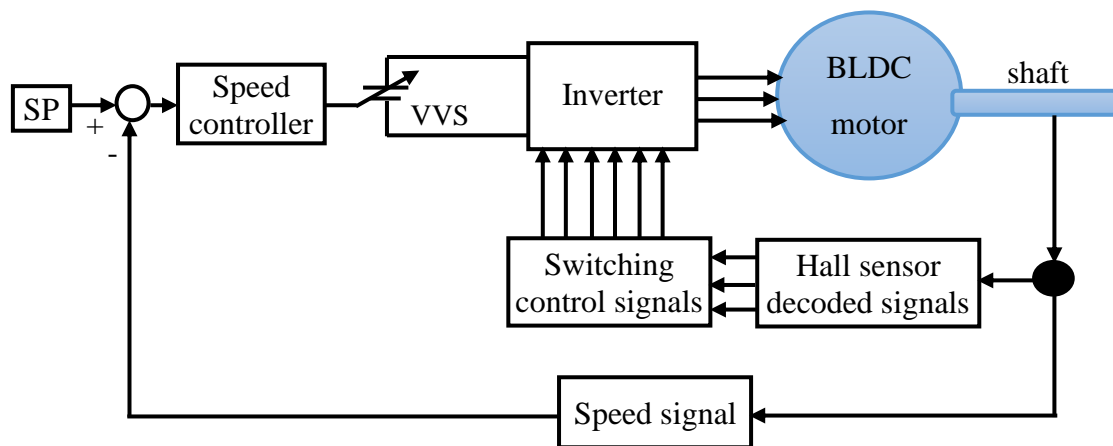


Figure 2.9 Variable voltage source based BLDC motor drive

2.4.2. Relay Based BLDC Motor Drive

Relay based BLDC motor drive is used in the application considering the effect of current harmonics. This inverter commutation drive technique is used for trapezoidal back-EMF brushless DC motor drive. It works based on the motor feedback current signal and the reference current signal generated from the speed controller output and hall sensor decoder [22]. The output of the speed controller will not directly control the input voltage of the BLDC motor as VVS. Figure 2.10 shows the block diagram of the relay based BLDC motor drive. This scheme has 20% current harmonics, which is better than VVS based drive developed and reported in the literature [22]. But the result of current harmonics in this scheme needs to be reduced to some extent using other driving techniques.

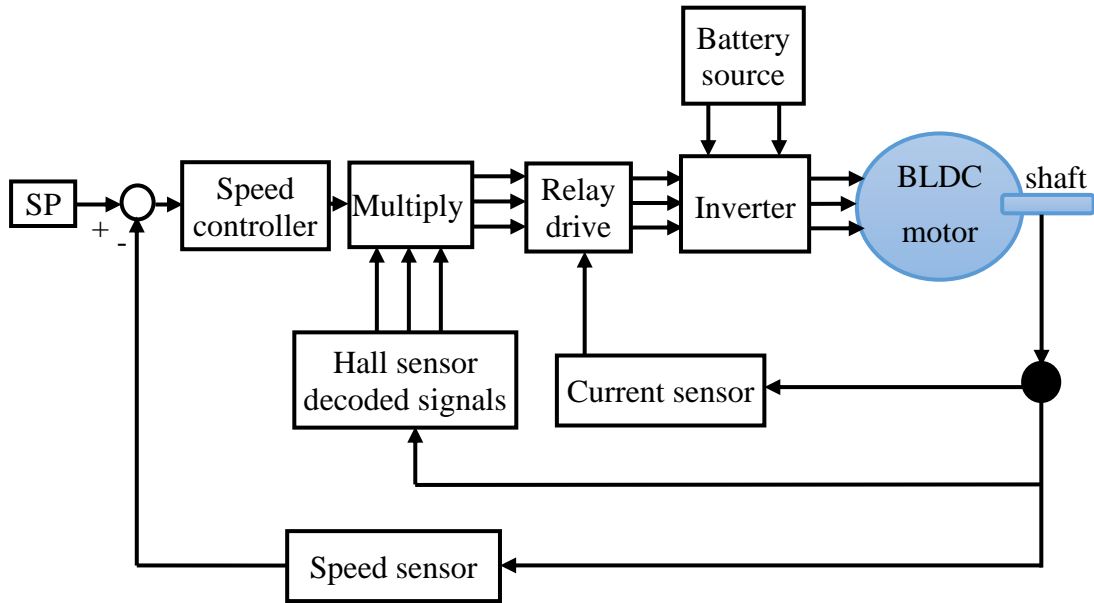


Figure 2.10 Relay based BLDC motor drive

The reference current of each phase is produced by multiplying the output of the speed control current signal and the decoded hall sensor signals. Then the difference of the reference current and the stator current passes through the relay bandwidth [23]. The output of the relay is a square wave signal determines the ON-OFF states of the inverter switches by using logical NOT circuits for each leg of the three phase inverter. In the case of the first leg when the upper switch S_1 is ON the lower switch S_4 is OFF and vice versa. Figure 2.11 depicts the process of relay inverter commutation drive.

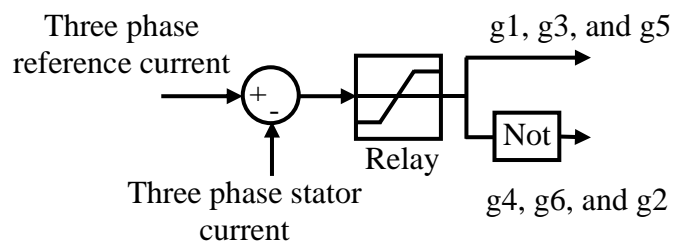


Figure 2.11 Relay based BLDC motor drive for each phase

2.4.3. Field Oriented Control (FOC) of BLDC Motor Drive

FOC is applicable for both sinusoidal and trapezoidal back-EMF types of BLDC motor drives. It is a vector control method based on stator current control in the field rotating reference flux [24] [25]. It works based on clark and park transformations, and space vector modulation (SVM). Fundamental requirements for the FOC are the knowledge of phase voltages and currents, and the rotor flux position [26]. The basic schemes of vector control

are indirect and direct methods of vector control. This method is applicable in torque and speed control applications and it is sophisticated for practical implementation. It is time consuming for debugging the program in the computer processor. This scheme is used relay control to implement the torque and flux control system [27]. It generates 15% current harmonics. Figure 2.12 depicts the application FOC in speed control of the motor.

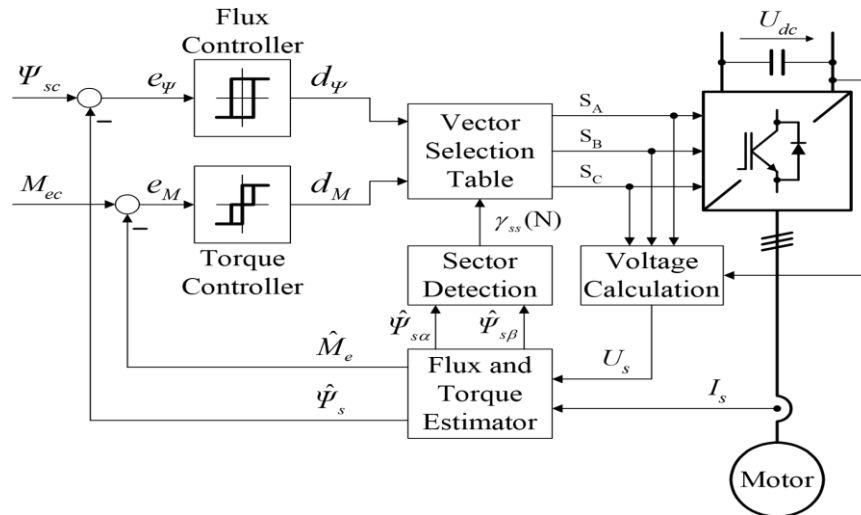


Figure 2.12 FOC based on direct torque control of BLDC motor [27]

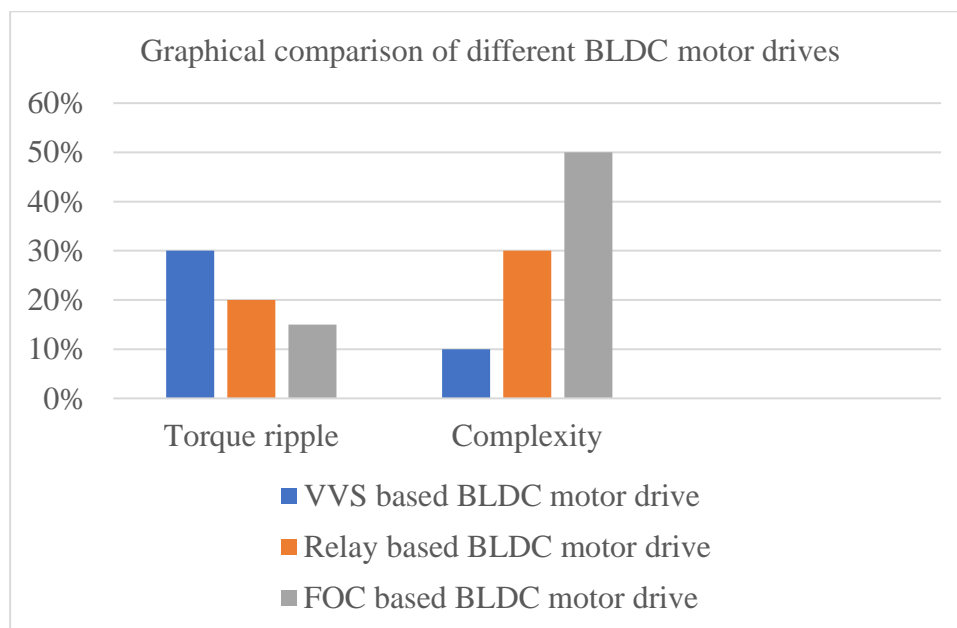


Figure 2.13 Graphical comparison of different BLDC motor drives

A graphical comparison of different motor drives has been performed as shown in Figure 2.13. It has been made based on torque ripple and complexity parameters. FOC has less torque ripple than other types but it is complex in case of implementation. VVS based BLDC motor drive has less complexity but it has high torque ripple than others.

2.5. Related Works on Cascade Control System of BLDCM

Several research papers reported on the BLDC motor cascade control system by using different tuning and optimization algorithms. The cascade control system of a BLDC motor is a combination of speed and current regulators. ON-OFF speed control firstly makes sense as the simplest control scheme but this control technique has less accuracy and stability [28]. On the other hand, the PID control method is accurate for speed control with disturbance rejection but it will give rise to produce high starting current which can be dangerous for control circuitry or motor for high capacity operation.

The cascaded PID configuration achieves better dynamic performance, gives the best setpoint tracking, disturbance regulation, and reduced starting current that can be used for low and high capacity motors [29]. The closely related works to the proposed research work with their corresponding output result merits and demerits are discussed. The discussions are made based on speed and current dynamic performances in the application of constant and variable setpoint as well as load conditions, current harmonics, and torque ripple.

The authors in [30] developed a comparative analysis of BLDC motor speed using ANFIS and PI controllers for EV. The EV is weighted about 1000kg and electric power consumption of 25kW per speed of 60km/hr is designed. In the case of speed ANFIS regulation, it has better dynamic performance than PI regulation, specifically the overshoot and settling time are 0% and 0.2sec respectively under variable and constant setpoint condition. But, settling time is relatively high compared with other related work [31] and needs to improve to some extent. The drawback of the paper is that it didn't discuss the current regulator, reduction of torque ripple, and speed dynamic performance due to variable load conditions.

The comparative analysis of the BLDC motor speed control system based on the PI and fuzzy-PI controllers under the VVS based inverter drive for pure EV was performed in literature [32]. The result of the study shows that the fuzzy-PI controller has a better speed dynamic performance than the PI controller. Its overshoot and settling time results are 0% and 0.025sec respectively under 3000rpm rated speed and constant load condition. The system is not simulated under variable setpoint and load conditions, and there is no mechanism to limit the motor starting current overshoot problem. These problems can be considered as a limitation of the study. The disadvantage of the study is, it has 30% of current harmonics and this leads to approximately 30% torque ripple which makes the vehicle vibrates.

BLDC motor speed control system using fuzzy-PID controller under variable load and setpoint condition for EV was developed in literature [33]. The system is simulated using VVS based inverter drive without a current control system and compared with the PID controller as shown in Table 2.4.

Table 2.4 Dynamic performance analysis of BLDC motor

Controller	Set Point (rpm)	Without load			With load		
		t_r (ms)	t_s (sec)	M_p (%)	t_r (ms)	t_s (sec)	M_p (%)
PID	600	35.12	-	1.74	79.26	-	1.68
	700	33.37	-	1.74	80.68	-	1.68
Fuzzy-PID	600	68.54	0.23	7.44	115.10	1.99	0.21
	700	68.76	0.23	7.44	115.10	1.99	0.21

where t_r , t_s , and M_p are rise time, settling time, and maximum overshoot respectively. The result shows that the fuzzy tuned PID can improve the performance of BLDC motor speed in variable setpoint and dynamic load conditions. Although the fuzzy-PID controller gives better performance than the conventional PID controller, its dynamic performance can be further improved. Also, the current harmonics are high due to VVS inverter drive and can be considered as a limitation of the study. VVS is not recommended for the propulsion of EV because it generates high torque ripple.

Speed control system for 1500rpm rated speed of BLDC motor using ANFIS controller was developed and compared with other types of controllers under variable setpoint and load conditions in literature [31]. The result shows that ANFIS speed control of BLDC motor has better dynamic performance than others. The result has 0.04sec rise time, 0% overshoot, and 0.05sec settling time. The system is simulated using relay based inverter drive and its torque ripple has a value of 20%. This is too high and can be further improved. The other drawback is that the system hasn't current regulator, and may lead to high current in the starting.

In a similar manner, the closed-loop speed control of the BLDC motor drive using position sensors is performed in literature [34]. The result shows that it has good speed dynamic performance but its torque ripple is about 15%. BLDC motor speed control is developed by using a fuzzy-PI controller and relay based inverter drive. The result shows that the speed dynamic performance of the motor have 0.05sec rise time, 10% overshoot, and 0.09sec

settling time. Even though the fuzzy-PI controller gives better control performance than the PI controller, it has high overshoot and settling time compared with the same controller used in the literature [32]. The other drawback of the study is, it has high current harmonics i.e. about (+20%) [35] [36]. And also, the authors didn't discuss the application of variable speed and load conditions, and current regulator.

Fuzzy-PID supervised online ANFIS speed controller has been presented for the comparison of the dynamic performance of BLDC motor in literature [37]. The system is simulated under constant and variable load as well as set point conditions. The result shows the fuzzy PID supervised online ANFIS controller has better performance than other controllers in various aspects. Its result has 0.02sec rise time, 0% overshoot, and 0.03sec settling time. The system is simulated using relay based inverter drive and its torque ripple has a value of +20%. The other drawback is that the system hasn't current regulator, this may lead to high current at starting.

In general, the performances of BLDC motor with PI, PID, fuzzy-PI and PID, ANFIS, and fuzzy PID supervised online ANFIS speed controllers for EV and other applications are discussed. Accordingly, a fuzzy PID supervised online ANFIS speed controller gives better dynamic performance than others. Although the performance of fuzzy PID supervised online ANFIS speed controller is better than others, the PID term is a linear controller and it is not recommended for the nonlinear systems. Hence, BLDC motor is a nonlinear machine, as a result in the PID controller a fixed gain is effective in a limited operating range, its performance degrades and it may become unstable in some cases when it is out of the range. This problem can be improved to some extent by introducing the nonlinear PID controller.

Form the reviewed literatures in this section, the BLDC motor current regulator is not discussed and proposed as a controller. Hence electric motors have high starting current (high overshoot), leads to heating in the motor winding and burning of the control circuitry. Therefore, the current regulator is required in cascaded with the speed controller. The current harmonics and torque ripple are very large in literatures. If the controller output is stable and smooth, the PWM inverter commutation technique is recommended because the signal depends on the stability and smoothness of the controller output signal. This research thesis focused on the analyses of speed and current dynamic performance of the BLDC motor and reducing the current harmonics by using PWM based inverter drive technique.

CHAPTER 3

3. METHODOLOGY

3.1. Introduction

This chapter deals with data collection and analysis, mathematical modeling of the vehicle dynamics and BLDC motor, and design of cascade control and inverter switching techniques for the BLDC motor drive. A nonlinear PID control technique is applied for speed control of the motor. The different artificial intelligence based nonlinear PID controller tuning techniques are performed for speed control of BLDC motor. Internal AI-based linear PI current regulator is developed to limit the starting current of the motor. Then modeling of the overall BLDC motor drive is performed. Finally, the system is simulated by using MATLAB/2016a software both in Simulink and script.

3.2. Materials

In this research work, software such as MATLAB/2016a, Microsoft office 2019, and MathType 6.0 equation are used. MATLAB is the computing software which consists of technical toolboxes and Simulink. Microsoft office is used for editing the thesis documentation. MathType 6.0 is used for writing mathematical formulas and equations in Microsoft offices word and PowerPoint presentation tools.

3.3. Methods

The method used in this thesis to accomplish the required task is shown in Figure 3.1. The closely related papers and literatures are reviewed. Then the necessary data used throughout this research are collected and analyzed. The electric bajaj vehicle and reducer including gear transmission ratio specification data were taken from gasoline based bajaj qute with similar size manufacturing company. Electric vehicle BLDC motor specifications have taken from the manufacturing company and some of the other specifications taken from literatures.

The collected data is analyzed mathematically and graphically for developing system modeling. The dynamics modeling and the maximum power requirement of electric bajaj qute vehicle are analyzed. The BLDC motor cascade control drive is designed with inverter commutation techniques. Based on the bajaj data and the motor controller result, the bajaj speed is analyzed in km/h with the battery state of charge. The proposed modeling and simulation result of the system is compared with different artificial intelligence based control

algorithms for speed and current control. Different three phase inverter commutation techniques are applied and compared throughout the work. The block diagram in Figure 3.1 summarizes the method followed throughout the research work.

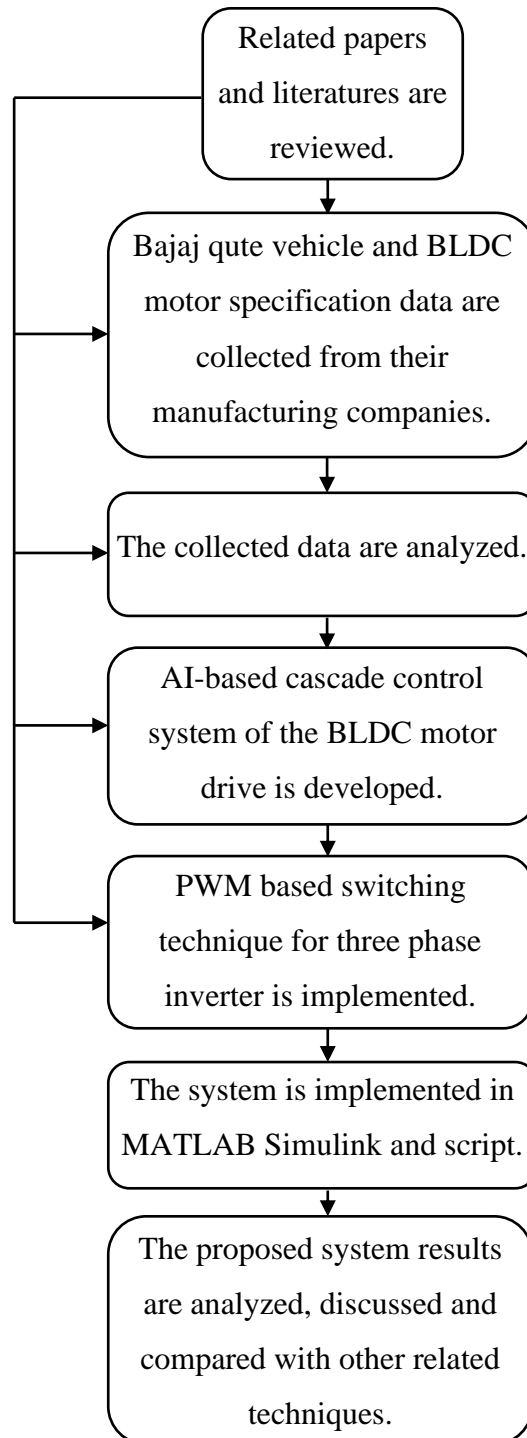


Figure 3.1 Block diagram of the research methodology

3.4. The Proposed Block Diagram of BLDC Motor Drive

The proposed system block diagram of the cascade control of the BLDC motor drive for the propulsion of electric vehicle bajaj qute is shown in Figure 3.2. The difference in the reference speed and actual rotor speed is controlled by using a speed regulator. For this, a neural network based NPID speed controller is proposed. Three phase reference current is generated from the speed controller output and hall sensor decoded signals.

Usually, the motor needs the current limiter due to the high starting current. Two phases of the stator current are taken as the stator current feedback because once the two current phases are known the third phase is a negative summation of the two phases. The difference of phase current and the corresponding reference current is controlled by using the GA-PI controller. The motor armature current has harmonics and leads to torque ripple. To reduce this effect PWM based three phase inverter commutation signal generation is performed and proposed. PWM consists of a comparator, output of the current controller converted to voltage, carrier signal including its switching frequency and the logical circuit which is used to generate inverter driving signals.

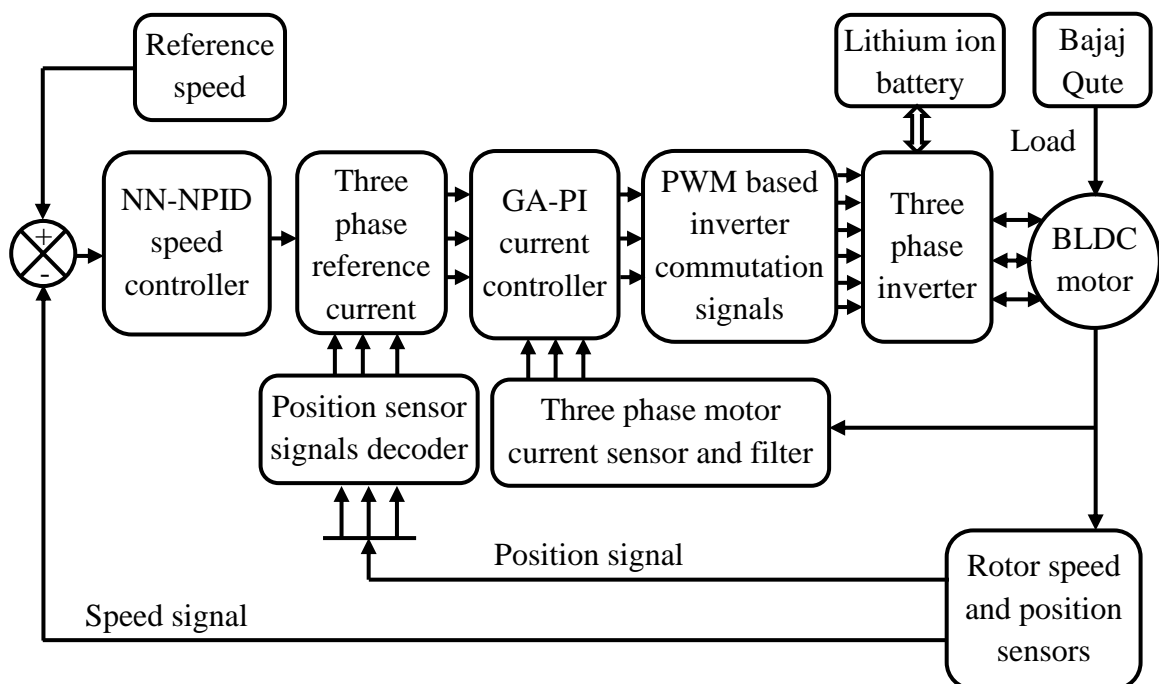


Figure 3.2 Block diagram of the proposed drive control system

3.5. Analysis of Bajaj Qute Electric Vehicle Dynamics

Pure electric vehicle power system train mainly includes the battery, drive motor, reducer, gearbox, clutch, etc. Among them, drive motor and battery are the core part. In order to

increase transmission efficiency and reduce the mechanical transmission device, the traditional automobile clutch can be omitted in the power transmission system of electric vehicle arrangement [38]. The power system of a pure electric vehicle designed in this work contained the motor, battery, mechanical driving device, and control system [39]. The structure diagram of the pure electric vehicle power system is shown in Figure 3.3. The double arrow indicates that the energy flow from the battery to the motor and vice versa converted to mechanical and electrical energy vice versa respectively.

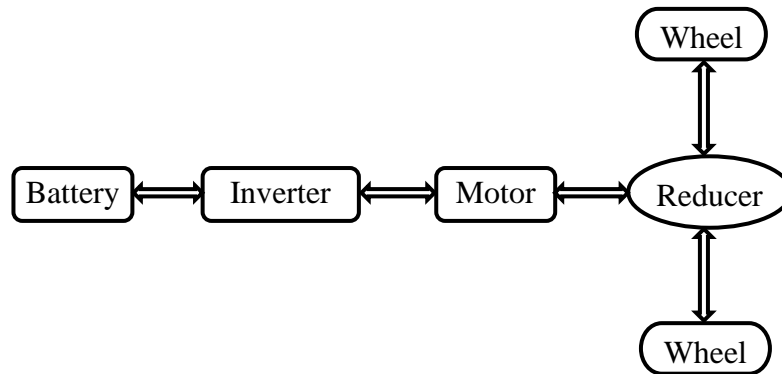


Figure 3.3 Pure electric vehicle power system structure

3.5.1. Driving Force and Power of Bajaj Qute Electric Vehicle

In this thesis, the drive motor and battery parameters are matched mainly according to the design specifications of four wheel bajaj vehicle dynamics. When deriving a mathematical model for the bajaj platform, it is important to study and analyses dynamics between the road, wheel, and vehicle platform [40]. Several forces are acting on the bajaj platform when it is running. The modeling of the bajaj vehicle dynamics involves the balance between the acting on the running platform forces, forces categorized into road-load, and driving force. The road-load force consists of the gravitational force at the inclined surface or hill climbing force, rolling resistance of the tires, the aerodynamic drag force, and so on [41]. The resultant force is the sum of all these acting forces i.e., the driving force.

It is seen in Figure 3.4 that, the changes of the inclination angle in the road surface introduce a disturbance to the system. Therefore, the controller must have the capability to eliminate disturbances. The disturbance torque to vehicle platform is the total resultant torque, generated by the acting forces, and can be expressed by:

$$F_t = F_r + F_c + F_o \quad (3.1)$$

where F_r is the rolling resistance force, F_c is the hill-climbing resistance force, and F_o is other forces.

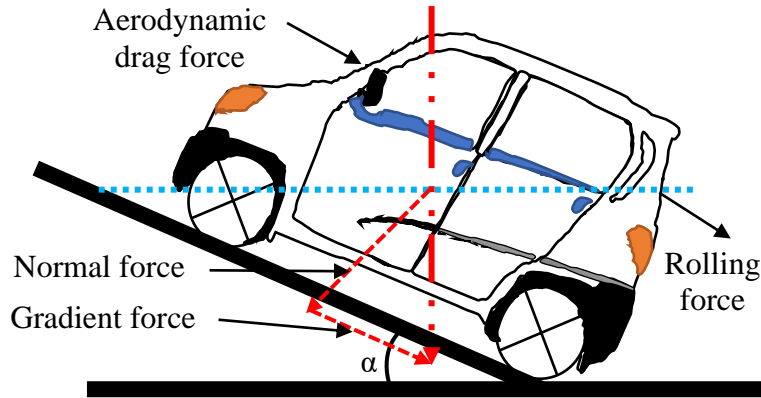


Figure 3.4 Forces acting on the moving four wheel bajaj vehicle platform

3.5.1.1. Rolling Resistance Force

Rolling resistance force is produced by flattening of the tire at the contact surface of the roadway [41] [42] [43]. The rolling resistance force is a conservative force with the possibility to partly recover. It depends on the platform's speed and is proportional to the platform weight. It is given by:

$$F_r = M \times g \times C_r \times \cos(\alpha) \quad (3.2)$$

$$F_r = 990\text{kg} \times 9.81 \frac{\text{m}}{\text{s}^2} \times 0.01 \times \cos(11.30^\circ) = 95.2363\text{N}$$

where M is the mass of the bajaj platform and cargo (kg), α is the gradient angle (rad), g is the acceleration due to gravity (m/s^2), and C_r is the rolling resistance coefficient. The power required to overcome the rolling resistance force is:

$$P_r = F_r \times \text{speed} \left(\frac{\text{m}}{\text{sec}} \right) = 95.2363\text{N} \times \frac{70000\text{m}}{3600\text{sec}} = 1.852\text{kW} \quad (3.3)$$

Table 3.1 shows the coefficient of friction for different types of surfaces.

Table 3.1 Coefficient of frictions for different types of surfaces [42] [43]

Contact surface	Coefficient of friction
Concrete surface (good/fair/poor)	0.010/0.015/0.02
Asphalt (good/fair/poor)	0.012/0.017/0.022
Macadam (good/fair/poor)	0.015/0.022/0.037
Snow/dirt	0.025/0.037
Mud (firm/medium/smooth)	0.037/0.09/0.15
Grass (firm/soft)	0.055/0.037
Sand (firm/soft/dune)	0.060/0.15/0.3

3.5.1.2. Hill-Climbing (Gradient) Resistance Force

While the vehicle platform is moving up or down the hill, the weight of the vehicle platform will create a hill-climbing resistance force directed downward [41] [42]. This force opposes or contributes to the motion. It is a conservative force, with the possibility to partly recover [43]. The component of gravity in the dimension of travel is the hill-climbing resistance force and it is expressed as:

$$F_c = M \times g \times \sin(\alpha) \quad (3.4)$$

$$F_c = 990\text{kg} \times 9.81 \frac{\text{m}}{\text{s}^2} \times \sin(11.30^\circ) = 1903.01\text{N}$$

where M is the mass of the vehicle platform and cargo (kg), g is the acceleration due to gravity (m/s^2), α is the road or the hill-climbing angle, road slope (rad.).

The power required to overcome the hill-climbing force at a speed of 35km/hr is:

$$P_c = F_c \times \text{speed} \left(\frac{\text{m}}{\text{sec}} \right) = 1903.01\text{N} \times \frac{35000\text{m}}{3600\text{sec}} = 18.5015 \text{ kW} \quad (3.5)$$

In Equation (3.5) the speed of the vehicle is assumed half of the maximum speed (i.e. 35km/hr) to increase the torque when climbing the hill.

3.5.1.3. Aerodynamic Drag Force

Aerodynamic drag force is the force opposing the motion of the vehicle platform due to air drag. When a bajaj is moving there will be a zone in front of the vehicle platform where the air pressure is high and a zone behind the vehicle platform where the air pressure is low. These two zones will oppose the motion of the platform. The resulting force on the vehicle is the shape drag [42] [43].

The second component of the aerodynamic drag is skin friction and created because two air molecules with different speeds create friction. Since the air, close to the vehicle platform, moves almost with the same speed as the vehicle platform, in contrast to the air speed far away from the bajaj vehicle, there takes place friction [44]. The aerodynamic drag force is a function of the vehicle platform linear velocity, V and can be written by

$$F_a = 0.5\rho \times A \times C_d \times (V + V_a)^2 \quad (3.6)$$

where A is the frontal area of the bajaj, C_d is the aerodynamic drag coefficient, V and V_a are the speed of bajaj and air, respectively. Hence, the air speed is less than the vehicle speed, and the power required to overcome it can be ignored. There are also other forces to consider when designing the bajaj electric vehicle dynamics like aerodynamic lift force, wheel force,

and others. Usually, they are minimal compared to the two forces mentioned above and can be considered as a maximum of 1.5kW. Therefore, the required maximum power for BLDC motor to drive a four wheel bajaj electric vehicle in all conditions of motion, that is, the maximum tractive power required to propel the vehicle will be:

$$P_{\text{out total(max)}} = 1.5\text{kW} + 1.852\text{kW} + 18.5015\text{kW} = 21.8535\text{kW} \quad (3.7)$$

In addition, the losses due to the transmission of power to the bajaj wheel must be considered [42]. The mechanical output power required to drive the vehicle is given by Equation (3.8).

$$\begin{aligned} P_{\text{total driving power}} &= \frac{P_{\text{out total(max)}}}{\eta_{\text{gear transmission efficiency}}} \\ &= \frac{21.8535\text{kW}}{0.95} \approx 23\text{kW} \end{aligned} \quad (3.8)$$

Equation (3.8) shows the total driving power of the motor for the propulsion of the bajaj quite. Based on this result, the motor rated specifications are selected as shown in Table 3.2.

3.5.1.4. The Effect of Bajaj Speed on the Power Requirement

The relationship between the speed and driving power of the bajaj is analyzed and plotted as shown in Figure 3.5. This shows that the vehicle power consumption and speed in km/hr have a linear relationship. As the speed of vehicle increases, its power consumption also increases [38] [39]. The vehicle can move at the speed of 70km/hr with a power consumption of 25kW. This relation fulfills with the identified maximum power requirement.

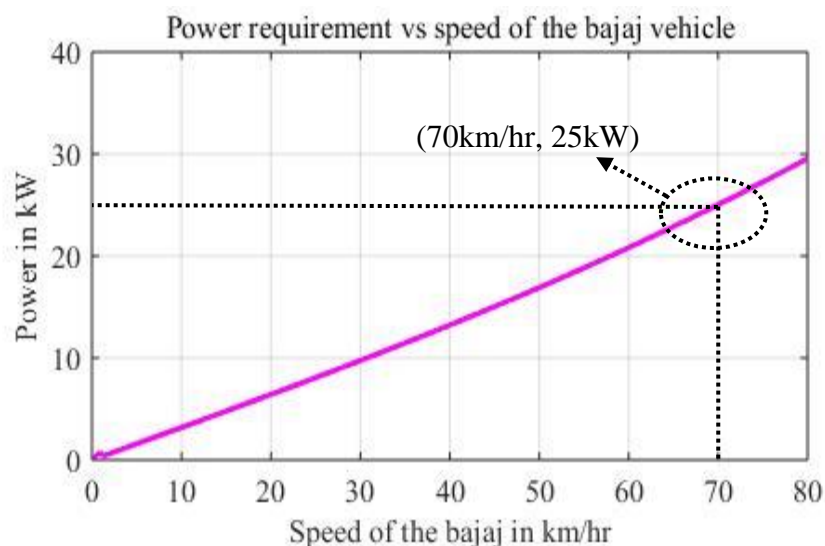


Figure 3.5 Driving power vs speed of the bajaj vehicle

3.5.1.5. Motor Rated Power and Peak Power Matching

The selection of rated speed, torque, and power of the BLDC motor should conform to the requirements of the torque versus speed characteristic curve [44]. When the vehicle starts, the motor speed is low and works in constant torque state, as long as the speed is higher than the rated speed, it works in constant power state [45]. The rated torque and power of the 1500rpm base speed electric vehicle BLDC motor have a value of 63.5Nm and 10kW respectively as shown in Figure 3.6.

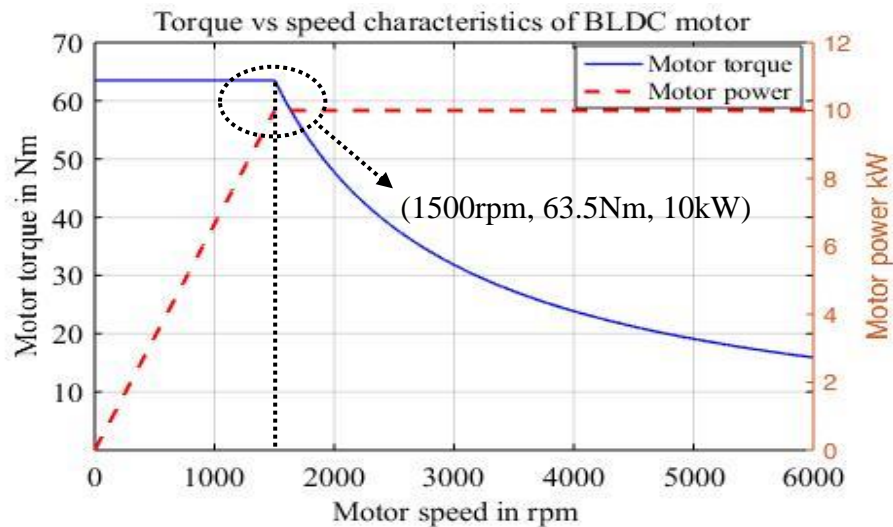


Figure 3.6 Torque versus speed characteristics of the BLDC motor

3.5.1.6. The Effect of Gradient Angle on the Power and Speed of Vehicle

The speed of the bajaj qute should be reduced while climbing the hill to increase torque.

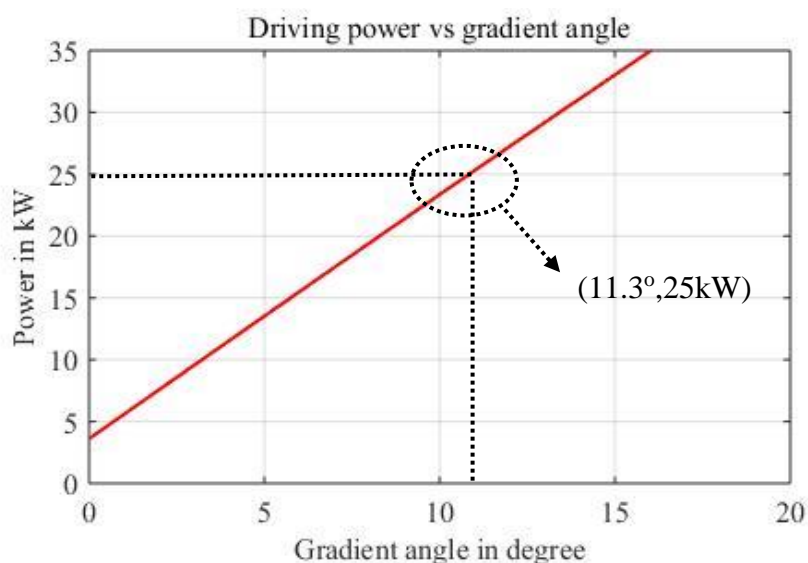


Figure 3.7 Driving power vs gradient angle of the vehicle

The vehicle needs more torque while climbing the hill [38] [39]. The maximum driving power is used when the vehicle is clamping the hill of maximum gradient angle which is 11.30° with its full load at a constant speed of 35km/hr. Figure 3.7 describes the power need to be supplied by the motor to drive the bajaj at a constant speed of 35km/hr with various gradient angle. From Figure 3.7, 25kW power is enough to propel the car over a maximum gradient angle of 11.3° at the fifth gear.

3.5.2. Electric Vehicle (Bajaj Qute) Specification

Table 3.2 shows the specifications of a four wheel bajaj electric vehicle and taken based on the gasoline bajaj qute from the manufacturing company [L1] [L4].

Table 3.2 Bajaj qute electric vehicle and driving motor specifications

Parameters	Value [Unit]
Maximum power	25 [kW]
Gross weight	990 [kg]
Rated power	10 [kW]
Maximum torque	130 [Nm]
Rated torque	63.5 [Nm]
Maximum speed	70 [km/hr.]
Rated speed	1500 [rpm]
Maximum gradient angle	11.3 [degrees]
Capacity of seating	4 [person]

3.5.3. Reducer and Gear Specifications

Reducers are frequently used in vehicles for power transmission because the torque requirement of a vehicle varies with speed [46]. The main functions of a reducer are as follows:

- It provides torque that is needed to move the vehicle under a variety of road, environment, and load conditions. It can be obtained by changing the gear ratio between motor crankshaft and vehicle drive wheels.
- It shifts gears to reverse so the vehicle can move in a backward direction.
- It shifts gears to neutral for rest and starting position.

The structure of a reducer or gearbox and a shaft for the general model of electric vehicle is shown below in Figure 3.8.



Figure 3.8 Reducer (gearbox) and shaft [L3]

Table 3.3 shows the specifications of the gearbox used in gasoline based four wheel bajaj. The required data are taken from the gasoline based vehicle manufacturing company.

Table 3.3 Gear box specifications [L3]

Parameters	Values
Maximum Speed	4000rpm
Maximum Torque	130Nm
Gear ratio	4.014

3.5.4. Traction Motor

While designing an EV, the first and foremost component to be selected is the electric motor because the internal combustion engine of conventional vehicles is replaced by an electric motor in an electric vehicle [47]. Therefore, the electric motor used in an EV must produce appropriate power and other characteristics that are required for traction purposes.

3.5.4.1. Selection of Traction Motor

In literature [4] [30] [32], it is shown that BLDC motor is the best selection for EV compared to an induction motor, SR motor and DC brushed motor. But PMSM motor is highly competent with BLDC motor especially in the case of weight, efficiency, and so on [26]. Even though these two motors are highly competent to each other, BLDC motor has better futures in case of having a higher power output, higher torque density, cost, and simplicity. Generally, BLDC motor has larger output power and torque density than PMSM but it is inferior to PMSM motor in high speed range and field weakening operational application. Furthermore, the BLDC motor has a higher torque ripple than PMSM [48]. Table 3.4 explains the performance comparison between the BLDC and PMSM motors.

Table 3.4 Performance comparison between BLDC and PMSM motors [26] [48]

Feature	BLDC motor	PMSM motor	Actual advantage
Speed/Torque characteristics	High	Moderate	If they have the same rated speeds, BLDC motor can have 15% more electric torque than PMSM.
Output Power/ Frame size (ratio)	High	Moderate	BLDC has a 15% power density than PMSM at equal copper losses.
Dynamic response	Fast	Fast	Lower rotor inertia because of the permanent magnet.
Torque ripple	High	Moderate	Because of trapezoidal back EMF and stator current generation, BLDC motor leads to less suitable in position control applications.
Rotor position sensor	Rotor position feedback is needed every 60-degree (less resolution sensor is required).	Continuous rotor position feedback is needed (high-resolution sensor is required).	This is an advantage of the BLDC over PMSM in speed control applications.
Controller/ driver cost	Less expensive	Very expensive	For this reason, we can't use PMSM for electric bajaj quite.

3.5.4.2. Traction Motor Specification

According to the maximum power of the bajaj quite, some of the BLDC motor specifications are taken from the manufacturing company and the others are taken from literature. The torque and back EMF constants are determined by the following derivations from the motor two phase equations [49]. The rated power of the motor is expressed by the product of the motor current and the back EMF for considering two phases.

$$\text{Power}_{(\text{rated})} = 2E_m \times I_m \quad (3.9)$$

The motor back-EMF is expressed in terms of rated power and current as follows:

$$E_m = \frac{\text{Power}_{(\text{rated})}}{2 \times I_m} = \frac{10\text{kW}}{2 \times 77\text{A}} = 64.935\text{V} \quad (3.10)$$

Hence, the back EMF of the motor is directly proportional to the motor speed.

$$\begin{aligned} K_b &= \frac{E_m}{W_{(\text{rated})}} = \frac{64.935\text{V}}{1500 \times \frac{2\pi}{60} \text{rad / sec}} \\ &= \frac{64.935\text{V}}{157.0796 \text{rad / sec}} = 0.4134\text{V sec / rad} \end{aligned} \quad (3.11)$$

For two phase operating system the constant back-EMF gain should be doubled.

$$K_b = 2 \times 0.4134 = 0.8268\text{V sec / rad}$$

The torque is directly proportional to the motor current and inversely with the motor speed, and it can be calculated as in Equation (3.12).

$$\text{Torque}_{(\text{rated})} = K_t \times I_m = \frac{2E_m \times I_m}{W_{(\text{rated})}} \quad (3.12)$$

Then the torque constant of the motor is calculated by

$$K_t = \frac{2 \times E_m}{W_{(\text{rated})}} = \frac{2 \times 64.935\text{V}}{157.0796 \text{rad / sec}} = 0.8268\text{Nm / A} \quad (3.13)$$

Table 3.5 shows the parameter specifications of three phase BLDC motor used for the study.

Table 3.5 Parameter specifications of BLDC motor used in this thesis [L4] [50]

Parameters	Value [Unit]
Number of poles	4
Power factor	0.85
Efficiency at rated	93.6 [%]
Control input rated voltage	144 [V]
Rated motor current	77 [A]
Rated motor power	10 [kW]
Armature phase winding resistance	2.875 [Ω]
Armature phase inductance	0.0085 [H]
Rated speed	1500 [rpm]
Viscous friction model	0.001 [N·s/m]
Torque constant	0.8268 [N·m/A]
Back emf coefficient	0.4132 [V·s/rad]
Inertia moment of the rotor	0.0089 [kg·m ²]

The motor rated power, voltage, current, torque, and speed are selected based on the requirement of the maximum power of the bajaj qute vehicle.

3.5.5. Battery Specifications

3.5.5.1. Matching Power Battery Parameters

The power source of the pure electric vehicles is a battery. A lithium battery is selected as the power source for electric vehicles due to its long life and high energy density [51]. It consists of the packs of standard lithium battery modules in serial. Each battery module has 4kWh storage. Hence the voltage rated of the motor is 144V and the lithium-ion battery has 90Ah as shown in Table 3.6. Then the total energy of the lithium battery is the product of the rated voltage and the ampere-hour rating of the battery and its result is 12960VAh (12.96kWh). Accordingly, there are four serially linked battery modules to fulfill the requirement of total energy. Therefore, the selection of battery parameters must meet the demand for endurance mileage requirements and the maximum power of the vehicle [52].

$$P = P_{\max} \times 0.15 + 0.85 \times P(\text{zero grad}) \quad (3.14)$$

$$P_m = \frac{P}{\eta_m} \quad (3.15)$$

$$W_{\text{road}} = P_m t = \frac{P_m S}{V} \quad (3.16)$$

$$\text{SOC}(\%) = \frac{(W_{\text{rated}} - W_{\text{road}}) \times 100\%}{W_{\text{rated}}} \quad (3.17)$$

where P is the power required for the vehicle at a constant speed, S is endurance mileage, W_{road} is the energy needed for mileage S , P_m is the input power of the motor drive and η_m is the efficiency of motor and motor drive assembly [49] [53].

Table 3.6 Parameter specifications of Lithium-ion battery [L4] [49]

Parameters	Value [Unit]
Cell type	Lithium-ion
Total battery power pack	16[kWh]
Capacity	90[Ah]
Rated voltage	144 [V]
Nominal voltage	4.2[V]
Energy density	154 [Wh/kg]
Operating temperature	-10 to 50 [°C]
Energy	666 [Wh]

3.5.6. Selection of Power Semiconductor Device

For this work, metal oxide semiconductor field effect transistor (MOSFET) is selected for the BLDC motor drive. MOSFET ratings are fulfilling the requirements of the BLDC motor drive. Hence in the application of switched mode power supply like inverter and chopper, MOSFET and (insulated gate bipolar transistor) IGBT are highly competent. Usually, they are selected based on their ratings [54]. MOSFET is a low voltage device. High voltage MOSFET is available up to 600V but with limited current and can be paralleled quite easily for higher current capability.

Ratings of MOSFET: Voltage $V_{DS} < 500V$, current $I_{DS} < 300A$ and frequency f are up to MHz. The gate drive circuit is simple, and turning on and off is very simple.

- To turn on: $V_{GS} = +15V$
- To turn off: $V_{GS} = 0 V$

IGBT is a combination of BJT and MOSFET characteristics. Gate behavior is similar to MOSFET and easy to turn on and off. Low losses like BJT due to low on-state collector to emitter voltage (2-3V). Ratings of IGBT are: Voltage: $V_{CE} < 3.3kV$, Current: $I_C < 1.2kA$ currently available. (Latest high voltage IGBT (HVIGBT): 4.5kV/1.2kA). The switching frequency of IGBT is up to 100kHz. Even though IGBT has a good performance than the MOSFET device, the rating is not suitable for the BLDC motor drive power requirement [54] [55]. Hence the rating of BLDC motor used in this work is 144V (input voltage) and 77A (current) for the propulsion of electric vehicle bajaj quite. MOSFET has the capability of carrying the requirement of the BLDC motor rating.

3.6. Modeling of BLDCM Drive for Electric Vehicle Propulsion

The electric vehicles power system component requires an accurate and precise model of electric motor drive design [56]. In order to design the BLDC motor control system for the propulsion of a four wheel bajaj electric vehicle, the precise model of BLDC motor is required. The three phase star connected BLDC motor with hall rotor position sensor control system is considered in this research work.

To study the various control schemes of the motor drive, an accurate model of the BLDC motor which gives, the precise values of rotor speed, armature current, torque, and back-EMF is required. In this section, the modeling of BLDC motor and the overall motor drive systems are discussed theoretically and mathematically.

3.6.1. Mathematical Modeling of Brushless DC Motor

BLDC motor is considered as an electronic motor and requires a three phase inverter in the front end as shown in Figure 3.9. In self-control mode, the inverter acts like an electronic commutator that receives the switching logical pulse from the position sensors [56]. The drive is also known as an electronic commutated motor. The BLDC motor has three stator windings and a permanent magnet on the rotor [57]. Rotor induced currents can be neglected due to the high resistivity of both magnets and stainless steel. The following assumptions are made to simplify the overall BLDC motor mathematical equation.

- The three-phase system is balanced on the motor.
- Magnetic circuit saturation is ignored.
- Inverter semiconductor switches are ideal.
- Hysteresis and eddy current losses are eliminated.
- No damper winding is included.

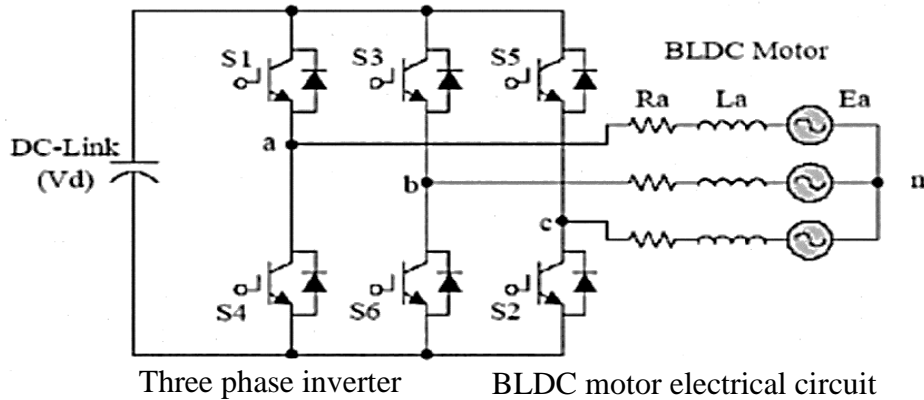


Figure 3.9 Stator connected three phase circuit diagram of BLDC motor winding [L5]

The circuit equations of the three windings in phase variables can be found in the literature [56] [58]. The per-phase circuit equations of the three phase windings are described by:

$$V_{as} = R_s i_a + L_a \frac{di_a}{dt} + L_{ab} \frac{di_b}{dt} + L_{ac} \frac{di_c}{dt} + e_a \quad (3.18)$$

$$V_{bs} = R_s i_b + L_b \frac{di_b}{dt} + L_{ba} \frac{di_a}{dt} + L_{bc} \frac{di_c}{dt} + e_b \quad (3.19)$$

$$V_{cs} = R_s i_c + L_c \frac{di_c}{dt} + L_{ca} \frac{di_a}{dt} + L_{cb} \frac{di_b}{dt} + e_c \quad (3.20)$$

It is assumed that resistances of all the windings are equal. It is also assumed that if there is no change in the rotor reluctance with angle because of no salient rotor and so that:

$$L_a = L_b = L_c = L \quad (3.21)$$

$$L_{ab} = L_{ba} = L_{ca} = L_{ac} = L_{bc} = L_{cb} = M \quad (3.22)$$

where R_s is the stator resistance per phase, L is the self-inductance per phase, and M is the mutual inductance per phase. The stator phase currents are considered to be balanced.

$$i_a + i_b + i_c = 0 \quad (3.23)$$

After rearranging Equation (3.23) and multiplying both sides by M gives:

$$Mi_b + Mi_c = -Mi_a \quad (3.24)$$

From Equations (3.18) and (3.22):

$$V_{as} = R_s i_a + L \frac{di_a}{dt} + M \frac{di_b}{dt} + M \frac{di_c}{dt} + e_a \quad (3.25)$$

$$V_{as} = R_s i_a + L \frac{di_a}{dt} + \frac{d}{dt}(Mi_b + Mi_c) + e_a \quad (3.26)$$

Substituting Equation (3.24) into (3.26) gives Equation (3.27):

$$V_{as} = R_s i_a + L \frac{di_a}{dt} + \frac{d}{dt}(-Mi_a) + e_a \quad (3.27)$$

The per-phase terminal voltage in terms of the motor armature parameters and back emf motor voltage is given by:

$$V_{as} = R_s i_a + (L - M) \frac{di_a}{dt} + e_a \quad (3.28)$$

The other phase voltage equations are obtained in a similar fashion:

$$V_{bs} = R_s i_b + (L - M) \frac{di_b}{dt} + e_b \quad (3.29)$$

$$V_{cs} = R_s i_c + (L - M) \frac{di_c}{dt} + e_c \quad (3.30)$$

Rearranging Equations (3.28), (3.29), and (3.30) gives the two phases of current differential equations as follows:

$$\frac{di_a}{dt} = \frac{V_{as}}{L - M} - \frac{R_s i_a}{L - M} - \frac{e_a}{L - M} \quad (3.31)$$

$$\frac{di_b}{dt} = \frac{V_{bs}}{L - M} - \frac{R_s i_b}{L - M} - \frac{e_b}{L - M} \quad (3.32)$$

$$\frac{di_c}{dt} = \frac{V_{cs}}{L - M} - \frac{R_s i_c}{L - M} - \frac{e_c}{L - M} \quad (3.33)$$

Equations (3.31), (3.32), and (3.33) can be represented in the form of a matrix as:

$$\frac{d}{dt} \begin{bmatrix} i_a \\ i_b \\ i_c \end{bmatrix} = \begin{bmatrix} -\frac{R_s}{L-M} & 0 & 0 \\ 0 & -\frac{R_s}{L-M} & 0 \\ 0 & 0 & -\frac{R_s}{L-M} \end{bmatrix} \begin{bmatrix} i_a \\ i_b \\ i_c \end{bmatrix} + \frac{1}{L-M} \begin{bmatrix} V_{as} \\ V_{bs} \\ V_{cs} \end{bmatrix} - \frac{1}{L-M} \begin{bmatrix} e_a \\ e_b \\ e_c \end{bmatrix} \quad (3.34)$$

The state space form is given by:

$$\frac{dx}{dt} = Ax + b(V - e) \quad (3.35)$$

where

$$A = \begin{bmatrix} -\frac{R_s}{L-M} & 0 & 0 \\ 0 & -\frac{R_s}{L-M} & 0 \\ 0 & 0 & -\frac{R_s}{L-M} \end{bmatrix}, V = \begin{bmatrix} V_{as} \\ V_{bs} \\ V_{cs} \end{bmatrix}, e = \begin{bmatrix} e_a \\ e_b \\ e_c \end{bmatrix}, b = \frac{1}{L-M} \quad (3.36)$$

3.6.1.1. Rotor Position Hall Sensors Modeling

Hall effect sensors provide the portion of information need to synchronize the motor excitation with rotor position in order to produce constant torque. They detect the change in the magnetic field. The rotor magnets are used as triggers for hall sensors [56] [57]. Three hall sensors placed 120° apart are mounted on the stator frame and used for sensing the rotor position. The output of the sensor signal is decoded to get the switching sequence of three phase inverter power semiconductor switches as shown in Table 3.7.

Table 3.7 Hall effect signals and inverter switches status of the BLDC motor [57] [58]

Electrical degree	Hall A	Hall B	Hall C	Inverter switch status					
				S ₁	S ₂	S ₃	S ₄	S ₅	S ₆
0-60	0	1	0	on	off	off	off	off	on
60-120	1	1	0	on	off	off	on	off	off
120-180	1	0	0	off	off	off	on	on	off
180-240	1	0	1	off	on	off	off	on	off
240-300	0	0	1	off	on	on	off	off	off
300-360	0	1	1	off	off	on	off	off	on

3.6.1.2. Modeling of Ideal Back-EMF

As mentioned before, it was assumed that back-EMF e_a , e_b , and e_c have trapezoidal wave from. The three-phase BLDC motor back-EMF can be described by the following equations:

$$\begin{bmatrix} e_a \\ e_b \\ e_c \end{bmatrix} = \omega_m \lambda_m \begin{bmatrix} f_{as}(\theta_r) \\ f_{bs}(\theta_r) \\ f_{cs}(\theta_r) \end{bmatrix} \quad (3.37)$$

Applying multiplication then the back-EMF voltages are as follows:

$$e_a = \omega_m \lambda_m f_{as}(\theta_r) \quad (3.38)$$

$$e_b = \omega_m \lambda_m f_{bs}(\theta_r) \quad (3.39)$$

$$e_c = \omega_m \lambda_m f_{cs}(\theta_r) \quad (3.40)$$

Hence the back-EMF voltages are a function of the electrical rotor angle θ_r , motor speed ω_m , and flux linkage λ_m . Each phase in the balanced three phase system is in phase with each other with a 120° phase shift. The rotor angle functions $f_{as}(\theta_r)$, $f_{bs}(\theta_r)$, and $f_{cs}(\theta_r)$ have the same shape as e_a , e_b , and e_c with a maximum magnitude of ± 1 . Equations (3.41), (3.42), and (3.43) show the mathematical functions of the rotor angle in a three phase system.

$$f_{as}(\theta_r) = \begin{cases} \frac{6}{\pi}\theta_r & 0 < \theta_r \leq \frac{\pi}{6} \\ 1 & \frac{\pi}{6} < \theta_r \leq \frac{5\pi}{6} \\ (-\frac{6}{\pi})\theta_r + 6 & \frac{5\pi}{6} < \theta_r \leq \frac{7\pi}{6} \\ -1 & \frac{7\pi}{6} < \theta_r \leq \frac{11\pi}{6} \\ (-\frac{6}{\pi})\theta_r - 1 & \frac{11\pi}{6} < \theta_r \leq 2\pi \end{cases} \quad (3.41)$$

Since in the balanced three phase system each rotor position sensor is separated by 120° , the rotor angle functions in phase-b and c are derived based on the function of the phase-a.

$$f_{bs}(\theta_r) = f_{as}(\theta_r + \frac{2\pi}{3}) \quad (3.42)$$

$$f_{cs}(\theta_r) = f_{as}(\theta_r - \frac{2\pi}{3}) \quad (3.43)$$

The back-EMF and the motor current are drawn along with the rotor position sensor signals as shown in Figure 3.10. The induced-EMFs do not have sharp corners because these are in trapezoidal nature in trapezoidal based BLDC motor drive.

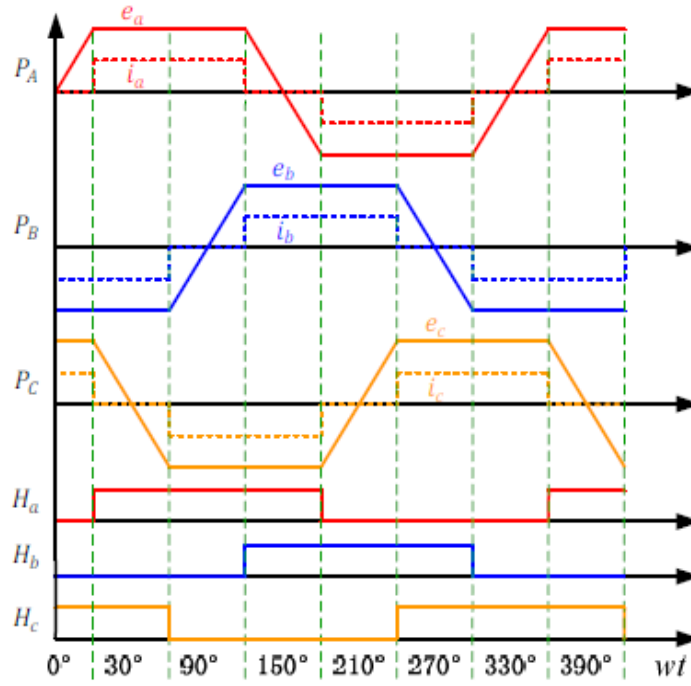


Figure 3.10 Back-EMF and rotor position hall sensor modeling [L5]

3.6.1.3. Dynamics Modeling of BLDC Motor

The electromagnetic torque for the three phase BLDC motor in Newton's is defined as:

$$T_e = \frac{P_{\text{rotor}}}{\omega_m} = \frac{i_a e_a + i_b e_b + i_c e_c}{\omega_m} \quad (3.44)$$

The moment of inertia is described by:

$$J = J_m + J_l \quad (3.45)$$

The equation of motion system with inertia J , friction coefficient B , and load torque T_l .

$$J \frac{d\omega_m}{dt} + B\omega_m = T_e - T_l \quad (3.46)$$

3.6.2. Modeling of Armature and Dynamics Transfer Functions of BLDCM

3.6.2.1. Armature Transfer Function

For the sake of easy reference, the armature model is derived in brief and given in the following equations [55] [59] [60]. During two phase conduction, the entire DC voltage is applied to the two phases having an impedance of:

$$Z = 2(R_s + \frac{d}{dt}(L - M)) = R_a + \frac{d}{dt}L_a \quad (3.47)$$

$$R_a = 2R_s \quad (3.48)$$

$$L_a = 2(L - M) \quad (3.49)$$

$$|Z| = \sqrt{R_a^2 + L_a^2} \quad (3.50)$$

The voltage equation for the stator is given by:

$$V_{is} = (R_a + \frac{d}{dt}L_a)I_{as} + E_{as} - E_{cs} \quad (3.51)$$

where the last two terms are the induced-EMFs in phase-a and phase-c, respectively. But the induced-EMFs in phase-a and phase-c are equal and opposite during the regular operation of the drive scheme and given as:

$$E_{as} = -E_{cs} = \lambda_m \Omega_m \quad (3.52)$$

where λ_m is the flux linkages per phase and Ω_m is the rotor speed. Substituting Equation (3.52) to Equation (3.51) gives the stator voltage equation as:

$$V_{is} = (R_a + \frac{d}{dt}L_a)I_{as} + 2\lambda_m \Omega_m \quad (3.53)$$

where the EMF constant for both the phases is combined into one constant as:

$$K_b = 2\lambda_m \text{ [V/rps]} \quad (3.54)$$

$$V_{is} = (R_a + \frac{d}{dt}L_a)I_{as} + K_b \Omega_m \quad (3.55)$$

$$\frac{I_{is}}{V_{is} - E_{is}} = \frac{1}{R_a + L_a s} \quad (3.56)$$

3.6.2.2. Motor Dynamics Transfer Function

Note that the electromagnetic torque for two phases combined is given by:

$$T_e = 2\lambda_m I_{as} \text{ Nm} \quad (3.57)$$

The machine contains an inner loop due to the induced-EMF. The inner current loop will cross this back-EMF loop creating complexity in the development of the model [59][60]. The interactions of these loops can be decoupled by suitably redrawing the block diagram. The load is assumed to be proportional to speed and is included in the feedback path [55].

$$T_l = B \Omega_m \quad (3.58)$$

The speed to air gap torque or dynamics transfer function can be evaluated as:

$$\frac{\Omega_m(s)}{T_e(s) - T_l(s)} = \frac{1}{B + Js} = \frac{1}{0.001 + 0.0089s} \quad (3.59)$$

where B is the friction coefficient of the motor and J is the inertia of the machine.

3.6.3. Modeling of Three Phase Inverter Transfer Function

The inverter is also represented as a first-order lag with a gain [55] as in Equation (3.60):

$$G_i(s) = \frac{V_{is}(s)}{V_c(s)} = \frac{K_i}{1 + T_i s} \quad (3.60)$$

where K_i is the gain and it is computed from inverter line to line voltage and the carrier voltage signal, T_i is the delay time of the inverter switches which is calculated as:

$$K_i = 0.65 \times \frac{V_{dc}}{V_{cm}} = 0.65 \times \frac{144v}{10v} = 9.36 \quad (3.61)$$

$$T_i = \frac{1}{2 \times f_c} = \frac{1}{2 \times 6000Hz} = 8.33 \times 10^{-5} \text{ sec} \quad (3.62)$$

Provided that, V_{dc} is the DC-link voltage input to the inverter, V_{cm} is the maximum control voltage, and f_c is the switching frequency of the inverter.

3.6.4. Modeling of Current Feedback Sensor Transfer Function

The noise signal generated by the current feedback sensor may not be small as compared to the motor current signal. In such a situation, it is necessary to design a low-pass filter in the input path of current sensing to improve measurement accuracy. In this work, a low-pass filter is used. The filter transfer function is given by:

$$G_f(s) = \frac{K_f}{1 + T_f s} = \frac{1}{1 + 0.0001s} \quad (3.63)$$

where K_f and T_f is the gain and the time constant of the filter and their parameter values are set to 1 and 0.0001sec, respectively.

3.6.5. Modeling of Speed Feedback Sensor Transfer Function

In general, the amplitude of the noise signal generated by the speed sensor is very small as compared to that of the motor speed. Since the vehicle itself works as a low-pass filter in this work, no filter is used in the speed feedback loop.

3.7. Cascade Control System for BLDCM Drive

In designing a vehicle control system, one major issue is to design a controller for stabilizing the speed of motor at the desired level under variable load and setpoint conditions. A fixed-parameter linear PID controller can perform satisfactorily as long as the vehicle is operating at a nominal operating point. However, it may have difficulty in maintaining the desired control performance when the operating point is shifted from one to another [61]. On the other hand, a nonlinear PID (NPID) controller gives very accurate results for speed control of BLDC motor. However, it may produce high current at starting [62] [63]. Therefore, to cope with these problems, designing a cascade controller incorporating the AI technique is

considered. Figure 3.11 shows the proposed cascade control system of the BLDC motor.

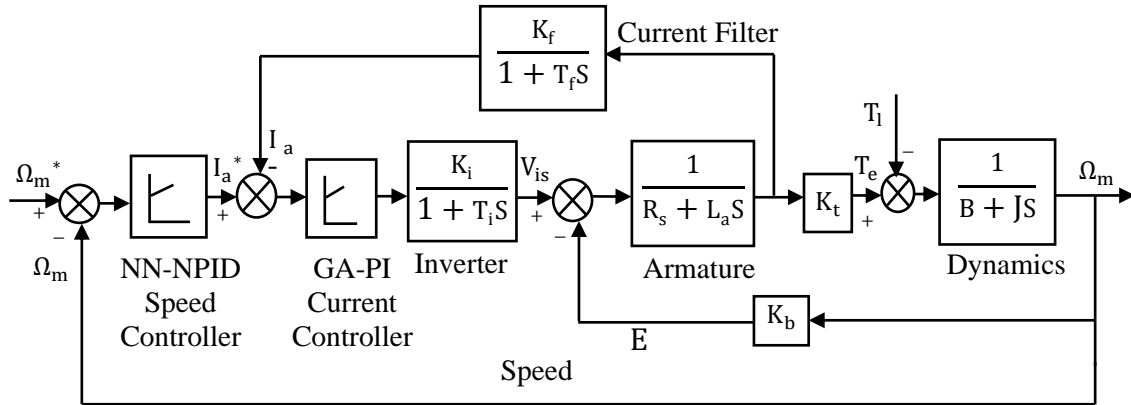


Figure 3.11 The proposed cascade control system block diagram of BLDC motor

3.7.1. Nonlinear PID Controller for BLDC Motor Speed Control

Although a fixed parameter PID controller is effective in an operating range, its performance may degrade and become unstable in some cases when it is out of the range. The integral term addresses how long and how far the output has been away from the setpoint and continuously sums up error e . Thus, even a small error, if it persists, will have a sum total that grows over time and the influence of the integral term will similarly grow. This problem can be solved to some extent by introducing a nonlinear PID (NPID) control structure.

Through the previous work [64], the authors proposed the structure of the NPID controller which consists of the linear PD-term and the nonlinear I-term employing a nonlinear gain in cascade with the integral action of a conventional PID controller. Figure 3.12 shows the closed loop control system with the NPID controller structure.

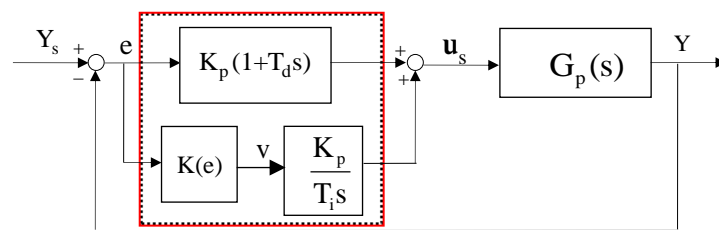


Figure 3.12 A NPID controller structure

$G_p(s)$ denotes the plant, Y_s , Y , and u_s are the setpoint, the plant controlled variable, and the control input, respectively and e is the error ($e = Y - Y_s$). The time domain equation of the NPID controller is given by:

$$u_s(t) = K_{ps}[e(t) + \frac{1}{T_{is}} \int V(t)dt + T_{ds} \frac{de(t)}{dt}] \quad (3.64)$$

$$= K_{ps}e(t) + K_{is} \int V(t)dt + K_{ds} \frac{de(t)}{dt}$$

where K_{ps} , T_{is} , and T_{ds} are the proportional gain, the integral time, and the derivative time respectively and $K_{is} = K_{ps}/T_{is}$ and $K_{ds} = K_{ps}T_{ds}$ are the integral gain, and the derivative gain of the speed controller, respectively [64]. The scaled error $V(t)$ in the integral term and the nonlinear gain $K(e)$ are given by in Equations (3.65) and (3.66) respectively.

$$V(t) = K(e) \times e(t) \quad (3.65)$$

$$K(e) = \exp\left(-\frac{e^2}{2\Delta Y_s^2}\right) \quad (3.66)$$

where ΔY_s is the speed setpoint change. An example of $K(e)$ is illustrated in Figure 3.13 with the typical values of $\Delta Y_s = 0.5, 1,$ and 1.5 . Its shape looks like the bell-shaped curve with a center 0. A small ΔY_s expects that e will be clustered around the center, whereas a large ΔY_s does that e will be spread out over a large range of values. It can be expected that about 99.7% of values of e will be within ± 3 times ΔY_s . It was demonstrated in [65] that the use of $K(e)$ in the integral loop can enhance the controller performance in terms of swiftness and closeness of the response without excessive control.

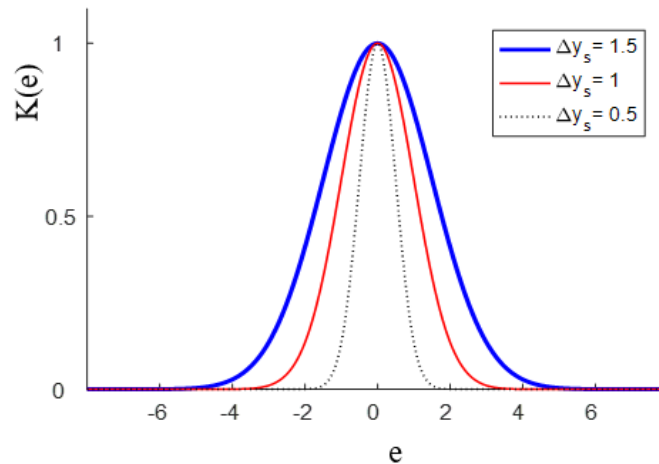


Figure 3.13 Shapes of $K(e)$ versus e for different ΔY_s

3.7.1.1. Implementation of Nonlinear Gain using Fuzzy Logic

In the previous section, a brief overview of the NPID controller was given. The nonlinear gain $K(e)$ was implemented by an exponential function. By the use of $K(e)$, when the error is large, the controller prepares for the occurrence of overshoot by scaling it down and when

the error is small, the controller reduces the steady state error by scaling to maintain its value. This section deals with implementing the nonlinear gain using fuzzy logic for the BLDC motor speed control system. Figure 3.14 depicts the implementation of nonlinear gain in the NPID controller using fuzzy logic.

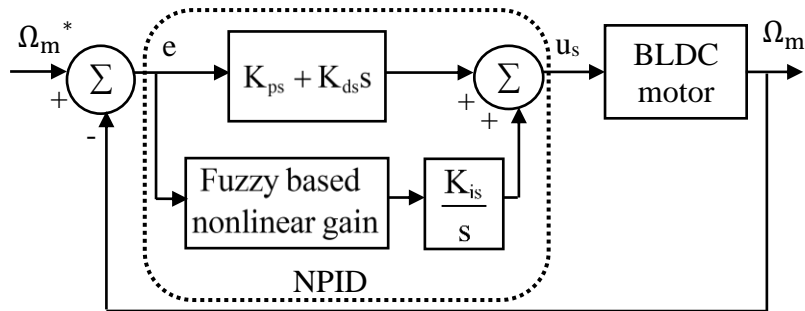


Figure 3.14 Implementation of nonlinear gain using fuzzy logic for NPID controller

Fuzzy logic is one of the types of artificial intelligence based techniques [66]. It works in three main steps: fuzzification, fuzzy inference with the knowledge base, and defuzzification which is shown in Figure 3.15. Fuzzification is the process of converting crisp sets into fuzzy sets. These sets are then mapped to output using fuzzy logic. This process is known as fuzzy inference [67]. There are two types of fuzzy inference systems that can be implemented in the fuzzy logic: Mamdani-type and Sugeno-type. These two types of inference systems differ in the way outputs are determined.

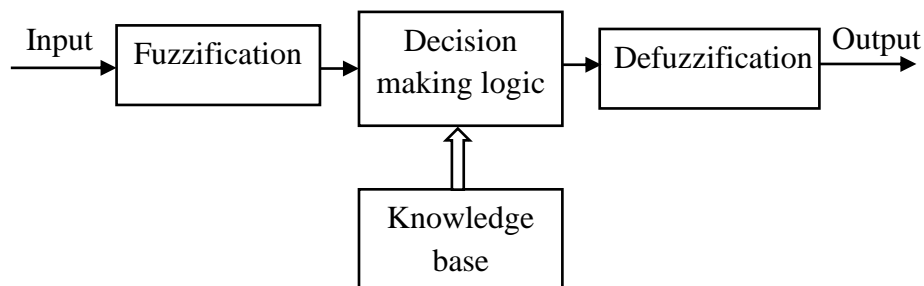


Figure 3.15 Fuzzy logic structure block diagram

For the actual system to use the output, the fuzzy logic must convert its internal fuzzy output variables into crisp values. This conversion process is called defuzzification [68]. In this study, Sugeno-type is considered for the design of the nonlinear gain. The integral gain is nonlinearly adjusted depending on the size of e using fuzzy logic. That is, it is decreased to prepare for the occurrence of overshoot when e grows and enlarged to reduce the steady-state error when e shrinks. Where, C_1 is user-defined positive constant, and N, Z, and P are fuzzy sets with the following membership function forms.

Figure 3.16 depicts the shapes of the membership functions of the fuzzy logic model. In this figure N, Z, and P are representing negative, zero, and positive respectively. The following codes are the if then rules of fuzzy logic input-output mapping of the nonlinear gain.

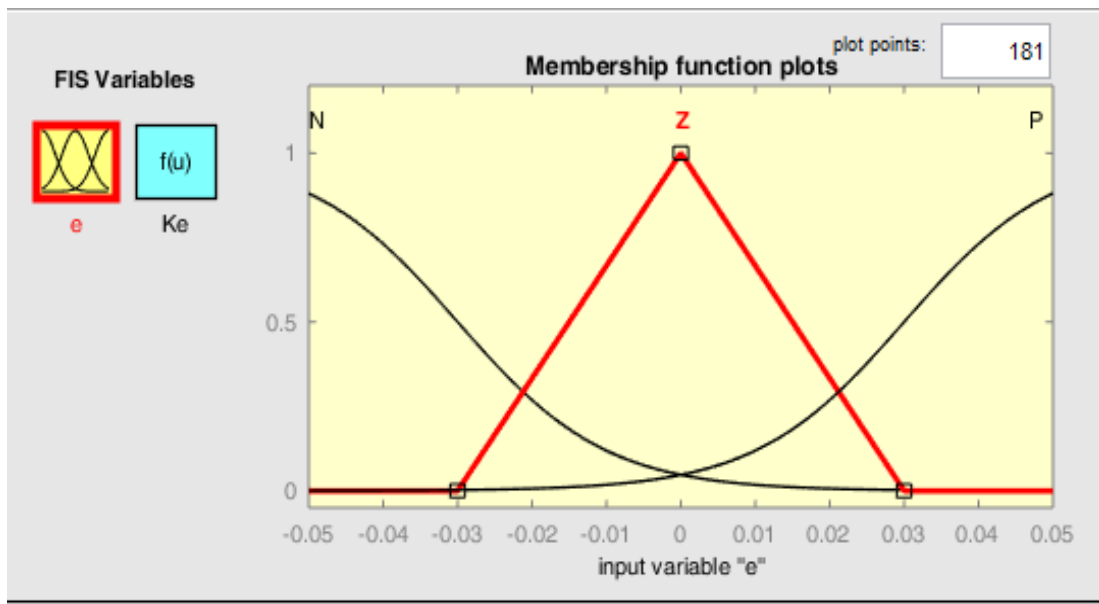


Figure 3.16 The input membership function of the fuzzy logic

- If e is N then K(e) is C_1
- If e is Z then K(e) is 1
- If e is P then K(e) is C_1

where C_1 is a positive constant determined by a user and it must be between 0 and 1. Figure 3.18 shows the shape of $K(e)$ in the typical values of C_1 . $K(e)$ converges to the value C_1 when $e = \pm \infty$ and to the value of 1 when $e = 0$. The final inferred output for $K(e)$ is the weighted average of the three rule outputs based on the Takagi Sugeno method.

$$K(e) = \frac{\sum_{j=1}^3 \alpha_j K^j(e)}{\sum_{j=1}^3 \alpha_j} = \frac{\alpha_1 C_1 + \alpha_2 + \alpha_3 C_1}{\alpha_1 + \alpha_2 + \alpha_3} \quad (3.67)$$

where α_j is the value when the nonlinear gain $K(e)$ curve converges to C_1 and one. Its values are $-e/3(\Delta Y_s)$, 0, and $e/3(\Delta Y_s)$. The rule view of the fuzzy model is shown in Figure 3.17. As an example when the input e is 0.000305 the output of $K(e)$ is about 0.988.

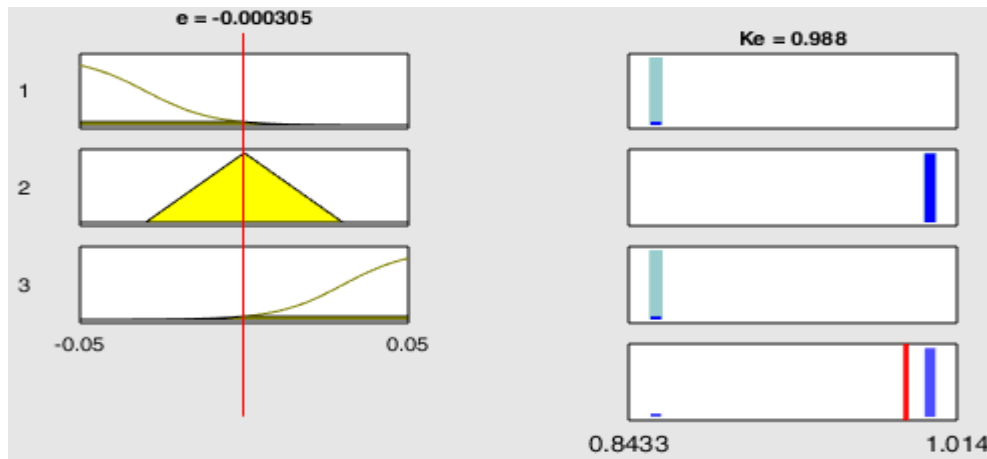


Figure 3.17 The fuzzy logic system rule view

The output of the designed fuzzy logic system in three and two dimensional views are shown in Figure 3.18. Its result is a nonlinear exponential graph.

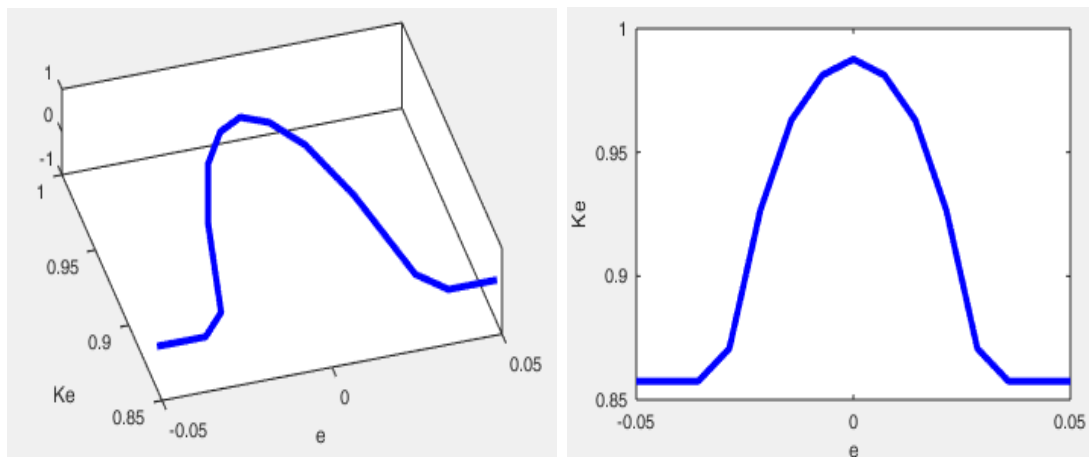


Figure 3.18 The surface view of the output in three 3D (left) and 2D (right)

The fuzzy logic based nonlinear gain $K(e)$ result is multiplied with speed error at every sampling time to optimize the linear gain of an integral controller in the specified operating range. Figure 3.19 depicts the Simulink implementation of the nonlinear gain $K(e)$.

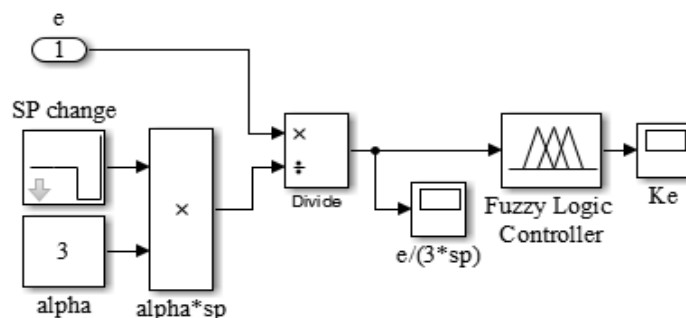


Figure 3.19 MATLAB/Simulink implementation of the nonlinear gain

Hence, practically the fuzzy model should be converted to user defined programming. The MATLAB code using math function to implement the nonlinear gain based on the fuzzy logic system used in this research work is shown in Appendix (D).

3.7.2. PI Controller for BLDC Motor Current Control

Usually in BLDC motor, the starting current is high, which may lead to heating in the motor stator windings and burning of the control circuitry. This problem can be solved by designing an appropriate current regulator in cascaded with the speed controller. The current controller then adjusts the stator current to maintain at the desired internal current level. The reference current is generated from the speed controller output signal. In this work, a linear PI current controller is considered to reduce the complexity in the cascade control system. Due to the application of low pass filter the derivative controller is not required. The controller time domain equation is given by:

$$u_c(t) = K_{pc}[e(t) + \frac{1}{T_{ic}} \int e(t)dt] \quad (3.68)$$

where K_{pc} and T_{ic} are the proportional gain and the integral time respectively and $K_{ic} = K_{pc}/T_{ic}$ is the integral gain of the current controller.

3.7.3. Implementation of BLDCM Cascade Control System using GA

The NPID controller has no specific tuning mechanism like the PID controller has Ziegler Nicholas. The only tuning mechanisms are either GA or particle swarm optimization (PSO). In this study, GA is considered to have an optimal linear and nonlinear gains because GA is easy to use and understand, and has almost similar characteristics with that of the PSO.

GA is a particular class of evolutionary algorithms that use techniques inspired by evolutionary biologies such as inheritance, mutation, selection, and crossover (also called recombination) [69]. Evolution usually starts from a population of randomly generated individuals and happens in generations. In each generation, the fitness of every individual in the population is evaluated, multiple individuals are selected from the current population (based on their fitness), and modified (recombined and possibly mutated) to form a new population [70]. The new population is then used in the next iteration of the algorithm. Traditionally, solutions are represented in binary as strings of 0s and 1s. Commonly, the algorithm terminates when either a maximum number of generations has been produced, or a satisfactory fitness level has been reached for the population [69] [70]. If the algorithm has terminated due to the maximum number of generations, a satisfactory solution may or may

not have been reached. The general stapes of GA optimization as the form of a flow chart is shown in Figure 3.20.

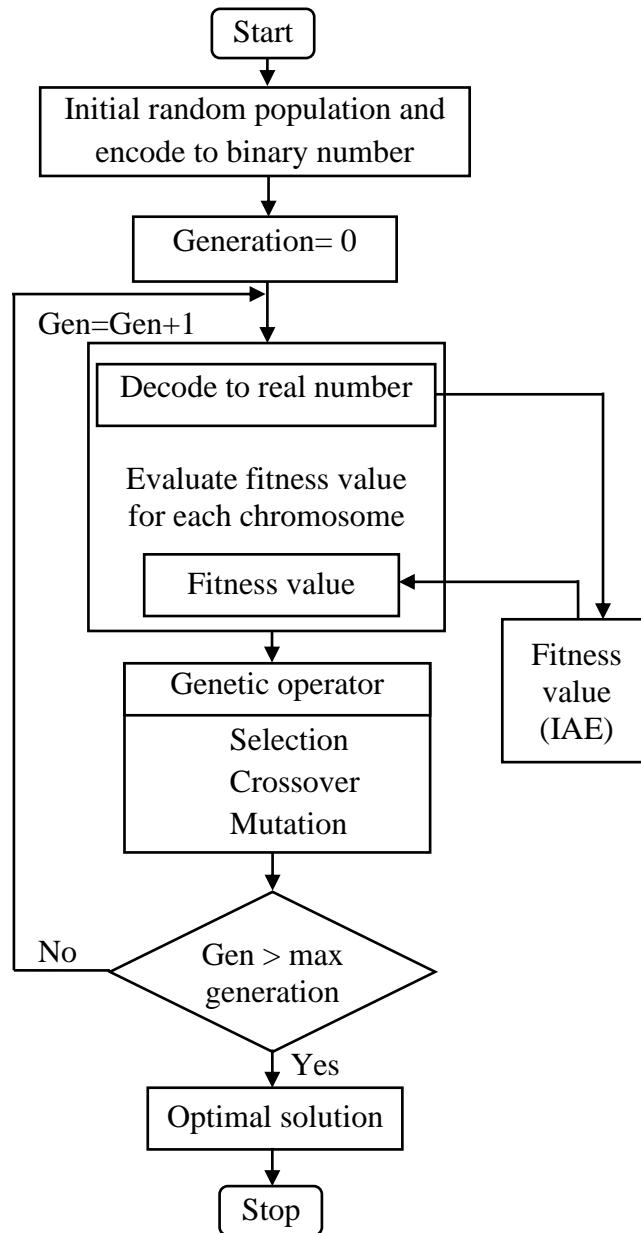


Figure 3.20 Flow chat of genetic algorithm optimization

The complete response of the system for each NPID and PI control parameter values and initial fitness value of integral absolute error (IAE) are computed and optimized using GA [64]. This process will be repeated every generation until the end of the generations where the best fitness value is achieved [71].

The ultimate aim of GA is to seek global NPID speed control values (K_{ps} , K_{is} , K_{ds} , and the fuzzy constant C_1) and PI current control values (K_{pc} , K_{ic}) with minimum fitness value to operate the BLDC motor cascade control system in the entire range. The block diagram

shown in Figure 3.21 depicts the implementation of GA optimization for the cascade control system of the BLDC motor.

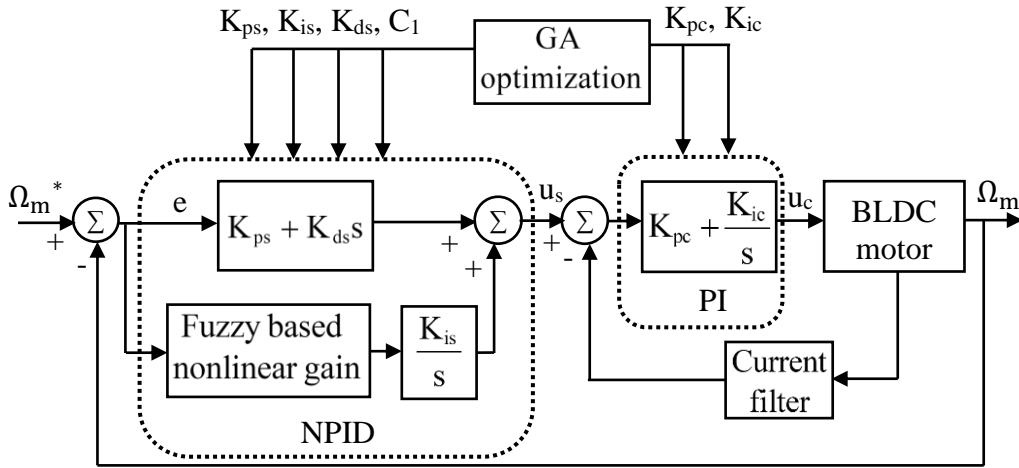


Figure 3.21 Block diagram of GA implementation in cascade control of BLDC motor

The GA is implemented in MATLAB programming. So, each subsystem transfer functions in the cascade control system are converted into an ordinary time domain differential equations. These equations are coded in MATLAB/script programming. As an example, the three phase inverter model is expressed as the form of input/output transfer function as shown in Equation (3.69).

$$G_i(s) = \frac{V_{is}(s)}{V_c(s)} = \frac{K_i}{1 + T_i s} = \frac{Y(s)}{U(s)} \quad (3.69)$$

By rearranging the terms in Equation (3.69) the simplified equation in the frequency domain of the three phase inverter is determined as follows:

$$sY(s) = \frac{-Y(s)}{T_i} + \frac{K_i \times U(s)}{T_i} \quad (3.70)$$

Conversion of the frequency domain into time domain of Equation (3.70) using inverse Laplace transformation is computed as follows:

$$\frac{dy(t)}{dt} = \frac{-y(t)}{T_i} + \frac{K_i \times u(t)}{T_i} \quad (3.71)$$

The general expression of the time domain state space equation in the form of state variables is shown in Equation (3.72).

$$\dot{x} = \frac{-x(t)}{T_i} + \frac{K_i \times u(t)}{T_i} \quad (3.72)$$

Using the built-in function, Equation (3.72) is converted into an m-file by assigning \dot{x} as the inverter output, x as the state variable, u as the inverter input, and t as the operating time.

```

function xdot= Inverter(t,x,u)
Kr= 9.36; Tr= 8.333e-5;
xdot=-x/Tr+Kr*u/Tr;

```

By following the same procedure of the inverter time domain analysis, other subsystems in the cascade control system of BLDC motor are converted into the time domain. The converted time domain functions are coded in MATLAB/script as shown in Appendix (B).

The time domain differential equation computations in the cascade control system are solved by Rang Kutta (RK4) 4th order method by setting the sampling time to 0.0001sec. RK4 function method is developed as a built-in function in MATLAB and it can be called easily by setting the appropriate input/output variables. The following code is an example of RK4 computing the output of inverter time domain function in the cascade control system.

```
xi= RK4(@Inverter,t,xi,ui_sat,h);
```

where xi is the updated output of the inverter function at every sampling time, ui_sat is the input of the inverter function, h is the sampling time, and t is the total operating time. The NPID controller programming is also developed in MATLAB as shown in the sample code.

```

function u= NPID(r,y,h,gains,dr,iv)
persistent ee, z;
ee= r-y;
% Retrieves the parameters of the NPID controller
Kp = gains(1); Ki = gains(2); Kd = gains(3);
e = r-y; % Error signal
up = Kp*e; % The proportional control implementation
fe = exp(-0.5*(e/deltar)^2)*e; %The nonlinear gain implementation
z = z+Ki*0.5*h*(fe+fee); % The integral control implementation
fee = fe;
ui = z;
ud = Kd*(e-ee)/h; % The derivative control implementation
u = up+ui+ud; % Returns the control input

```

The detail of NPID speed and PI current cascade controller of BLDC motor MATLAB/script programming code is shown in Appendix (B).

3.7.3.1. Parameter Tuning of Cascade NPID and PI Controller

The NPID and PI cascade controller has six tuning parameters: K_{ps} , K_{is} , K_{ds} , C_1 , K_{pc} , and K_{ic} . The details of GA optimization parameters used in the simulation including the maximum generation, population, and parameter boundary are shown below in Table 3.8.

Table 3.8 Parameter settings of the genetic algorithm optimization

Parameter	Type and value
Maximum generations	30
Population size	30
Encoding	Binary
Selection	Uniform
Crossover	Single point crossover
Mutation	Uniform
No of parameters	6
Lower boundary	[0 0 0 0 0 0]
Upper boundary	[30 10 1 1 10 10]

The graphical result of the optimized object function (IAE) parameter of the cascade control system is shown below in Figure 3.22. Its value after many times re-optimization is 3.1303.

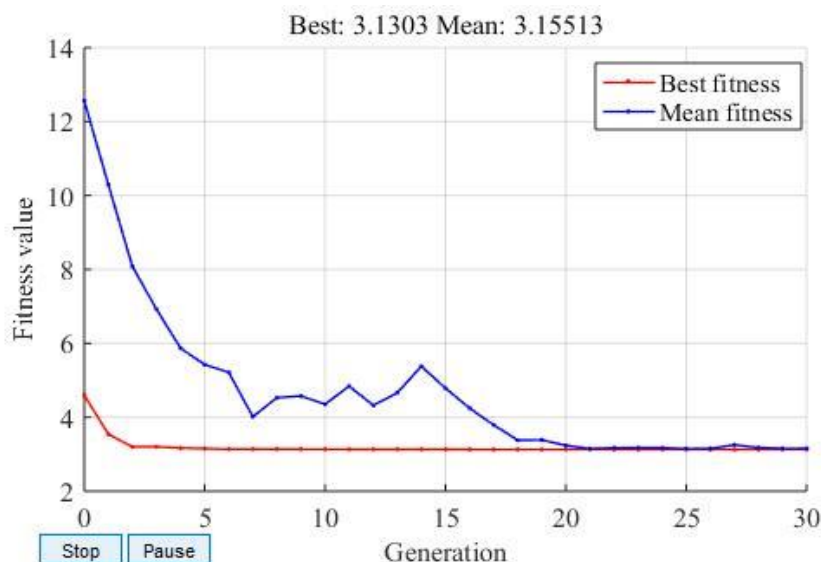


Figure 3.22 Fitness values vs generation for object function

The model of the cascade control system of BLDC motor NPID and PI controller is performed in GA optimization. The parameters of the NPID speed (K_{ps} , K_{is} , K_{ds} , and C_1) and PI current (K_{pc} , K_{ic}) controllers based on GA are obtained as shown in Table 3.9.

Table 3.9 The GA optimized parameters of the cascade NPID and PI controllers

Controllers	Optimized parameters	Optimized results
NPID speed controller	K_{ps}	23.8933
	K_{is}	1.4326
	K_{ds}	0.0237
	C_1	0.8575
PI current controller	K_{pc}	4.3912
	K_{ic}	0.4587

Then the system is simulated at different speed ranges based on the motor rated speed as shown in Figure 3.23. The GA based NPID speed controller result of the brushless DC motor is zoomed out at a simulation time of 0.5sec and a speed of 1500rpm. The result shows that the speed overshoot is about 0% and the settling time is about 0.03sec, this shows that the controller has good speed dynamic performance.

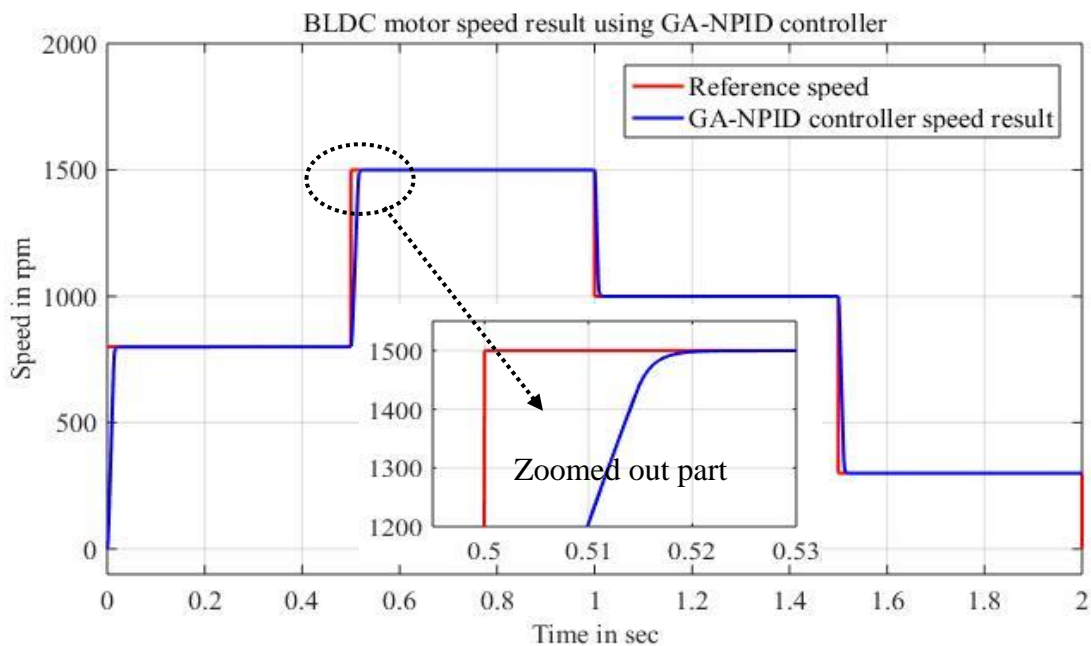


Figure 3.23 GA based NPID speed controller result of BLDC motor

In the cascade control system, the current controller has the setpoint from the speed controller output. The speed controller output has a limiter between ± 77 because the rated current of the motor is 77A. Based on steady state values (i.e. when the Laplace term $s=0$) the current controller limiter is designed at the value of ± 28 for rated speed of the motor. The GA-PI controller of BLDC motor output current result is shown below in Figure 3.24.

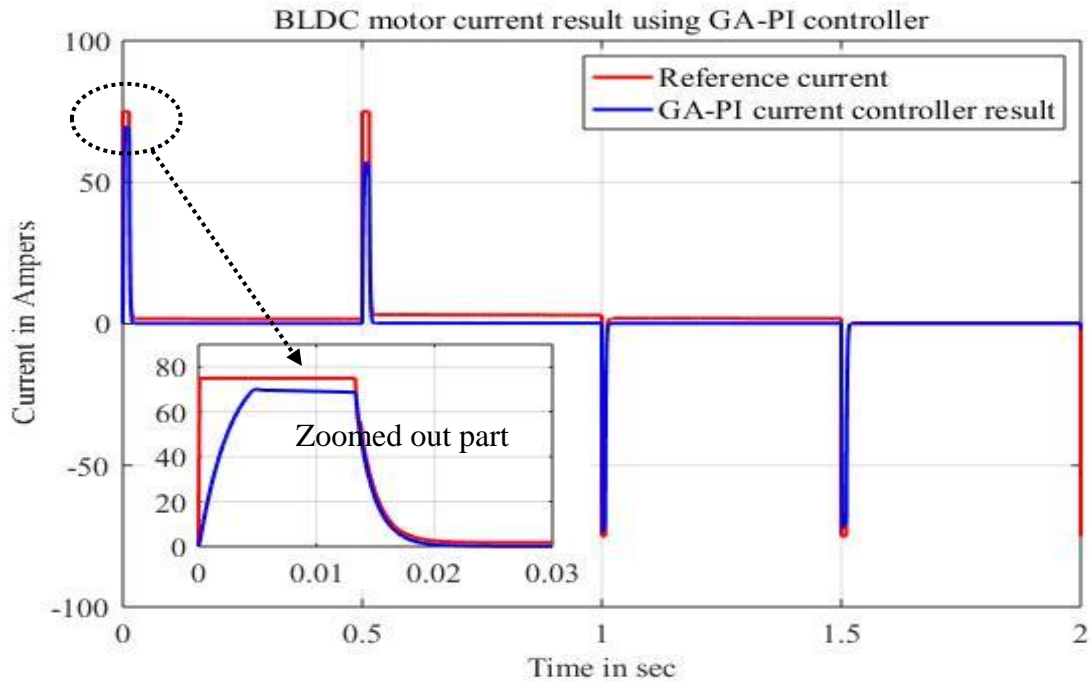


Figure 3.24 GA based PI current controller result of BLDC motor

The GA based PI current controller result of the BLDC motor is zoomed out at a simulation time of 0sec and a current of 75A. GA based cascade control system of BLDC motor has good speed dynamic response and current overshoot minimization under a constant load. But due to the effect of road types, carrying capacities, and other factors every time the vehicle has variable load conditions. In this case, the motor speed is affected and sometimes it cannot follow the desired speed. To reduce this effect to some extent, the system should integrate neural network (NN) based auto-tuning technique in the speed regulator side.

3.7.4. NN-NPID Speed and GA-PI Current Cascade Control of BLDCM

Figure 3.25 depicts the proposed cascade control system of the BLDC motor. The NPID speed controller is tuned online using neural networks and the fuzzy-based nonlinear gain and the PI current controller gains are optimized using a genetic algorithm. In this study, in order to train and validate the NN, several measured of the NPID speed controller gains were used to train the networks. The present work applies a feed forward back propagation NN in four layers. The input, two hidden and output layers have 3, (6, 4), and 1 neuron, respectively as shown in Figure 3.26.

The number of neurons in the hidden layer is a very important part of network architecture. The hidden layer does not directly interact with the external environment [72]. This layer has a significant effect on the final output and the number of neurons in this layer must be

selected very carefully. Using too few and too many neurons in the hidden layers will result in underfitting and overfitting problems respectively. The problem of underfitting is the signal, especially in a complicated system, cannot be detected sufficiently. Overfitting can result in several problems because the limited amount of information contained in the training set is not enough to train all of the neurons in the hidden layers. It causes an increase in training time [73] [74].

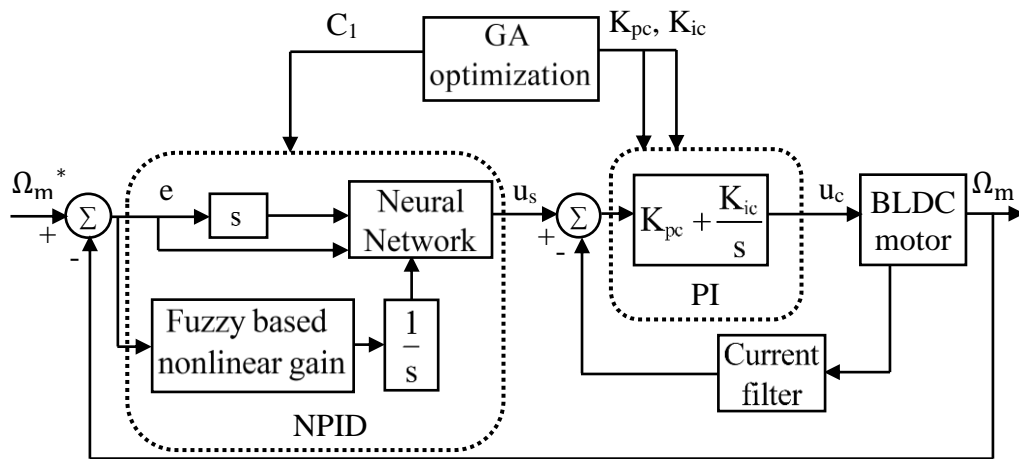


Figure 3.25 The proposed cascade control system

The selection of NN architecture is done by trial and error using a forward selection method to find the optimum network architecture. To design and establish the network behavior a sigmoid function is used as an activation function. A sigmoid transfer function can introduce nonlinearity in the model and/or to make sure that certain signals remain within a specified range. Figure 3.26 shows the final neural network structure used in this work.

The procedure to create and train a network using the toolbox is as follows [75] [76]:

1. Inputs (error, derivative of the error, and nonlinear based integral of the error) and target vectors are generated and loaded to the workspace in MATLAB.
2. A four layer feed forward back propagation network created in the MATLAB/script
3. Trainlim and Tansig were chosen as training and transfer function, respectively.
4. Input and target vectors were introduced to the created network.
5. Training parameters such as the epochs and error goal were adjusted.
6. The specified network was trained gradually. This process is finished when the defined error was reached. During the training, weights and biases of the network were iteratively adjusted to minimize the network performance function.
7. Finally, after training the network, the Simulink block is generated.

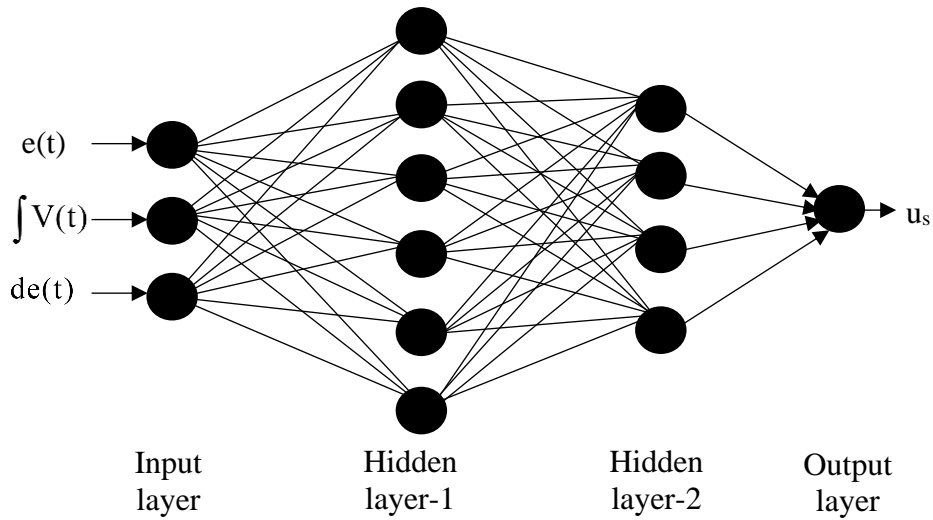


Figure 3.26 Neural network structure used in this thesis

where the idea of u_s (control signal) is taken from Equations (3.64) and (3.65) of the NPID control system structure time domain analysis.

Figure 3.27 depicts the flowchart of the neural network training of the proposed neural network structure in the speed control system of the BLDC motor.

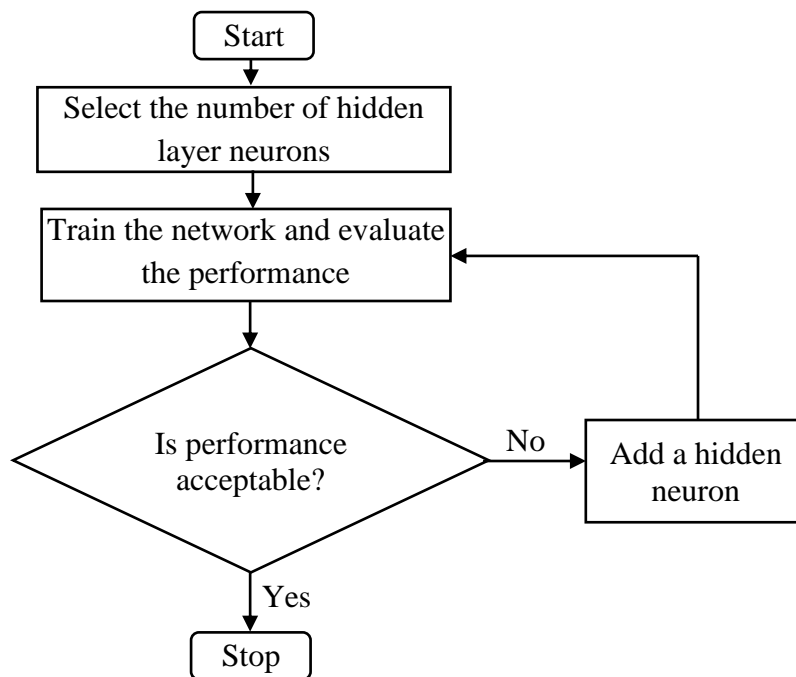


Figure 3.27 Flow chart of the neural network training

The input and output data are generated from the GA optimization based result Simulink implementation as shown in Figure 3.28. After the simulation time is completed, the data are transferred from Simulink to the workspace in the form of vectors.

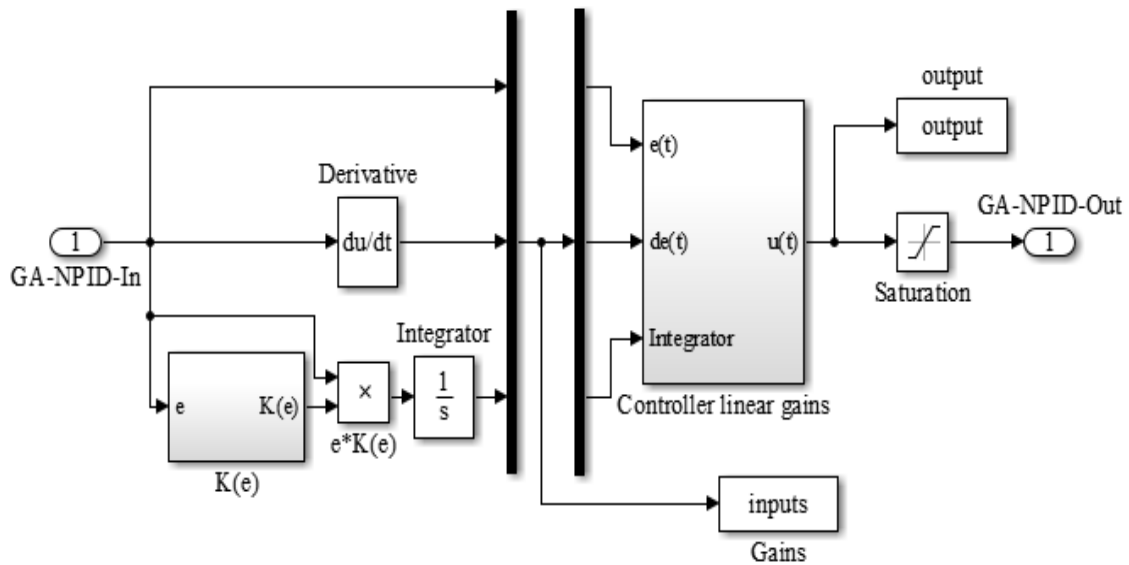


Figure 3.28 Generating the input and output data from the GA-based control system

Below the MATLAB/code is the sample code for the neural network used in this thesis. The Levenberg-Marquardt backpropagation is used to train the network and Tansig is the default transfer (activation) function of the network. The network has three input parameters and one output parameter as described above. Each input and one output have 5000 data. After several trainings of the network based on trial and error, the number of hidden layers and their neurons are selected based on the performance evaluation toolbox results.

```

x = inputs'; % inputs - input data.
y = output'; % output - target data.
% 'trainlm' is usually the fastest.
% Levenberg-Marquardt backpropagation.
trainFcn = 'trainlm';
% Create a fitting network
hiddenLayerSize = [6 4];
net = fitnet(hiddenLayerSize,trainFcn);
% Setup division of data for training, validation, testing
net.divideParam.trainRatio = 80/100;
net.divideParam.valRatio = 10/100;
net.divideParam.testRatio = 10/100;
net.trainParam.epochs= 1000;
% Train the network
[net,tr] = train(net,x,y);

```

```

% Test the network
y = net(x);
e = gsubtract(x,y);
performance = perform(net,x,y)
%To generate the NN on Simulink block
gensim(net)

```

After executing the above code, several performance measurements of the trained network are available. The Figure 3.29 depicts the validation of the mean squared error and its value. At the training epoch of 1000 the mean squared error is 0.0013407.

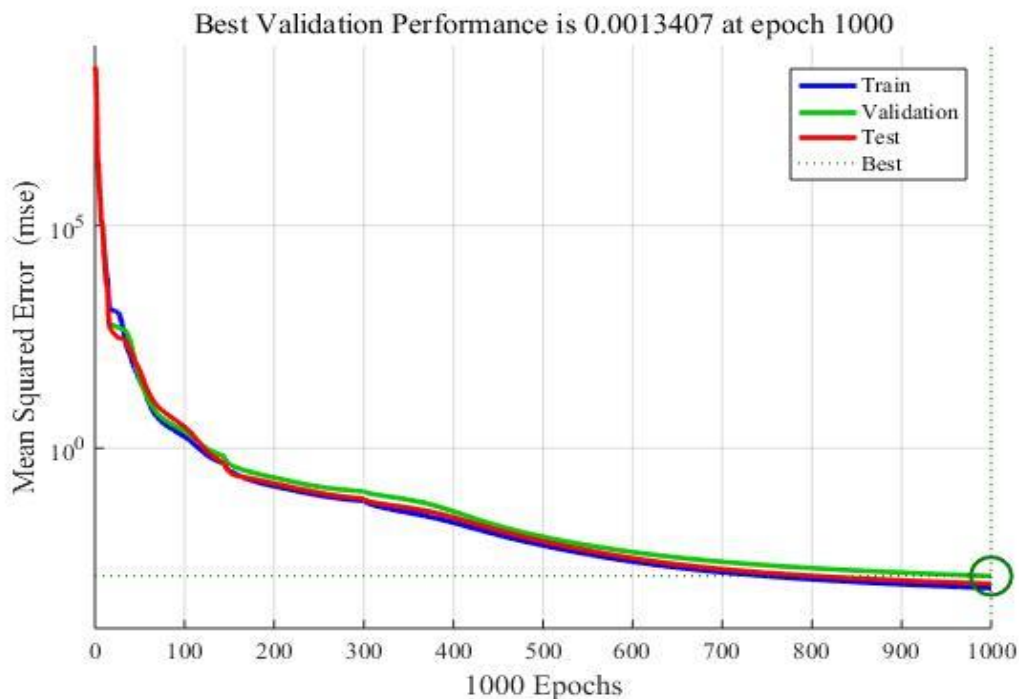


Figure 3.29 Validation of the mean squared error

The regression plots also display the network outputs with respect to targets for training, validation, and test sets as shown below in Figure 3.30. For a perfect fit, the data should fall along a 45-degree line, where the network outputs are equal to the targets. In this work, the neural network has been retrained many times to have the perfect fit for its output and target. This is done by changing the hidden layers and their neurons. This change updates every time the weights and biases of the network, and it produce an improved network after retraining. For this work, the fit is perfect for all data sets, with R values in each case is 1.

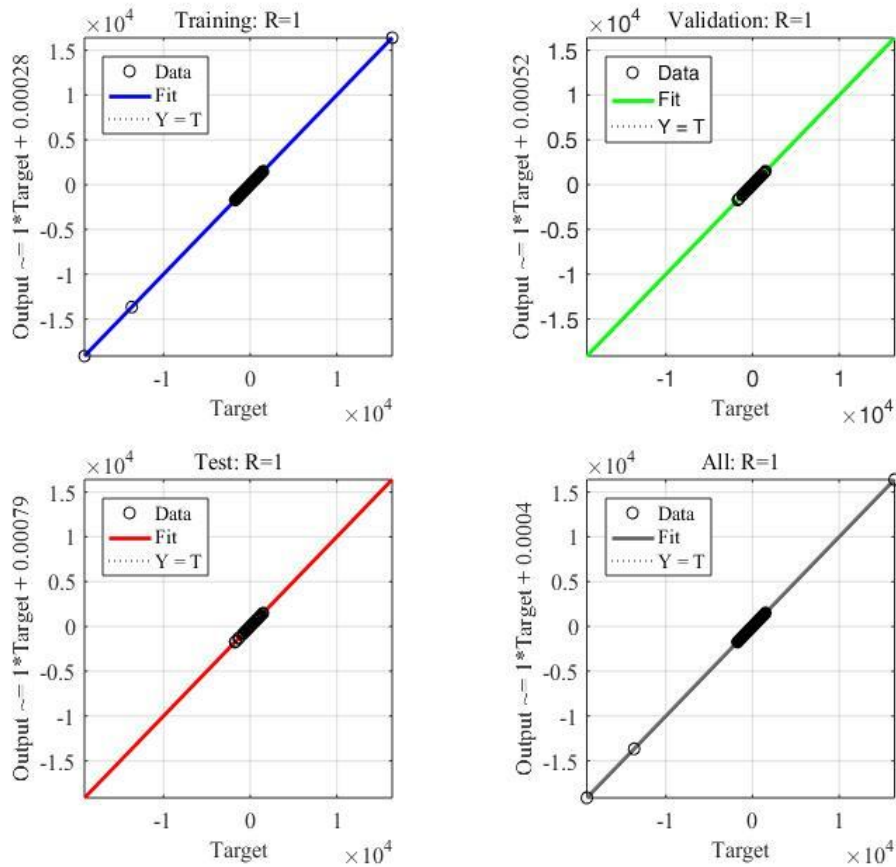


Figure 3.30 Regression plots of the training, validation, and test sets

After training of the network, the following Simulink block in Figure 3.31 is generated. It includes the input and output of trained data, the structure of the network, the weights, and the biases of each layer and neurons.

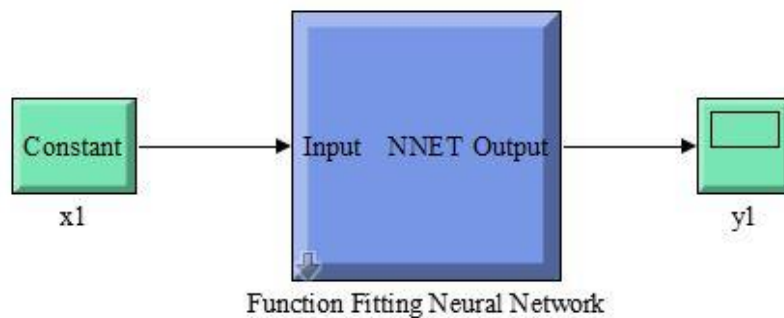


Figure 3.31 The Simulink block of the trained neural network structure

Figure 3.32 demonstrates the proposed speed control system of the BLDC motor in the cascade control system. The diagram consists of GA tuned fuzzy logic based nonlinear gain for integral control, and the neural network based proportional, integral, and derivative gains for the NPID speed controller of BLDC motor.

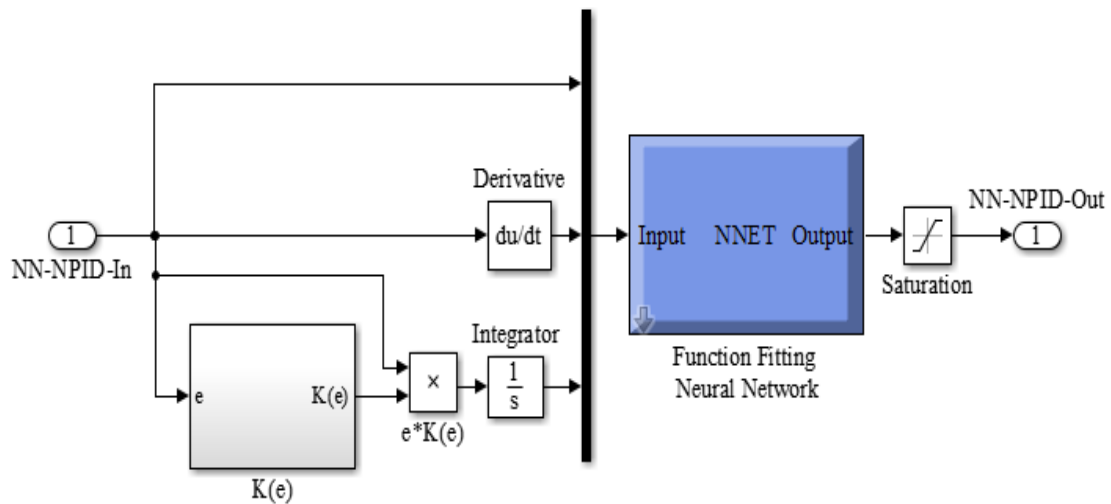


Figure 3.32 Neural network based NPID speed control system of the BLDC motor

Below Figure 3.33 shows the result of the proposed NN-NPID speed controller of the BLDC motor. The system is simulated based on the linear and nonlinear Simulink model of the BLDC motor drive. The result shows that the speed overshoot is about 0% and the settling time is about 0.0275sec, this shows that the controller has better speed dynamic performance parameters than the GA-NPID speed controller.

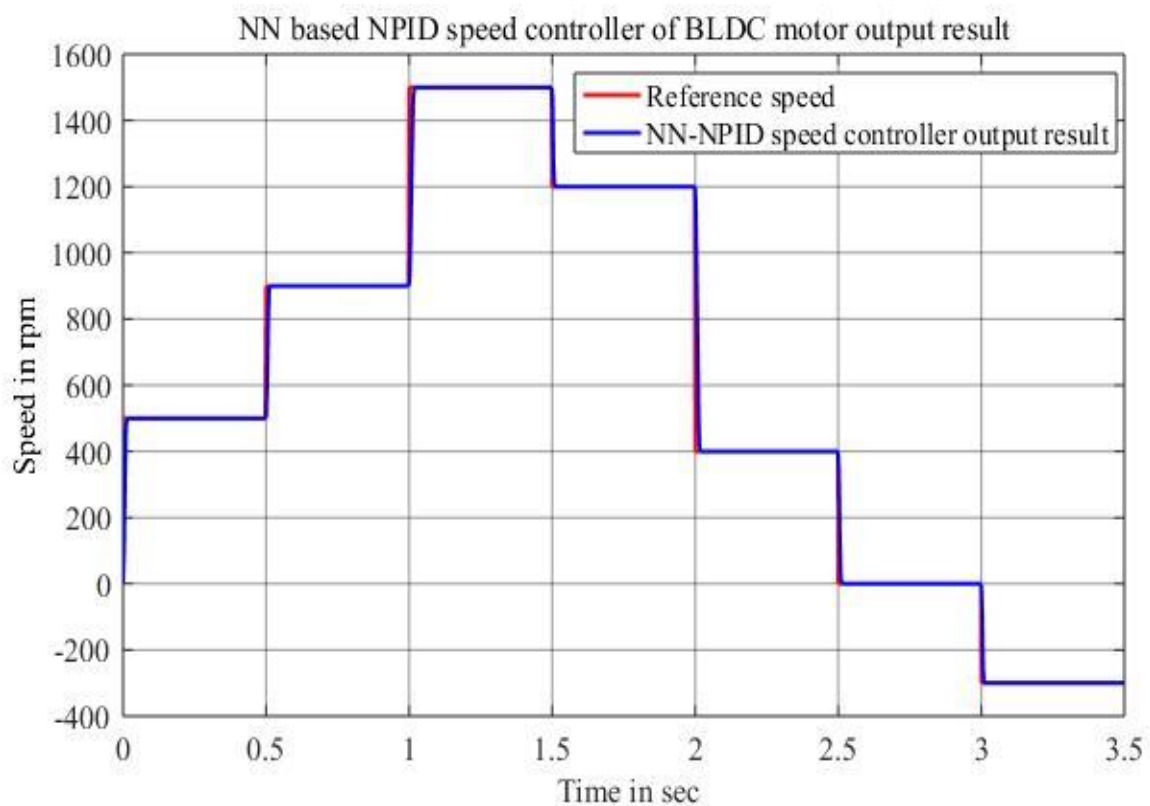


Figure 3.33 NN based NPID speed controller of the BLDC motor output result

3.7.5. ZN Based PID Speed and PI Current Controllers of BLDCM

Ziegler Nicholas (ZN) PID tuning is frequently used in the industrial process control systems. In this thesis also Ziegler Nicholas based linear PID controller is implemented for performance comparison purposes.

3.7.5.1. Tuning of PID Controller Using ZN Based Relay Control

Astrom and Haggglund's method determines the ultimate point using a relay test signal as the system input [77] [78]. The test signal is automatically produced as described in Figure 3.34. The method is based on the fact that system with a phase lag of at least π at high frequencies can oscillate under the ultimate period T_u .

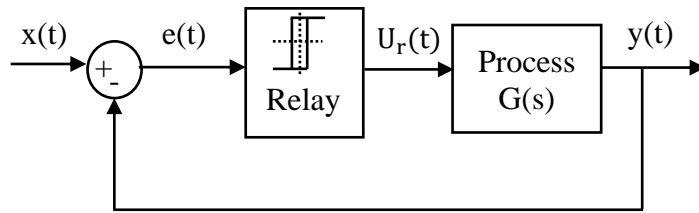


Figure 3.34 Block diagram for ultimate point estimation

The square signal of the relay output is represented by a Fourier series as in Equation (3.73):

$$u_r(t) = \frac{4d}{\pi} \sin(\omega t) + \frac{4d}{3\pi} \sin(3\omega t) + \frac{4d}{5\pi} \sin(5\omega t) + \dots \quad (3.73)$$

By neglecting higher frequencies terms:

$$u_r(t) \approx \frac{4d}{\pi} \sin(\omega t) \quad (3.74)$$

where d and a are the amplitude of the relay square wave and output signal of the process. Neglecting higher frequencies is possible since most physical systems act as low pass filters. The transfer function of the relay for a sine wave input with amplitude a is given by:

$$N(a) = \frac{4d}{\pi a} \quad (3.75)$$

The system will show continuous cycling when the following condition is satisfied.

$$1 + N(a) \times G(i\omega_u) = 0 \quad (3.76)$$

Placing Equation (3.75) into Equation (3.76) will result in:

$$G(i\omega_u) = -\frac{1}{N(a)} = -\frac{\pi a}{4d} \quad (3.77)$$

Note that the imaginary part of $G(i\omega_u)$ is zero. So, the frequency is the ultimate frequency of the process and the ultimate gain is $1/G(i\omega_u)$.

$$\omega_u = \frac{2\pi}{T_u}; K_u = \frac{4d}{\pi a} \quad (3.78)$$

Once the ultimate frequency and gain have been estimated, a PID controller can be tuned using ZN closed loop tuning rules. Table 3.10 provides the tuning parameters for the given ultimate gain and period of the process.

Table 3.10 ZN-PID parameters according to the ultimate point

Controller	K_p	T_i	T_d
P	$0.5K_u$	-	-
PI	$0.45K_u$	$T_u/1.2$	-
PID	$0.6K_u$	$T_u/2$	$T_u/8$

3.7.5.2. Design of PI Current Controller of BLDCM using ZN Tuning

Applying the feedback calculation on the motor dynamics and moving the back-EMF constant to the left of the torque constant block. Then the reduced block of the motor dynamics along with armature transfer function is shown in Figure 3.35.

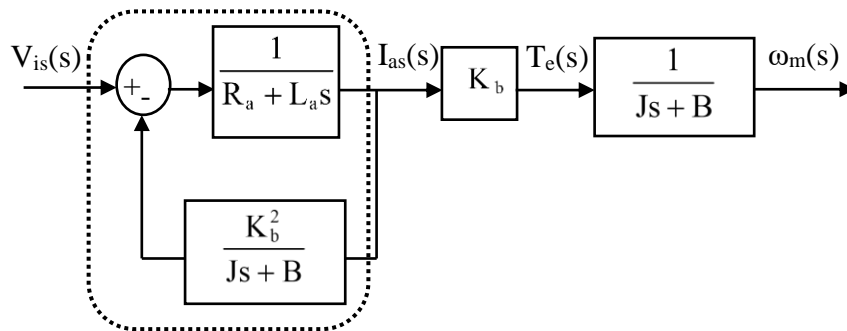


Figure 3.35 Reduced block diagram of the internal loop of the main block diagram

Considering the armature transfer function and its feedback block diagram, the internal current controller of the BLDC motor block diagram is developed as shown in Figure 3.36.

The PI controller gains are determined by applying and replacing with a relay current controller. The system is implemented in MATLAB/Simulink as shown in Figure 3.37. The setpoint of the relay current controller is set as zero and the relay current controller parameters are adjusted to have a sinusoidal output current signal.

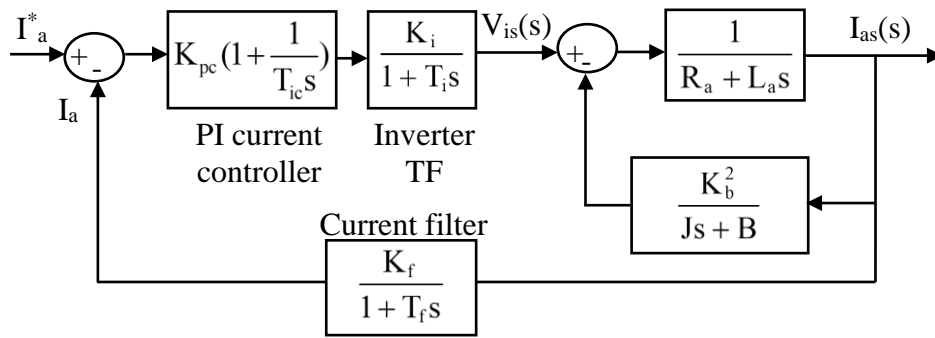


Figure 3.36 Internal current controller of the BLDC motor block diagram

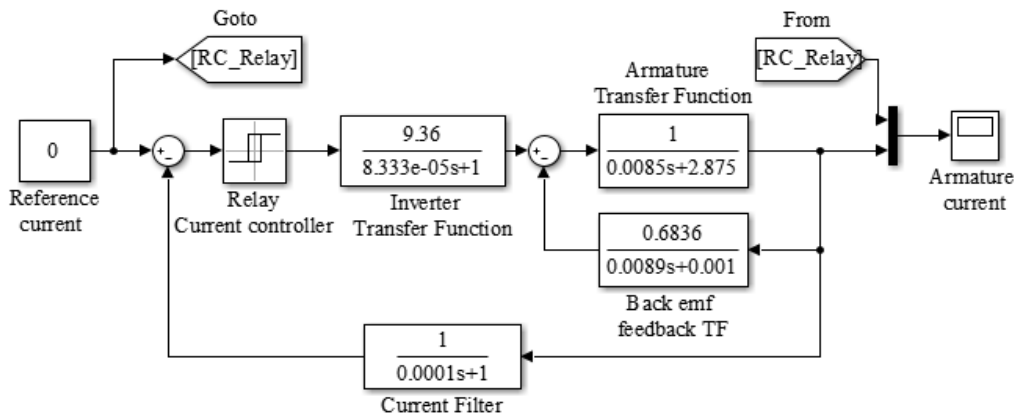


Figure 3.37 Simulink model of BLDC motor internal loop using a relay controller

The output is a sinusoidal current signal for a zero current setpoint as shown in Figure 3.38.

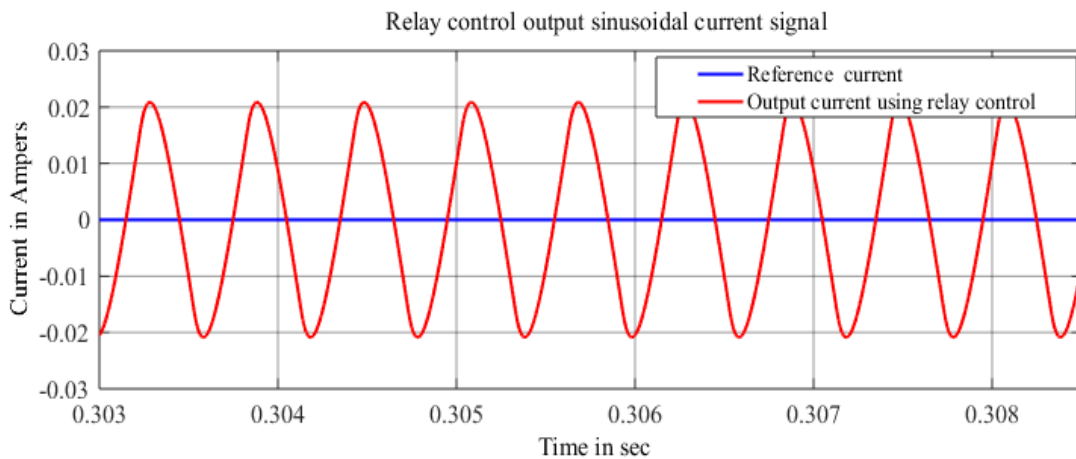


Figure 3.38 Output armature current based on relay current controller

The amplitude of the relay square wave internal signal and its value is the average of a peak to peak of the square wave.

$$d = \frac{U_{\text{high}} - U_{\text{low}}}{2} = \frac{0.2 - (-0.2)}{2} = 0.2 \quad (3.79)$$

The amplitude of the output current signal and its value is determined in Equation (3.80).

$$a = 0.02086 \quad (3.80)$$

The ultimate gain is determined from the parameters in a relay and controlled output signal.

$$K_{uc} = \frac{4d}{\pi a} = \frac{4 \times 0.2}{\pi \times 0.02086} = 12.2075 \quad (3.81)$$

The value of T_u is determined by measuring the time for one full cycle from Figure 3.38. Taking points from 0.3045 to 0.3075 for 5 full cycles then the difference of these two points is 0.0030. The result is divided by 5 to get one full cycle time.

$$T_{uc} = \frac{0.0030 \text{ sec}}{5} = 0.0006 \text{ sec} \quad (3.82)$$

The proportional integral controller gains can be calculated according to Table 3.10.

$$K_{pc} = 0.45 \times K_{uc} = 0.45 \times 12.2075 = 5.4934 \quad (3.83)$$

The integral time can be calculated as:

$$T_{ic} = \frac{T_{uc}}{1.2} = \frac{0.0006 \text{ sec}}{1.2} = 0.0005 \text{ sec} \quad (3.84)$$

The integral gain is determined in Equation (3.85) from proportional gain and integral time.

$$K_{ic} = \frac{K_{pc}}{T_{ic}} = \frac{5.4934}{0.0005} = 10987.43 \quad (3.85)$$

Then the controller transfer function is easily determined from the proportional gain and integral time (integral gain) as follows:

$$G_c(s) = K_{pc} \times \left(1 + \frac{1}{T_{ic}s}\right) = 5.4934 \times \left(1 + \frac{1}{0.0005s}\right) \quad (3.86)$$

$$G_c(s) = \frac{5.4934s + 10987.43}{s}$$

The internal current loop under the cascade control system is simulated by modeling in MATLAB/Simulink independently. Figure 3.39 shows the MATLAB/Simulink model of the BLDC motor internal current loop using ZN tuning based PI controller. The reference current is given manually based on the rated current. But the actual reference current is generated from the speed controller output in the cascade control system.

Figure 3.40 shows the result of output current using Ziegler Nicholas PI current controller. The system implemented without a speed control system. As a result, the controller performance is analyzed based on the reference current given manually below the motor rated current.

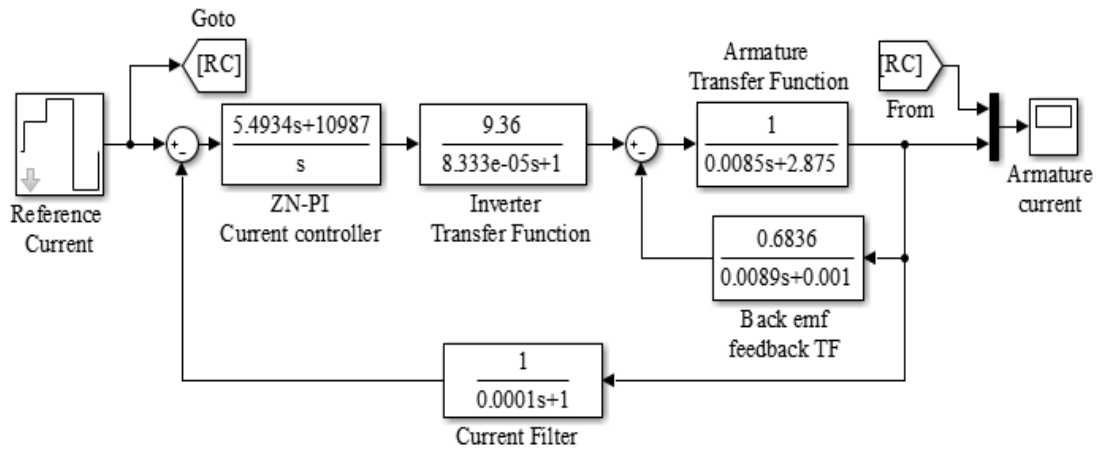


Figure 3.39 The MATLAB/Simulink model of internal current loop using PI controller

The PI current controller result of the BLDCM is zoomed out at a simulation time of 0.5sec and 70A. The result shows that the current overshoot is about 33% and the settling time is about 0.002sec.

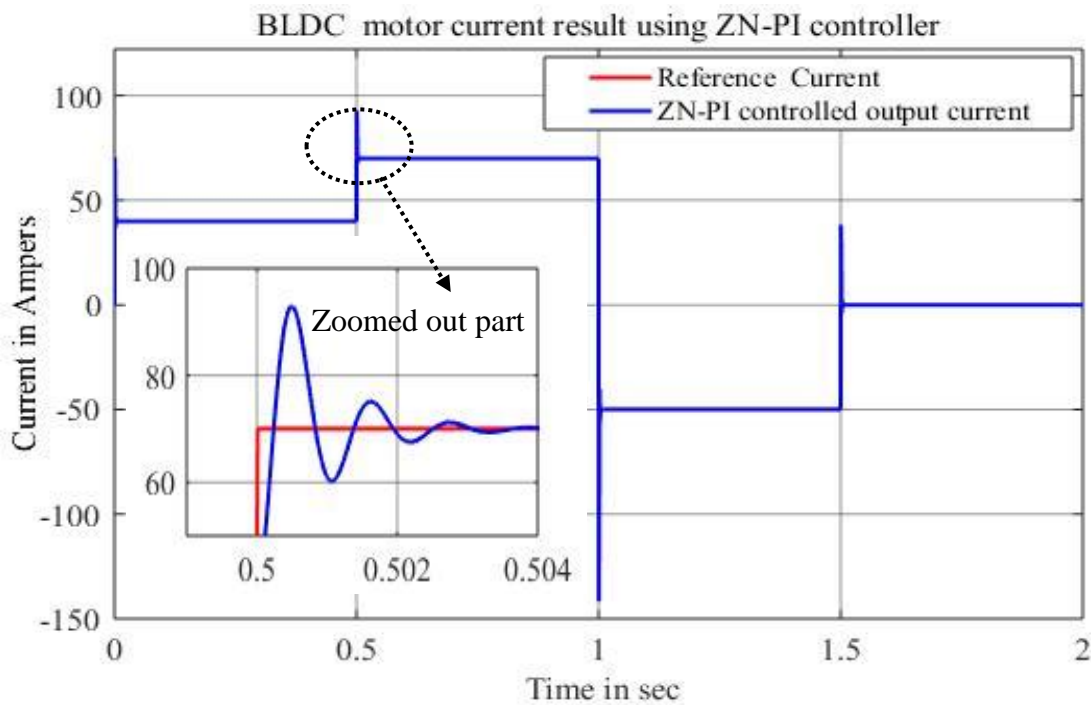


Figure 3.40 BLDC motor output current result using ZN-Pi current controller

3.7.5.3. Design of PID Speed Controller of BLDCM using ZN Tuning

In this portion, the PID speed controller is designed based on ZN tuning technique by cascaded with the PI current controller designed in the previous section. The MATLAB/Simulink diagram using the relay controller is implemented as shown in Figure 3.41.

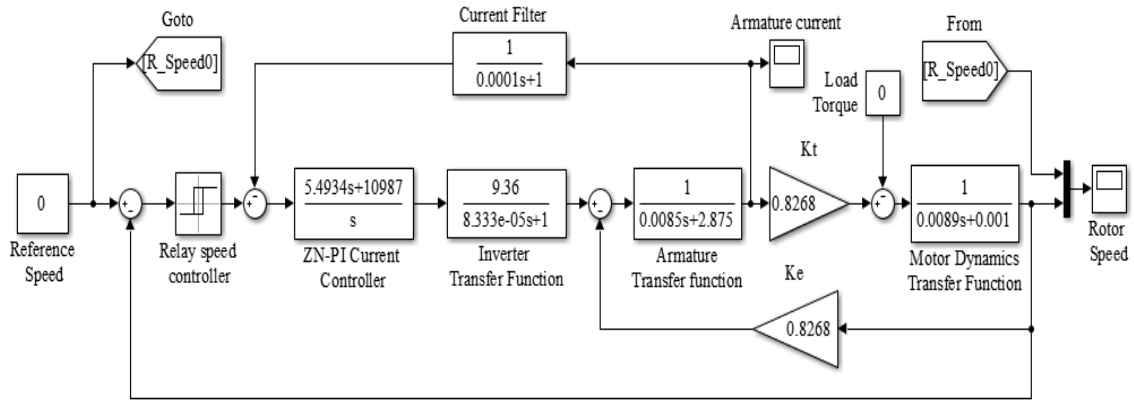


Figure 3.41 MATLAB/Simulink model of BLDC motor relay based speed controller

Using the sinusoidal output speed signal as shown in Figure 3.42, the PID speed controller gains are determined based on ZN manual closed loop tuning technique.

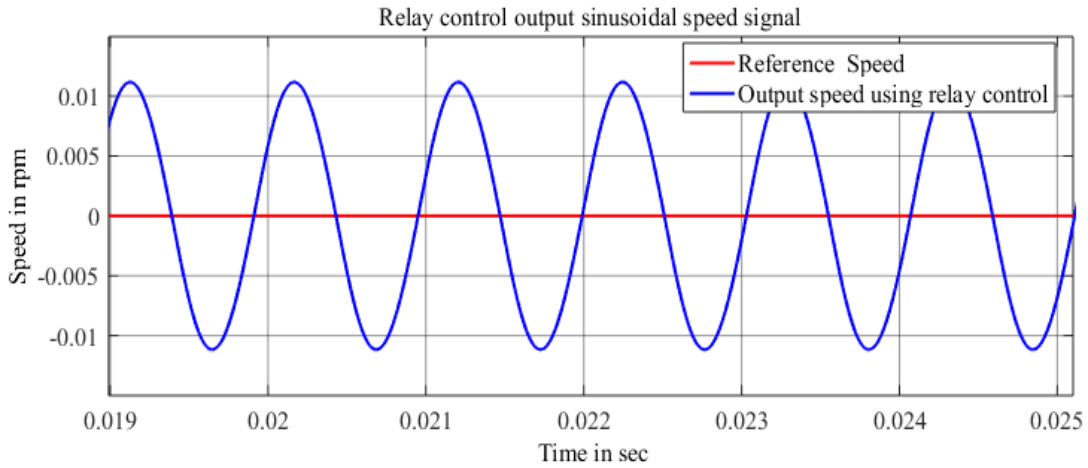


Figure 3.42 Output motor speed result based on relay controller

By applying the same procedure as in relay current controller tuning technique, the speed controller PID gains are determined. The amplitude of the internal relay square wave signal is calculated in Equation (3.87).

$$d = \frac{U_{\text{high}} - U_{\text{low}}}{2} = \frac{0.2 - (-0.2)}{2} = 0.2 \quad (3.87)$$

The amplitude of output speed sinusoidal signal a is 0.010707 and the ultimate gain is determined in Equation (3.88).

$$K_{us} = \frac{4d}{\pi a} = \frac{4 \times 0.2}{\pi \times 0.010707} = 23.783311 \quad (3.88)$$

From Figure 3.42, between time values from 0.02 to 0.021025 the sine wave signal contains one full cycle. The value of T_u can be determined by subtracting these two-time values.

$$T_{us} = 0.001025 \text{ sec} \quad (3.89)$$

The proportional integral derivative controller gains are calculated according to Table 3.10.

$$K_{ps} = 0.6 \times K_{us} = 0.6 \times 23.783311 = 14.26998 \quad (3.90)$$

The integral time is calculated as:

$$T_{is} = \frac{T_{us}}{2} = \frac{0.001025 \text{ sec}}{2} = 0.0005125 \text{ sec} \quad (3.91)$$

The derivative time is determined as:

$$T_{ds} = \frac{T_{us}}{8} = \frac{0.001025 \text{ sec}}{8} = 0.000128125 \text{ sec} \quad (3.92)$$

The integral gain is determined in Equation (3.93) from proportional gain and integral time.

$$K_{is} = \frac{K_{ps}}{T_{is}} = \frac{14.26998}{0.0005125} = 27843.86 \quad (3.93)$$

The derivative gain can be also calculated from proportional gain and derivative time.

$$K_{ds} = K_{ps} \times T_{ds} = 14.26998 \times 0.000128125 = 0.00182834 \quad (3.94)$$

The PID speed controller of BLDC motor gains are determined mathematically. Fine tuning is applied along with ZN tuning to increase performance. The system is simulated at different speed ranges and its result is shown below in Figure 3.43.

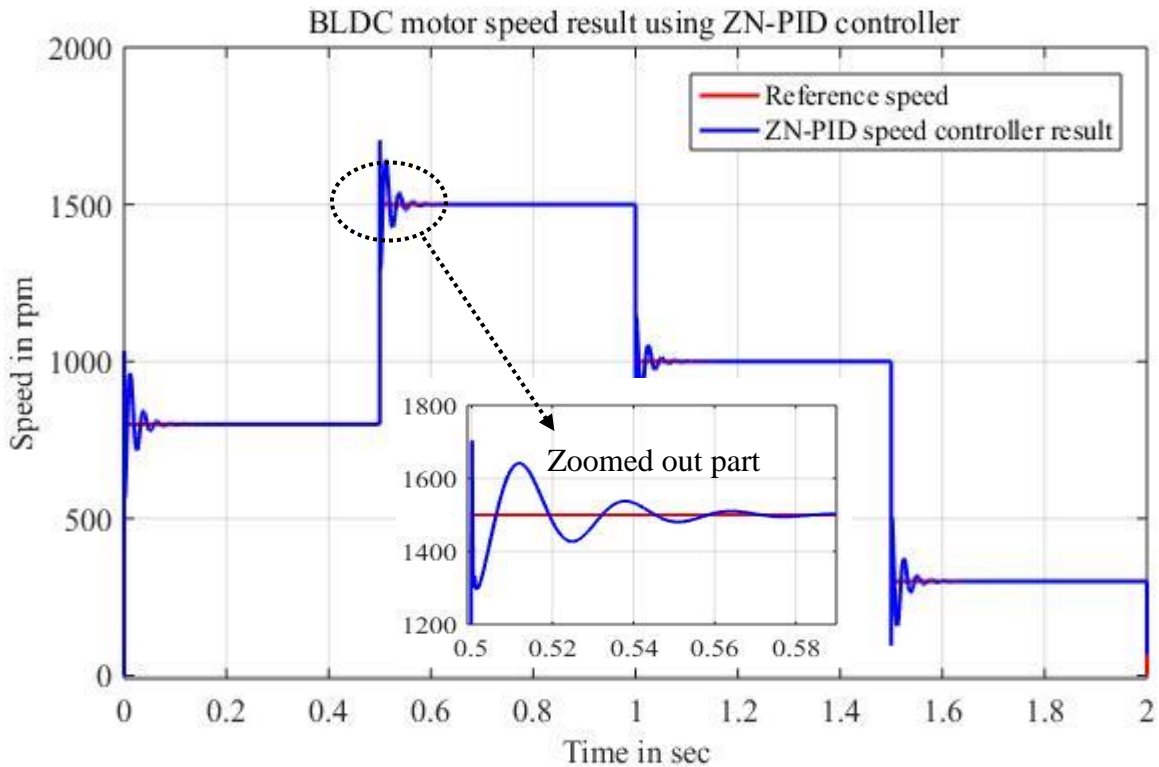


Figure 3.43 BLDC motor speed result using ZN-PID speed controller

The PID speed controller result of the BLDC motor is zoomed out at a simulation time of 0.5sec and a speed of 1500rpm. The result shows that the speed overshoot is about 30% and the settling time gives 0.09sec.

ZN-PID speed and PI current cascade controller is performed. Figure 3.44 depicts the current result under the cascade control system, the reference current is generated from the speed controller output. Hence the system hasn't any limiter especially in speed controller output. So, the current result shows it has very high current at starting and setpoint change conditions because of the reference current has +50% overshoot. Even though the reference current is very high at setpoint change conditions, the output current tracks the reference current. The result shows that the current overshoot is about +50% and the settling time is about 0.09sec.

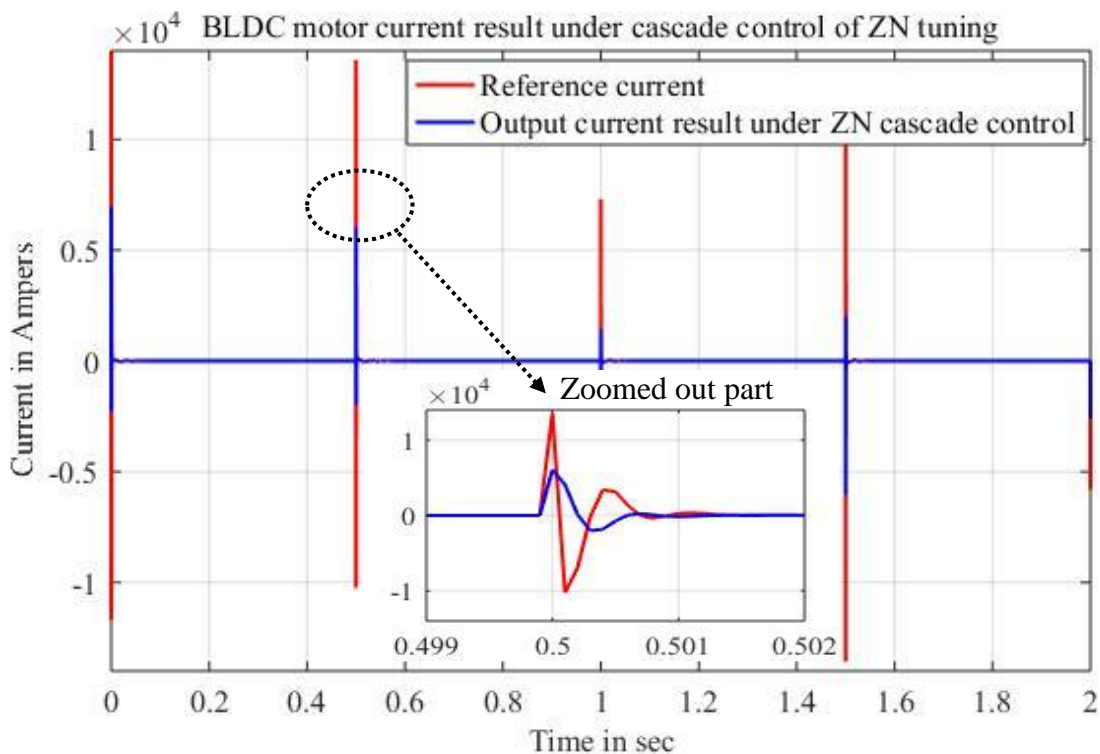


Figure 3.44 Current result of linear PID-PI cascade control system

3.7.6. GA Tuning of Cascade PID and PI Controller

ZN based tuning of linear PID speed and PI current cascade controller has poor performance especially in case of overshoot, it is very high. The GA based PID speed and PI current cascade controller is implemented. The details of the GA optimization parameters setting used in the simulation for the tuning of linear PID and PI cascade controller of BLDC motor control are shown in Table 3.11.

Table 3.11 Parameter settings of the genetic algorithm optimization

Parameter	Type and value
Maximum generations	30
Population size	30
Encoding	Binary
Selection	Uniform
Crossover	Single point crossover
Mutation	Uniform
No of parameters	5
Lower boundary	[0 0 0 0 0]
Upper boundary	[30 10 1 10 10]

The graphical result of the optimized object function (IAE) parameter of the cascade control system is shown in Figure 3.45. Its value after many times re-optimization is 7.67077 which is greater than the GA-NPID controller result and shows it is less efficient.

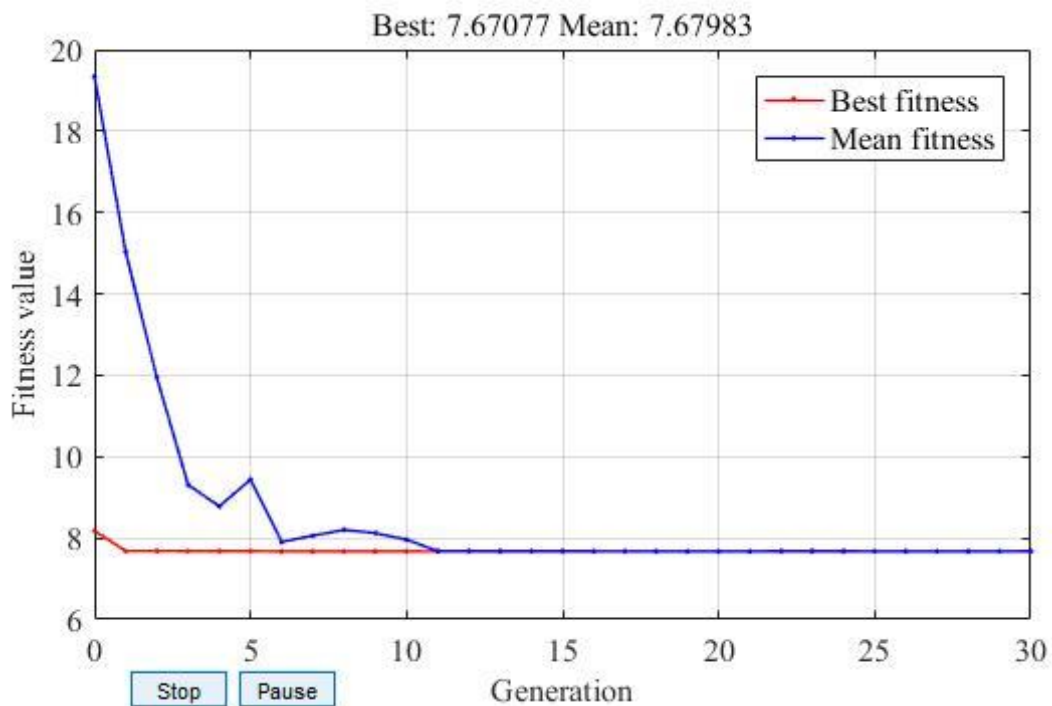


Figure 3.45 Fitness values vs generation for object function

The model of the cascade control of BLDC motor PID and PI controller is performed in GA optimization. The parameters of the PID speed (K_{ps} , K_{is} , K_{ds}), PI current (K_{pc} , K_{ic}) controllers based on GA are obtained as shown below in Table 3.12.

Table 3.12 The GA optimized parameters of the cascade PID and PI controllers

Controllers	Optimized parameters	Optimized values
PID speed controller	K_{ps}	9.8296
	K_{is}	0.3190
	K_{ds}	0.0364
PI current controller	K_{pc}	9.3062
	K_{ic}	0.7038

Figure 3.46 depicts the result of GA optimization based linear PID speed control of BLDC motor output speed. The result of the brushless DC motor output speed is zoomed out at a simulation time of 0.5sec and a speed of 1500rpm. The result shows that the speed overshoot is about 0% and the settling time is about 0.05sec, this shows that the GA-PID controller has better speed dynamic performance than ZN based speed controller results. But it is inferior to NN-NPID and GA-NPID speed controller results. The current controller has the same performance parameter result with the cascade NPID speed and PI current controller result.

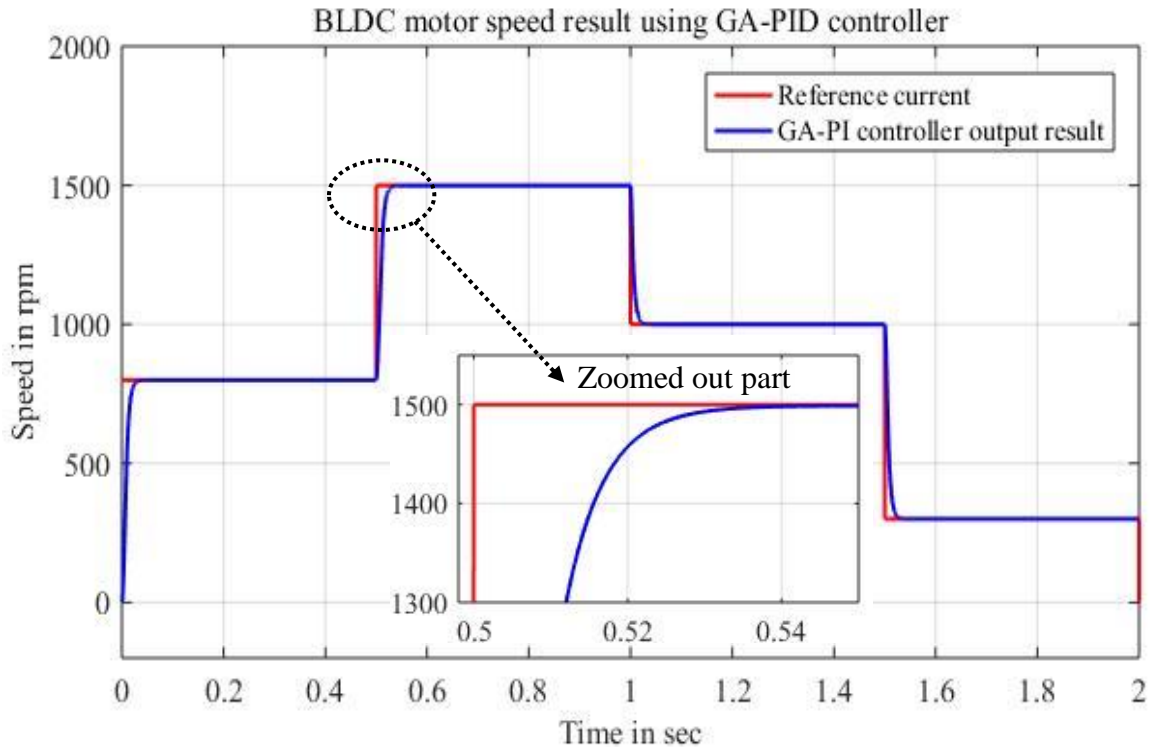


Figure 3.46 GA-PID controller speed result

3.8. The Proposed BLDC Motor Drive Setup

The Simulink design of a nonlinear BLDC motor system with NN-NPID speed and GA-PI current cascade controller, and PWM based inverter switching technique are performed and proposed for the propulsion of electric vehicle bajaj qute. The entire proposed linear and nonlinear BLDC motor drive Simulink block with each subsystem is shown in Appendix (D).

3.8.1. Lithium-Ion Battery Source

Because of its advantages mentioned in the previous sections, the lithium-ion battery is selected and proposed for the power source of the BLDC motor drive and the entire power system source of the four wheel electric vehicle bajaj qute.

3.8.2. Three Phase Inverter BLDC Motor Drive

Three phase inverter with MOSFET power semiconductor switches is considered for this research work. For energy flow from motor to battery during braking operation and reverse motion, the freewheeling diode is connected in parallel with each MOSFET in the inverter drive as shown in Figure 3.47. Since a signal from the hall sensor changes every after 60° , six steps are necessary for the completion of an electrical cycle.

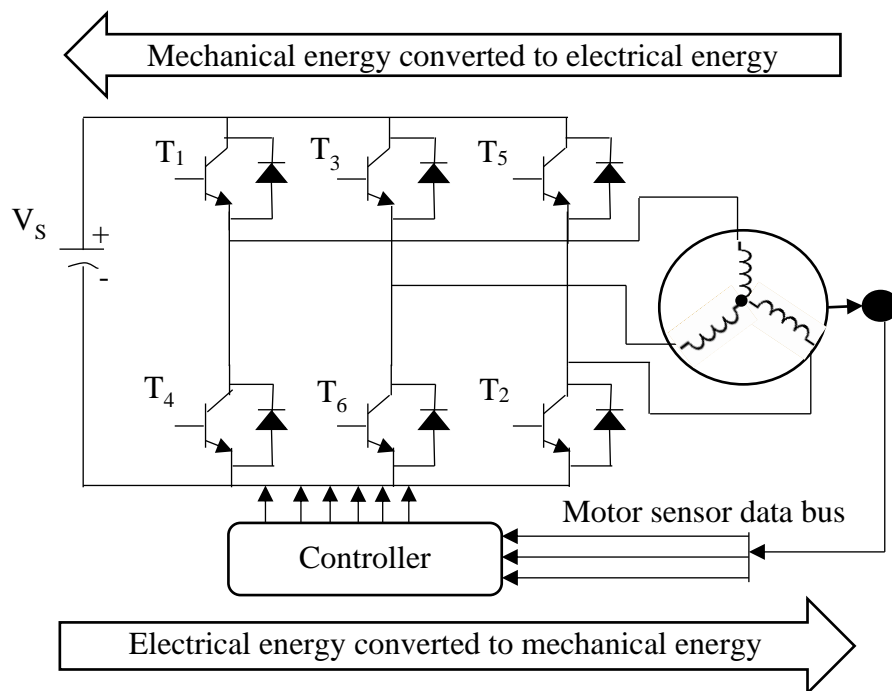


Figure 3.47 Three phase inverter and energy flow for BLDC motor

The phase commutation sequence is AB-AC-BC-BA-CA-CB and each conducting stage is called one step. Only two phases conduct at a time and the third phase is floating. To produce maximum torque, the inverter should be commutated after every 60° so that the current is in

phase with the back EMF. In this work, three PWM is used for the purpose of inverter switching signal generation.

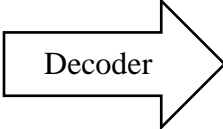
3.8.3. The Proposed Cascade Control System

The different cascade control systems of BLDC motor are applied and compared based on speed and current controllers dynamic performance parameters. Among them ZN tuned PID-PI, GA tuned PID-PI, GA tuned NPID-PI, and NN-NPID and GA-PI cascade controllers are performed in the previous sections. The results show that NN-NPID and GA-PI current cascade controller gives better speed and current dynamic performance than other controllers. As a result, the obtained cascade controller parameters in MATLAB/code are used in the nonlinear MATLAB/Simulink BLDC motor model.

3.8.4. BLDCM Rotor Position Sensor Signal Decoder Implementation

The hall sensor signal is generated based on the rotor position. These signals are decoded into rectangular based three level signals to create emf type reference motor current [56]. Logical based hall sensor decoder is used to convert the signals form each hall sensor into a rectangular three level signals with -1, 0, and 1 which represent the normalized ideal phase currents to injected in the motor phases. The hall sensor decoder can be performed by using the following truth Table 3.13.

Table 3.13 Truth table of hall sensor decoder [57] [58]

No	Hall sensors			Decoder	Decoded signals amplitude		
	H1	H2	H3		emf_a	emf_b	emf_c
0	0	0	0		0	0	0
1	0	0	1		0	-1	+1
2	0	1	0		-1	+1	0
3	0	1	1		-1	0	+1
4	1	0	0		+1	0	-1
5	1	0	1		+1	-1	0
6	1	1	0		0	+1	-1
7	1	1	1		0	0	0

By using Table 3.13 the Simulink modeling of hall position sensor signal decoder is developed as shown below in Figure 3.48. This block is used to extract the induced EMF information from the hall signals and it includes logical and arithmetic operations.

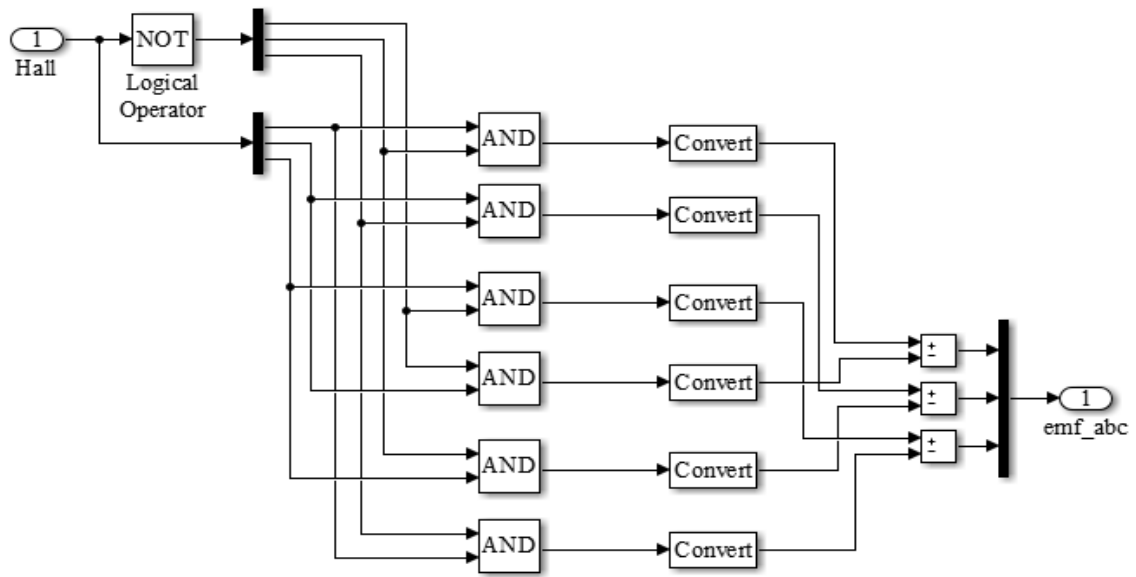


Figure 3.48 MATLAB/Simulink model of hall sensor signal decoder

The output signals of the decoder with the corresponding hall effect sensor signals are drawn as shown below in Figure 3.49. The hall sensors are shifted from each other by 60 degrees. The upper inverter switches (S_1 , S_3 , and S_5) are on when the rotor reaches nearby the corresponding hall sensor.

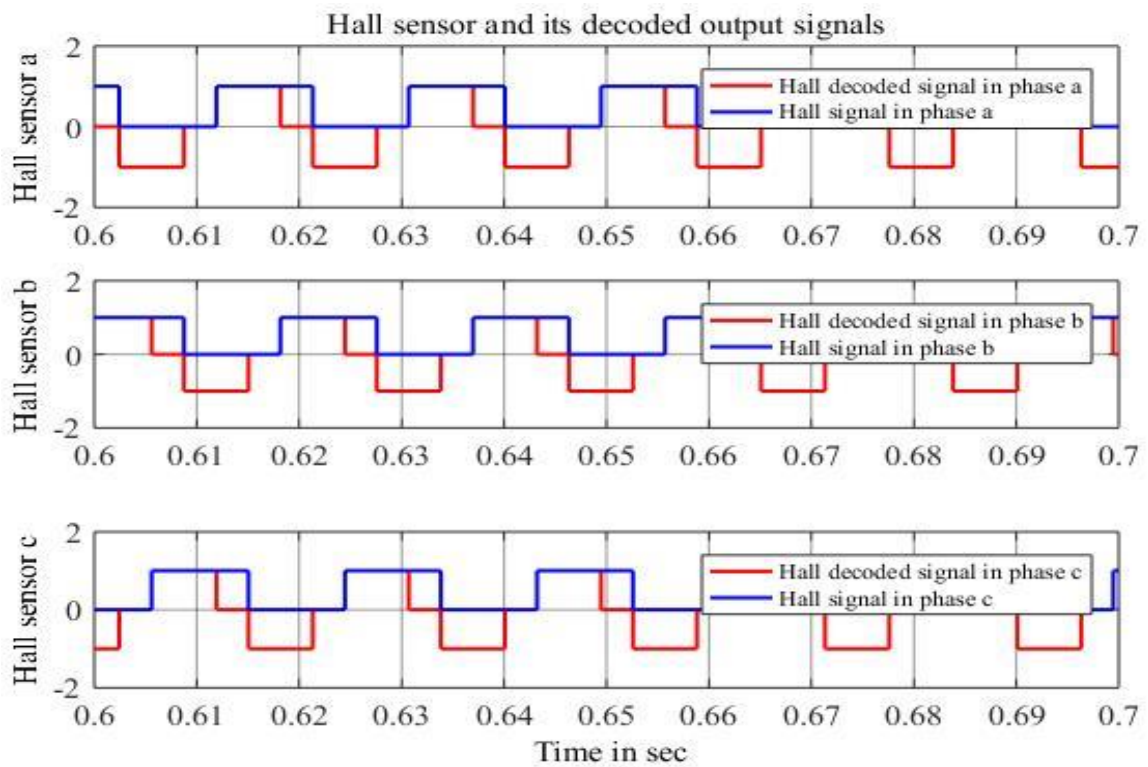


Figure 3.49 Three phase hall sensor and its decoded signal

3.8.5. Reference Current Generation

The three phase reference current is generated based on the multiplication of the decoded hall position sensor signals and the current signal from the speed controller output. Hence the wave shape of the reference signals is similar to the decoded hall signals as shown in Figure 3.50.

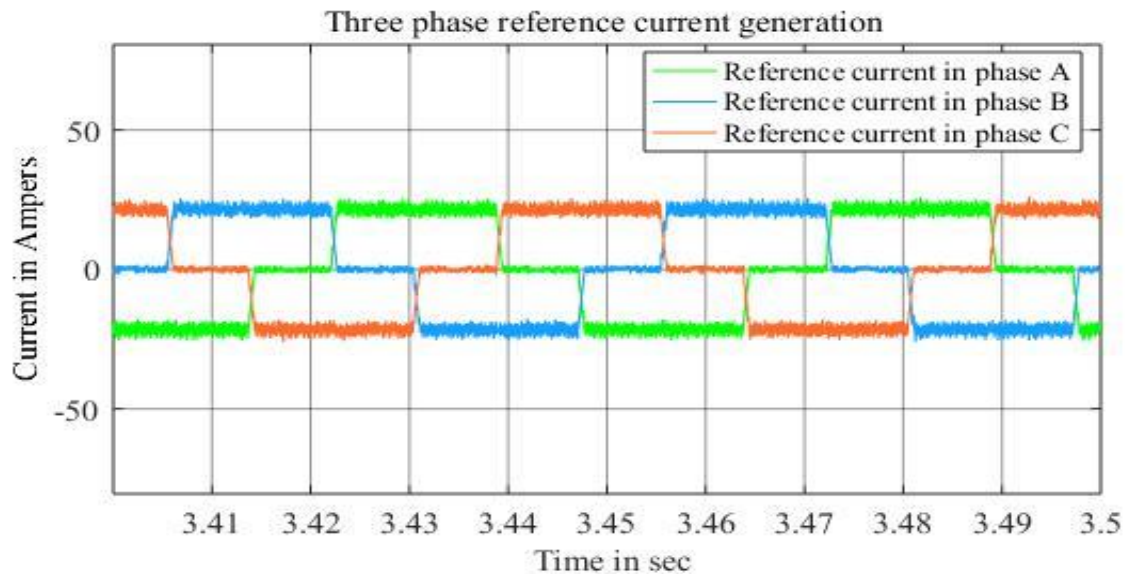


Figure 3.50 Three phase reference current signal

3.8.6. Pulse Width Modulation (PWM) Based BLDCM Drive

PWM works for any type of signal and it needs two signals for operation. These are controlled and carrier signals. Usually, the frequency of the carrier signal must be at least twice that of the modulating signal frequency. By comparing these two signals the rectangular wave switching signal can be generated. In this work, PWM based inverter drive is considered and it consists of the voltage signal, carrier signal, comparator, and logical circuit. The output of the current controller is converted into a voltage signal by applying an appropriate resistance based on the selected carrier voltage amplitude. The result gives the corresponding phase voltage controlled modulating signal V_a , V_b , and V_c as shown in Simulink Figure 3.51.

The controlled voltage signal is compared with a triangular carrier signal. If the controlled voltage signal is greater than the amplitude of the carrier signal, the switching signal is one and the corresponding switch will be ON and if the controlled voltage signal is less than the amplitude of the carrier signal the switching signal is zero and the corresponding switching state will be OFF. The output signal of PWM is connected to the logical NOT in each phase

for switching the semiconductor switches in the same leg. When the upper switch is ON the lower switch should be OFF and vice versa under the same leg of the inverter.

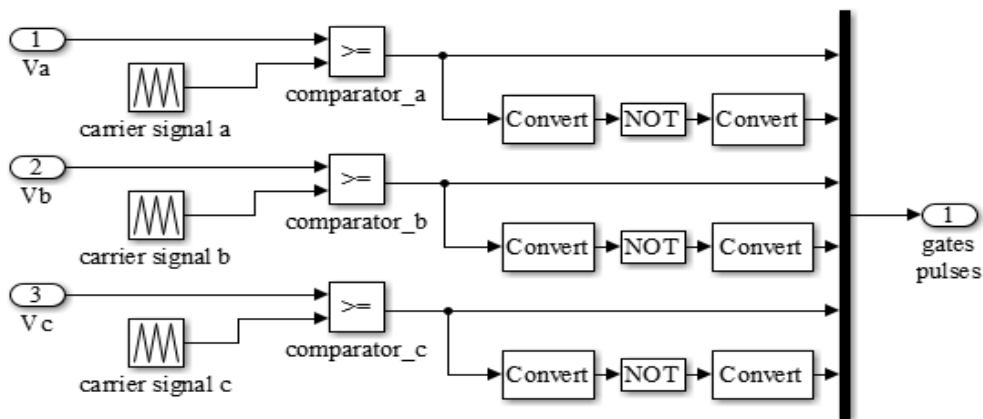


Figure 3.51 The proposed PWM based BLDC motor drive Simulink diagram

The triangular carrier signal is generated by considering the inverter switching frequency of 6kHz and the amplitude of 10v. The amplitude is selected based on the modulation index (0.9) criteria because the maximum controlled voltage has 9v. The selection of switching frequency is depending on the inverter loss. If the switching frequency is more the loss will be less and vice versa. The generated carrier signal is shown in Figure 3.52.

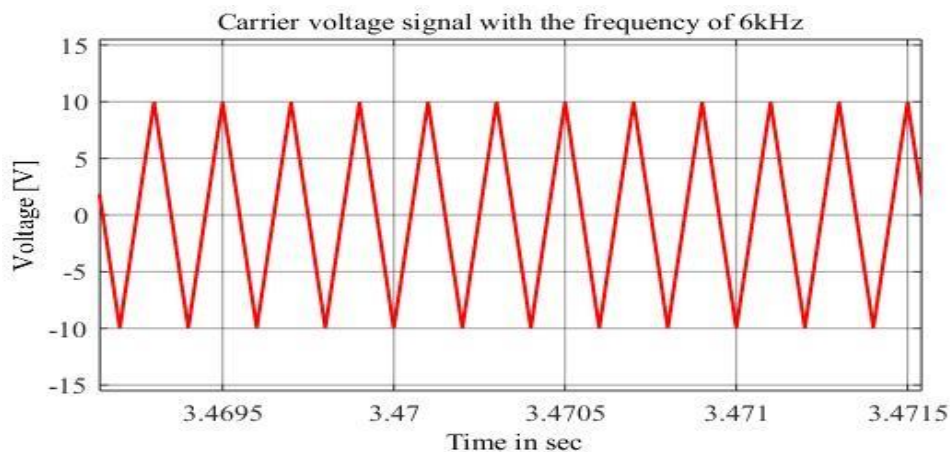


Figure 3.52 Triangular carrier voltage signal

3.8.7. Relay Based BLDCM Drive

In this work relay based BLDC motor drive is performed for comparison purpose. When the current controller is used like PI controller, relay based inverter drive will not applicable to trigger the inverter power semiconductor switches. Because it works based on the comparison between the stator current and the corresponding reference current. The error signal is given to a two level relay comparator. Each phase requires one relay comparator.

The output of the relay comparator becomes one or zero based on the bandwidth of the relay. The advantages of this scheme are, its simplicity and easy to implement practically. Its disadvantages are, it has high current overshoot, leads to harmonics due to the bandwidth of the relay comparator. Figure 3.53 depicts the implementation of switching signal generation in Simulink. The output relay comparator is connected to the logical NOT in each phase for switching the semiconductor in the same legs. When the upper switch is ON the lower switch should be OFF and vice versa under the same leg of the inverter.

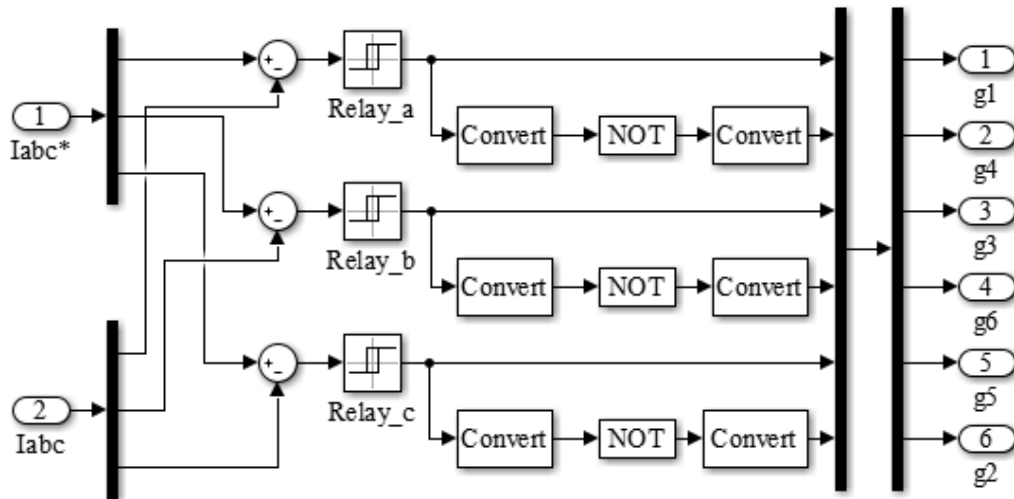


Figure 3.53 Relay based BLDC motor inverter drive

CHAPTER 4

4. RESULTS AND DISCUSSIONS

This chapter includes the result and analysis of the proposed cascade control system and drive system of the BLDC motor for a bajaj quite electric vehicle. The simulation results of the proposed system are compared with the related works mentioned in the literature to fulfill the specific objectives of the research. The simulation results explained in this chapter are performed for the same values of the system parameters under study. In this research work, both the linear and nonlinear MATLAB models of the BLDC motor drive is used. The linear system generally used to simulate the speed and current controllers of different artificial intelligence tuning techniques. Also, the nonlinear Simulink system is used to analyze the current harmonics and torque ripple of the motor. Besides, the nonlinear Simulink system helps to analyze the BLDC motor output result like induced back-EMF, stator current, electromagnetic torque, three phase inverter output voltage, and battery state of charge along with the speed of the electric vehicle bajaj quite so on.

4.1. The Proposed BLDCM Control and Drive System Result

In this work, the NN-NPID and GA-PI current cascade controller with PWM based BLDC motor drive are proposed. The results are explained in detail in the following sections.

4.1.1. The Proposed Cascade Control System Results of BLDCM

An autotuning (neural network) based NPID speed and GA-PI current cascade controller is simulated in both linear and nonlinear BLDC motor drive. The result of the speed controller in both drives has a similarity of 98% in the speed dynamic performance. Different cascade control techniques are discussed and compared.

4.1.1.1. NN Based NPID Speed Controller Result of BLDCM

Figure 4.1 depicts the result of an autotuning of the NPID proposed speed control system of the linear brushless DC motor drive system. The result shows that the speed of the motor follows its reference speed with better dynamic performance (settling time, rise time, peak time, overshoot, and steady state error). The speed result in Figure 4.1 has similar speed dynamic performance with the result under the nonlinear Simulink model of BLDC motor shown in Figure 4.9. The system is simulated in different speed setpoint values because the vehicle moves at different speeds.

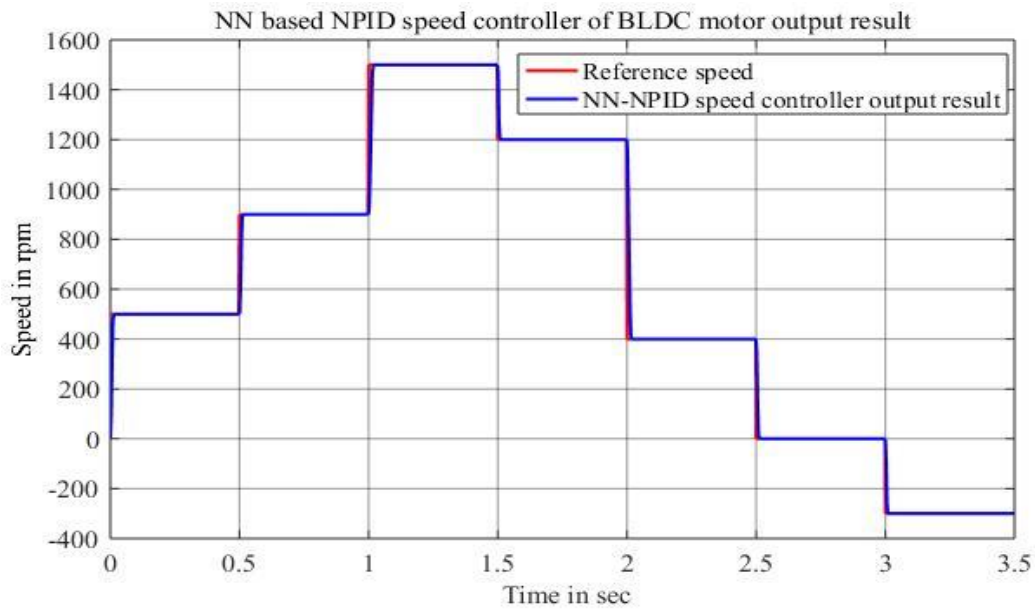


Figure 4.1 The proposed speed control result of the BLDC motor

4.1.1.2. GA-PI Current Controller Result of BLDCM

The linear BLDC motor system of MATLAB simulation of the GA-PI current controller result is shown in Figure 4.2. The motor current tracks the reference current from the proposed speed controller output. The result of the proposed current control system of the brushless DC motor has good current overshoot (0%), and it is always below the rated motor current. Hence the rated current of the motor is 77A, the result shown in the figure below is less than 77A and it is about 75A. Theoretically, the motor drive is in a safe condition.

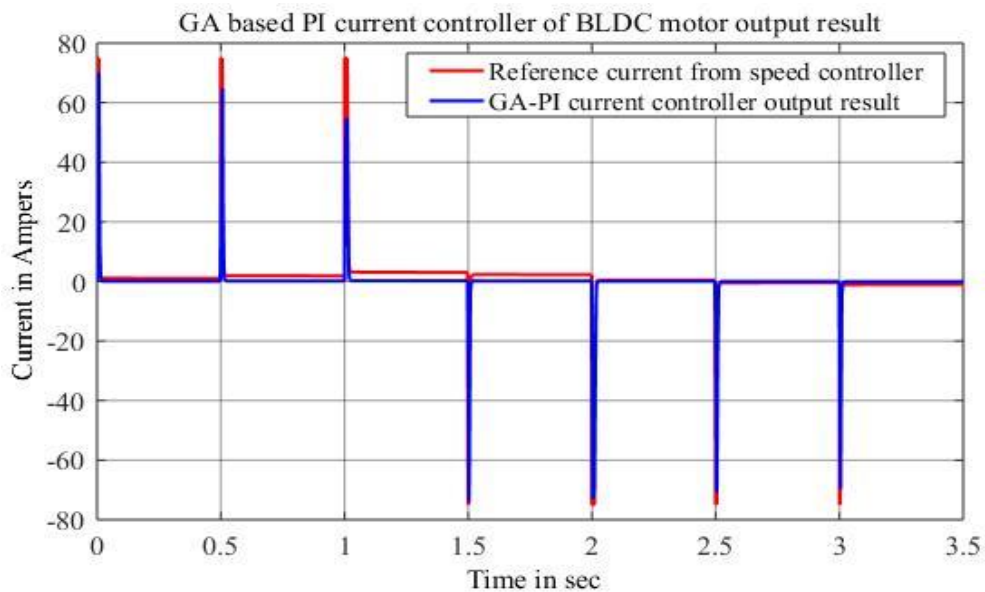


Figure 4.2 The proposed current control result of the linear BLDC motor drive system

4.1.2. PWM Based Nonlinear BLDCM Drive Output Results

4.1.2.1. BLDCM Stator Current Result

The BLDC motor has always current harmonics and one of the objectives of the thesis is to reduce the distortion to some extent. Figure 4.3 shows the three phase stator current of the motor under the PWM based BLDC motor drive study and its harmonics value in percentage is 6%. The stator current frequency is directly proportional to the motor speed. When the speed is large/minimum the frequency of the stator current is large/minimum respectively. As an example, when the time between 1 to 1.5sec the speed is 1500rpm and the frequency is large, and when the speed is 0 between the time 2.5 to 3sec the frequency is zero.

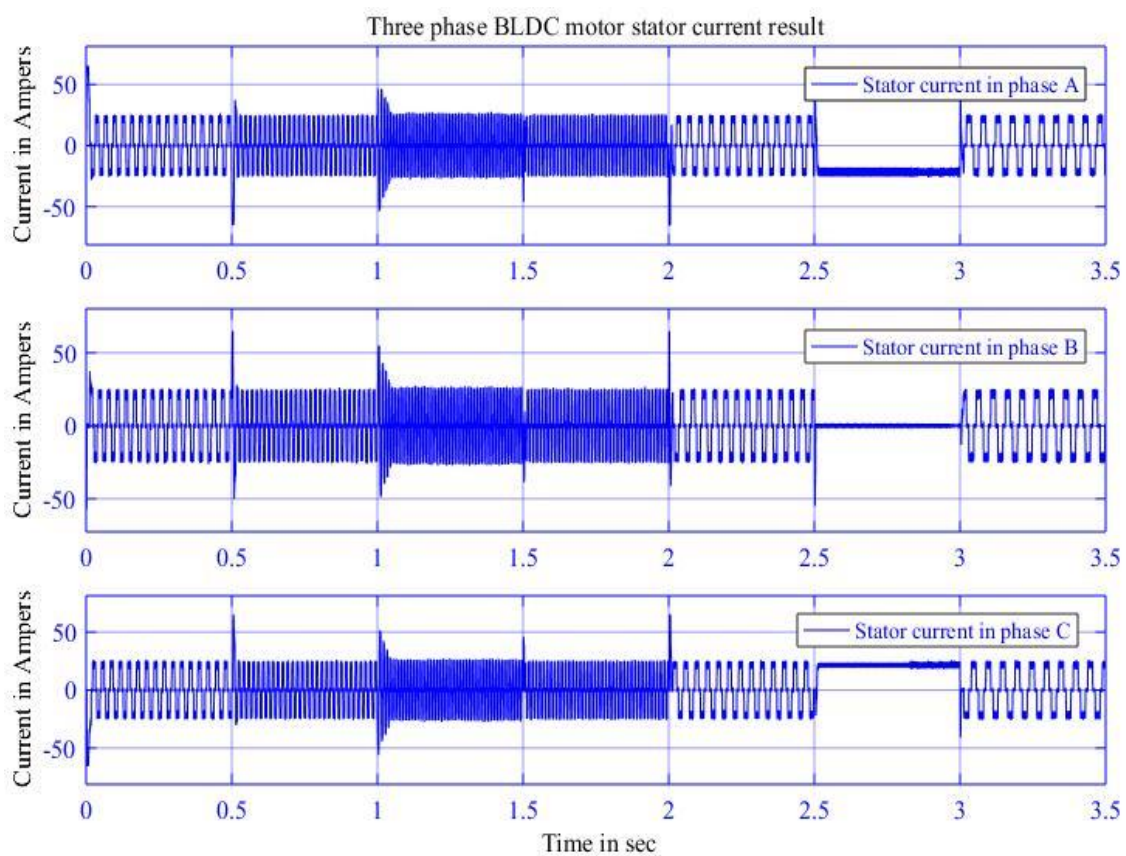


Figure 4.3 Three phase BLDC motor stator current result

4.1.2.2. BLDCM Three Phase Trapezoidal Back-EMF Result

The three phase BLDC motor trapezoidal back-EM waveform result is generated as shown in Figure 4.4. It is taken at the same simulation time with that of the nonlinear model speed dynamic performance shown in Figure 4.9. From the result, when the speed is increasing the induced back-EMF is also increasing. As an example, from the simulation time of 2.5 to 3sec the speed is zero correspondingly the induced back-EMF is also zero. And also, from

time 1 to 1.5sec the speed is 1500rpm and the back-EMF is about 75v. This result shows that the speed and induced back-EMF voltage are directly proportional to each other.

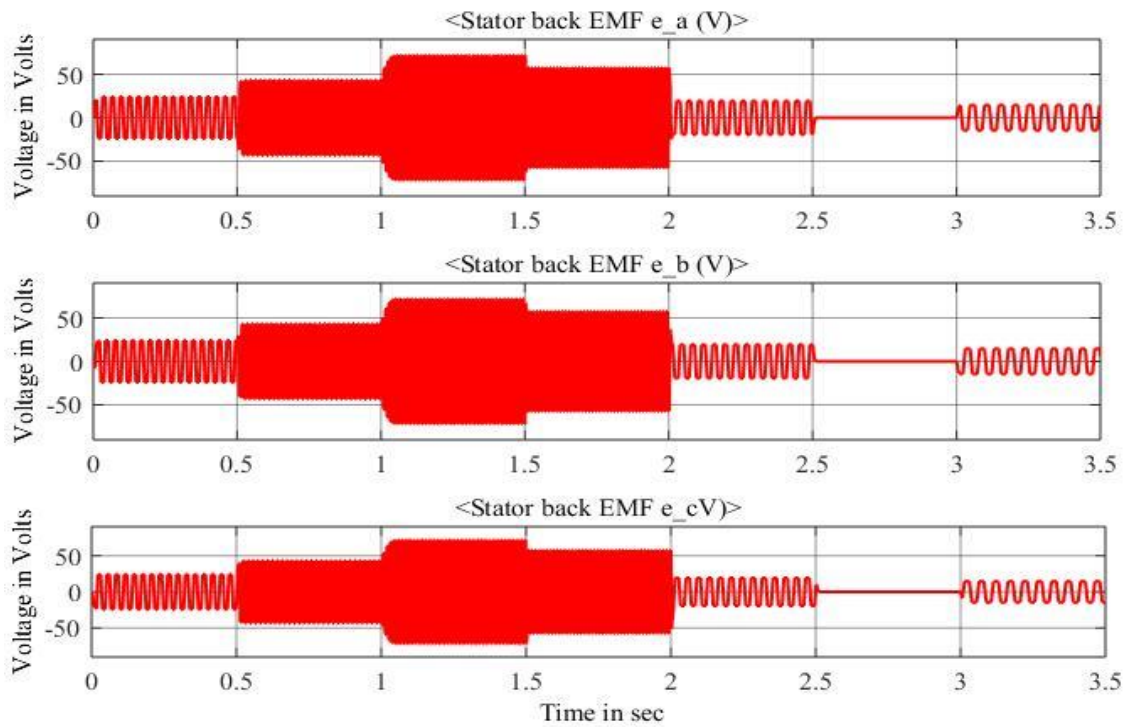


Figure 4.4 BLDC motor three phase back-EMF result

Figure 4.5 shows the trapezoidal back-EMF zoomed out result from the simulation time of 0.5 to 0.6 sec. The figure explains the structure of induced back-EMF waveform.

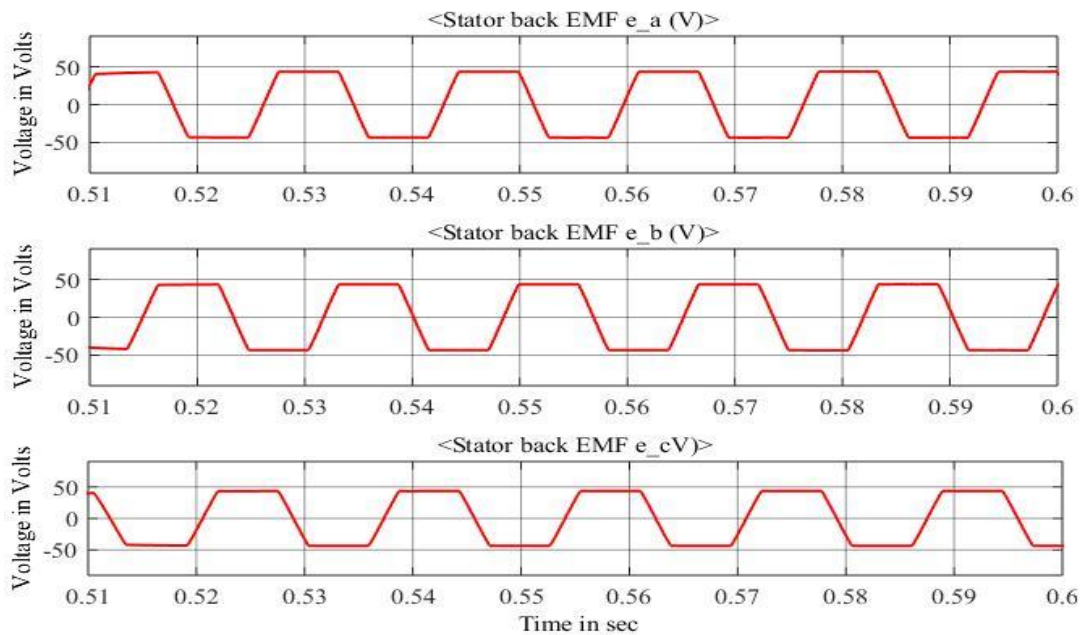


Figure 4.5 BLDC motor three phase trapezoidal back-EMF zoomed out result

4.1.2.3. BLDCM Electromagnetic Torque Result

The electromagnetic torque and stator current of BLDC motor are directly proportional to each other. As a result, the stator current harmonics of the BLDC motor leads to torque ripple. Figure 4.6 explains the result of electromagnetic torque vs the applied load torque of BLDC motor under the nonlinear MATLAB/Simulink drive system. Its torque ripple is about 6%, the result shows it is proportional to the stator current harmonics result. The system is simulated about a constant load of 20Nm for different speed setpoints below its base speed i.e. 1500rpm. Hence in speed versus torque characteristics below base speed, the torque is constant. The result shows also the torque is constant below the rated speed.

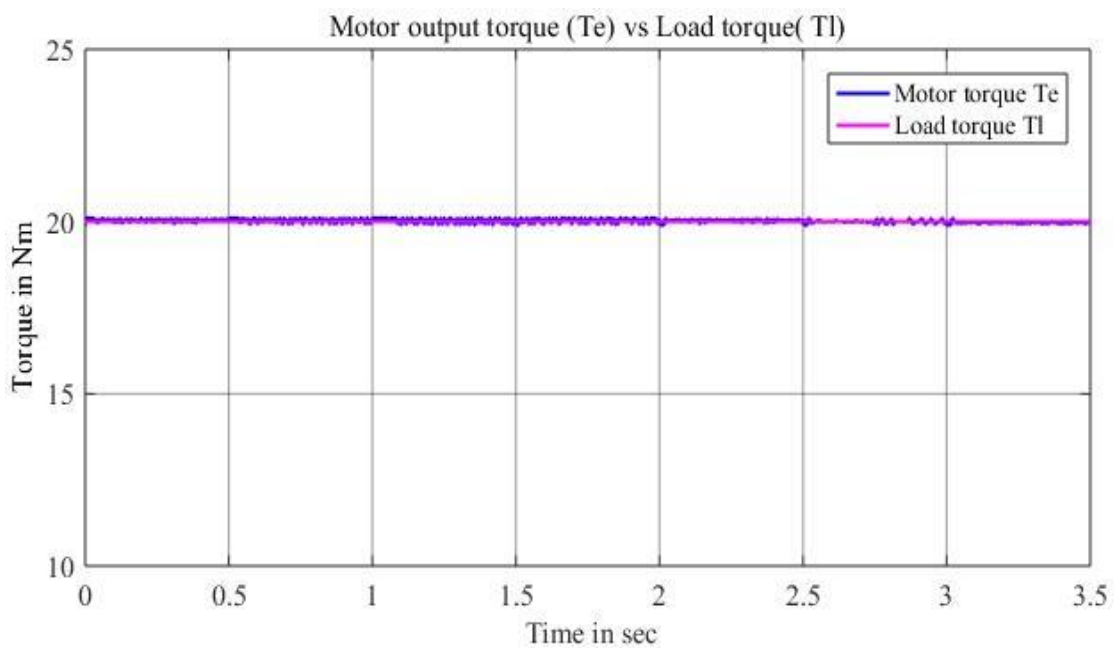


Figure 4.6 BLDC motor electromagnetic torque result

4.1.2.4. Three Phase Inverter Output Voltage of BLDCM

The output of the three phase inverter voltage of the BLDC motor is generated as shown below in Figure 4.7. Its output waveform is a rectangular wave type with a switching frequency of 6kHz. The three phase inverter switching commutation signal is designed based on a PWM switching technique. The inverter output voltage follows the inverter switching frequency. However, because of stator inductance the stator phase current can't follow the inverter switching frequency rather it follows the frequency of its reference current generated from the speed controller output signal and decoded hall output signals.

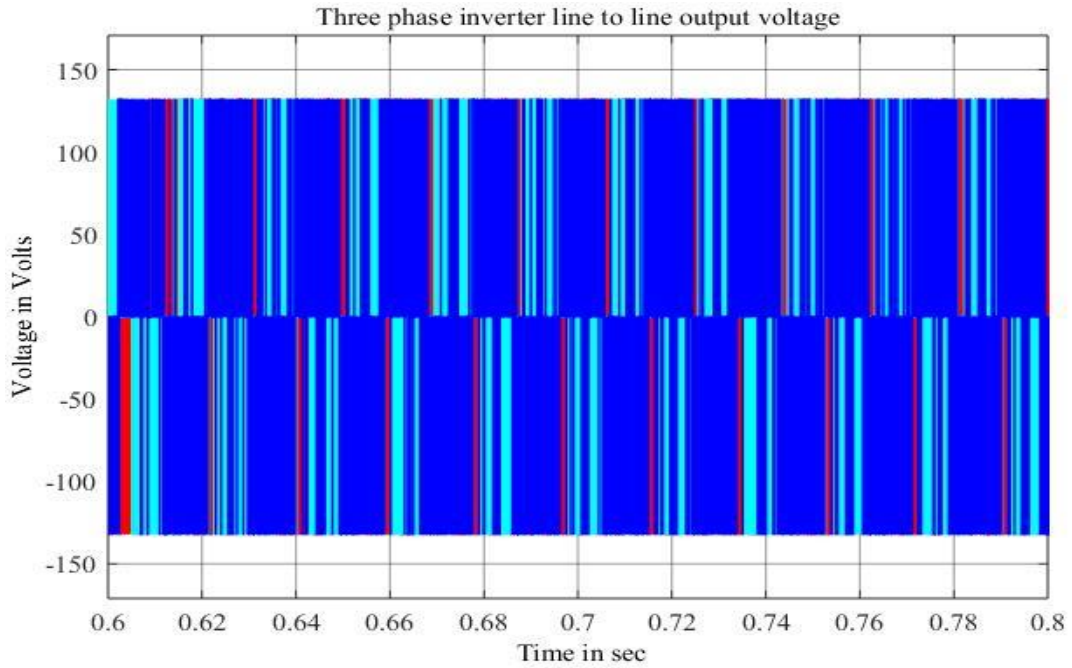


Figure 4.7 Three phase inverter output voltage

The output power of the BLDC motor is the product of the speed and electromagnetic torque. Figure 4.8 depicts the result of the output power of the BLDC motor, when the speed of the motor is 1500rpm (157.079 rad/sec) at 20Nm then the output power is 3.142kW. The system is simulated about a constant load for different speed setpoints below its base speed i.e. 1500rpm. Hence in the speed versus torque characteristics curve below base speed, the power is variable. The result also shows the power is variable below the rated speed.

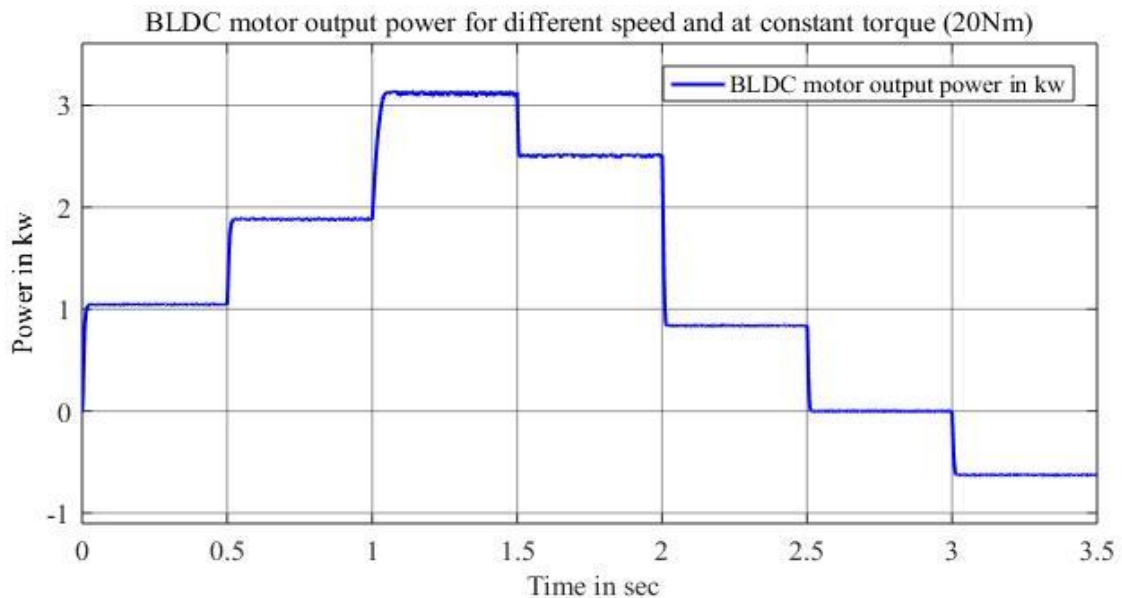


Figure 4.8 The power output of BLDC motor under the nonlinear drive system

4.1.2.5. Vehicle Speed vs Battery State of Charge

The result of electric vehicle bajaj qute speed versus battery state of charge is shown in Figure 4.9. The speed of electric bajaj follows its command speed with a better dynamic performance like the motor speed result. It is computed in km/hr based on the output of the motor speed, the reducer (gear transformation), and the radius of the wheel or tire.

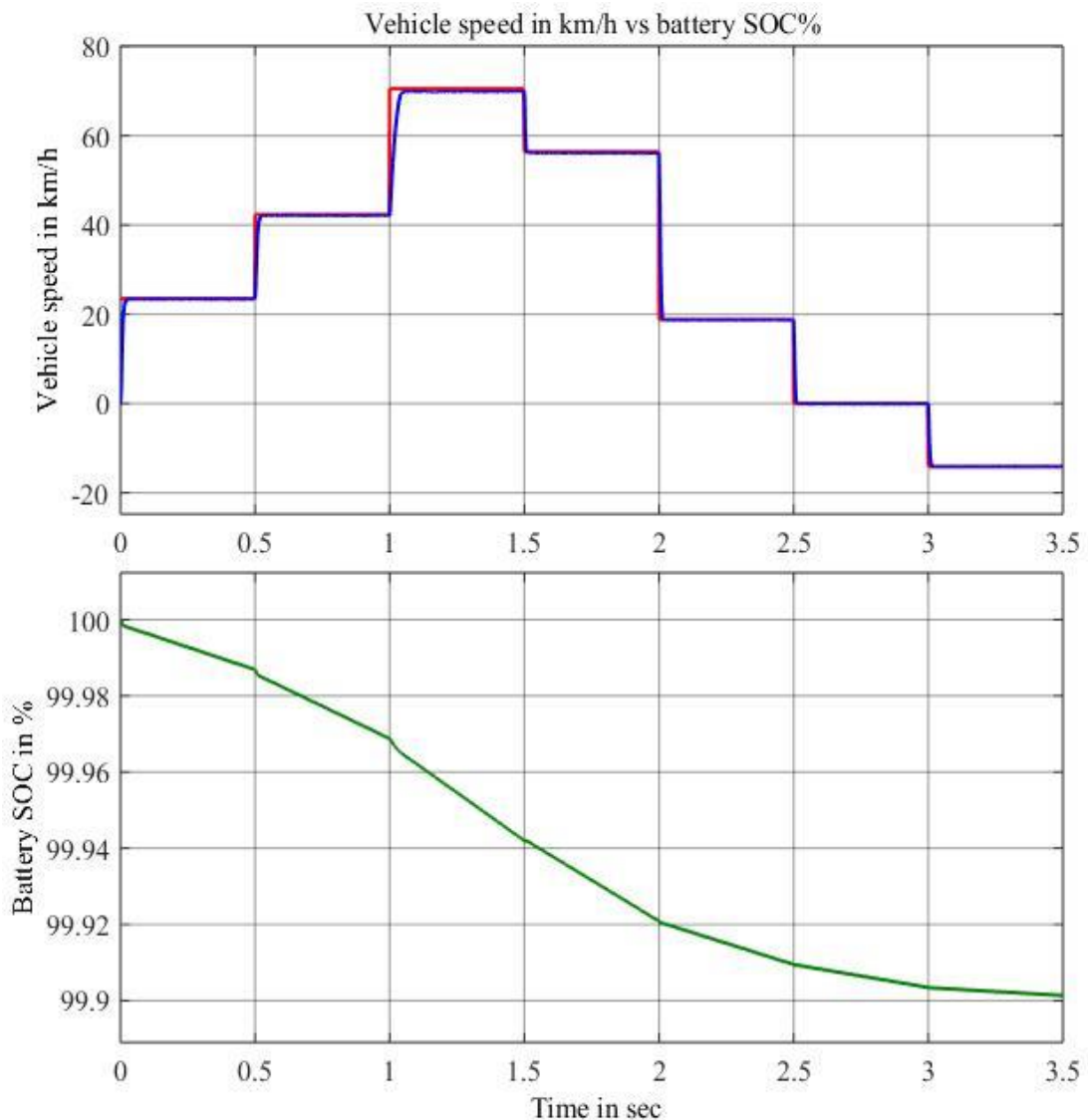


Figure 4.9 Vehicle speed vs percentage of battery state of charge

In addition, the state of charging in the range of different vehicle speed performance is also shown in the result. Accordingly, in the case when the speed of the vehicle or motor is increasing the discharging rate of the battery also increases (i.e. the slope of the state of charge is increasing negatively). In another case when the direction of the rotation of the rotor vehicle movement is reversed, specifically from 3 to 3.5 sec, the battery is getting the charge through the freewheeling diode in the inverter and its slope of the state of charge is

tries to become positive. In this case, the motor acts as the generator. The relationship between electric vehicle battery state of charge versus distance in km is performed and its result is shown in Figure 4.10 below. The vehicle drives at 70km/hr constant speed on road by ignoring the impact of external factors and the environment. As can be seen from Figure 4.10, battery SOC decreased with increasing mileage. Mileage which can be seen from the figure is 90km, achieves the performance index of the mileage for at least 70km.

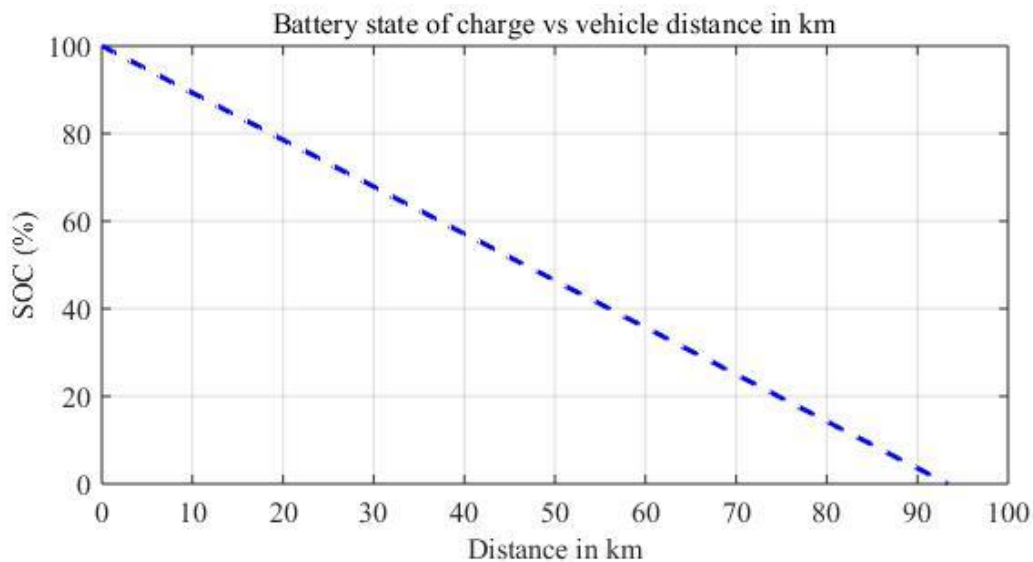


Figure 4.10 SOC versus mileage in kilometer at 70km/hr constant speed

4.2. Discussion of Results

In this portion, the results of the cascade controllers and inverter switching techniques of the BLDC motor drive are discussed in detail. The comparison of each speed and current controllers and inverter switching techniques are described in tabular and graphical forms.

4.2.1. Discussion of BLDCM Cascade Control System Result

Different cascade control systems are performed for BLDC motor speed and current control. The results of each controller are compared and discussed in tabular and graphical forms.

4.2.1.1. Speed Dynamic Performance of BLDCM

In this study, different speed controllers are performed. These are ZN-PID speed controller, GA-PID speed controller, GA-NPID speed controller, and the proposed NN-NPID speed controllers. For the comparison purpose, the simulation is performed in constant and variable setpoint conditions. Figure 4.11 shows the constant setpoint condition speed result (at 1500rpm). The comparison result is from the modeling of linear BLDC motor drive system. From control system theory, the system is said to have better dynamic performance if it has

the lower rise time, lower percent overshoot, lower settling time, and lower peak time.

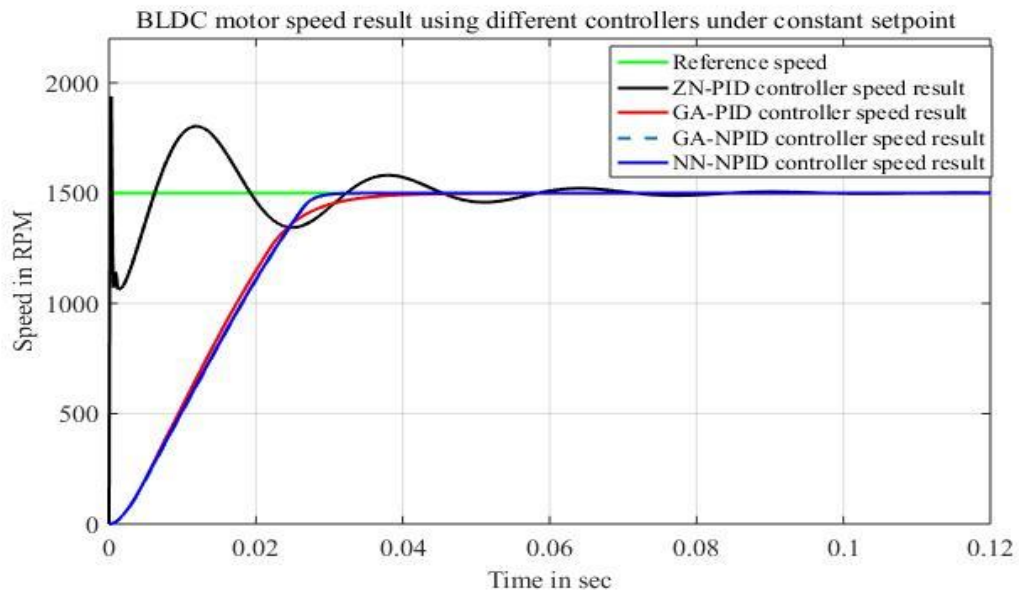


Figure 4.11 BLDC motor speed result using different controllers

The speed result of Figure 4.11 is zoomed out from the simulation time of 0 to 0.09 sec and the speed from 1100 to 2000 rpm as shown in Figure 4.12. The result shows that the NN-NPID speed controller has good speed dynamic performance as shown in Table 4.1.

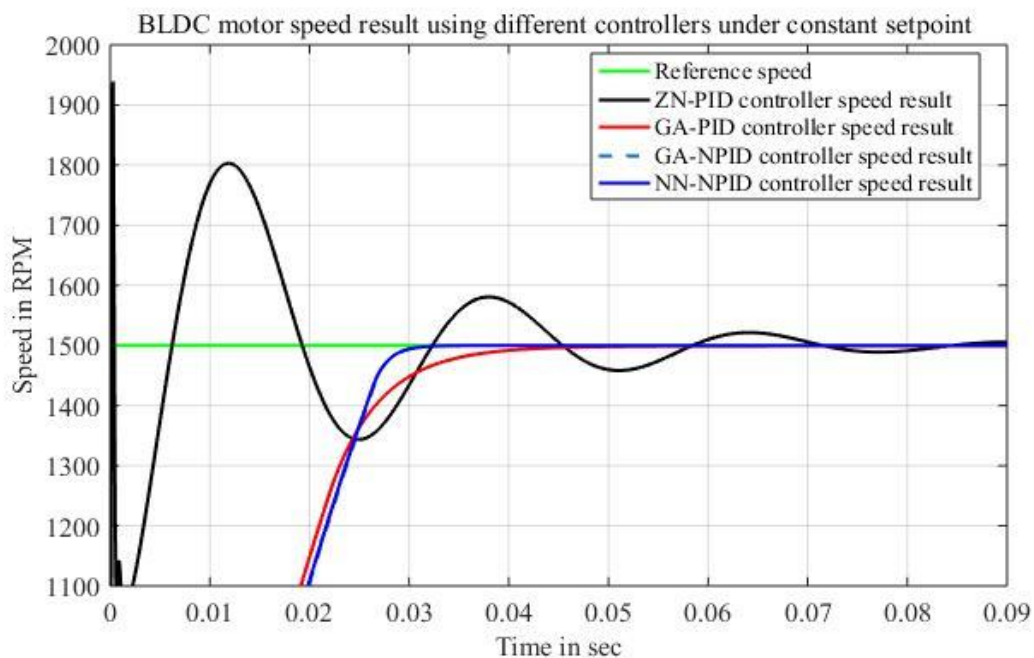


Figure 4.12 BLDC motor speed zoomed result using different controllers

Table 4.1 shows the detailed speed dynamic performance parameters of each controllers result. ZN-PID speed controller has poor performance than others especially in the case of

overshoot and settling time. It has a 30% overshoot and settling time of 0.09sec. The GA-PID controller has a better result in case of overshoot (0%) and settling time (0.05sec) than ZN-PID controller. But the BLDC motor is the nonlinear motor due to this the linear PID speed controller of BLDC motor is not suitable.

Table 4.1 Speed controller comparison of performance parameter results

Speed Controllers	Performance parameters result in constant 20Nm load condition				
	Settling in time sec	Rise time in sec	Peak time in sec	Percentage overshoot	Steady- state error
ZN-PID controller	0.09	0.027	0.04	30%	0%
GA-PID controller	0.05	0.04	0.045	0%	0%
GA-NPID controller	0.03	0.02	0.025	0%	0%
NN-NPID controller	0.0275	0.02	0.022	0%	0%

The nonlinear PID controller is recommended for the BLDC motor speed control due to nonlinear coupling between winding currents and rotor speed. The GA-NPID speed controller is performed and it has good speed dynamic performance in all aspects. But, in case of load change conditions, the motor speed cannot track the desired speed. As a result, the steady state error is increased when the load is increased and its value is $>0.7\%$ (i.e. $>10\text{rpm}$ speed error) as shown in Figure 4.15. To reduce this effect to some extent neural network is used based on the GA-NPID result. Neural network tunes the NPID controller gains online. The result of the NN-NPID speed controller shows that it has better performance than GA-NPID speed controller results as shown in Table 4.1.

The speed control systems are simulated under setpoint change condition, and all have similar performance parameter results with the results listed in Table 4.1. The result of all speed control systems together is shown in Figure 4.13. The system is simulated with similar parameters considered under study. For the comparison purpose, the simulation time is taken 2sec because it is easy to see the effect of the setpoint change condition and also it is easy to zoom out at the particular setpoint change condition.

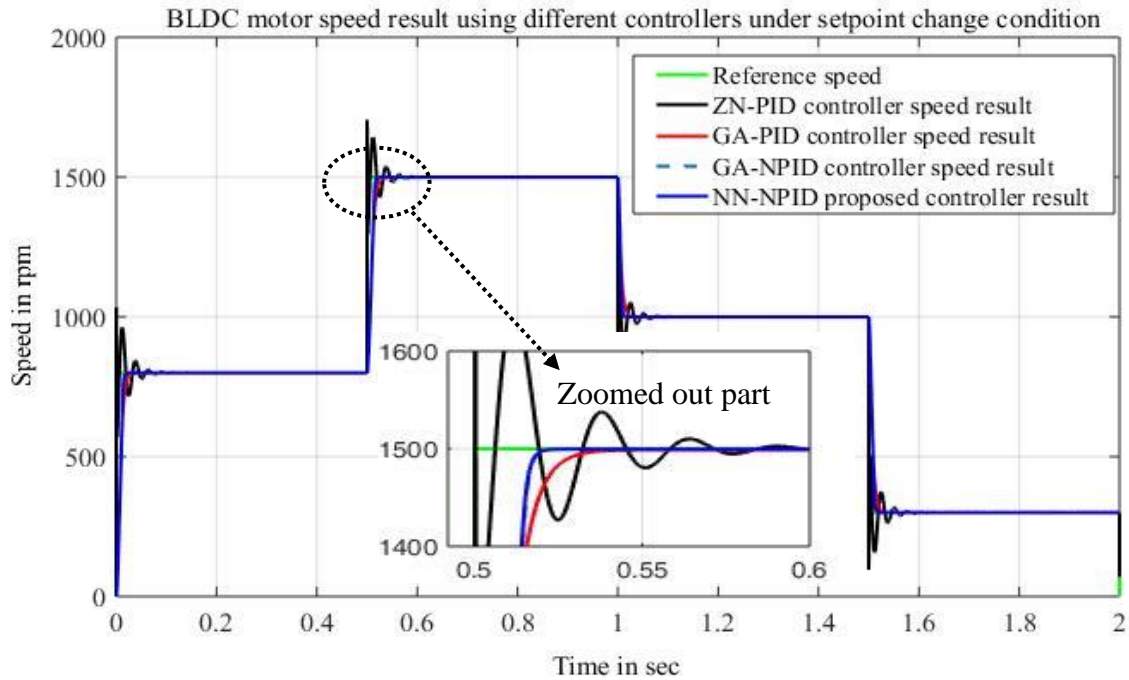


Figure 4.13 BLDC motor speed result using different controllers for setpoint change

Figure 4.14 demonstrates the speed dynamic performance parameters (settling, rise, and peak times) graphical results of each speed controller. The graph shows that the NN-NPID speed controller has better performance parameters than the others.

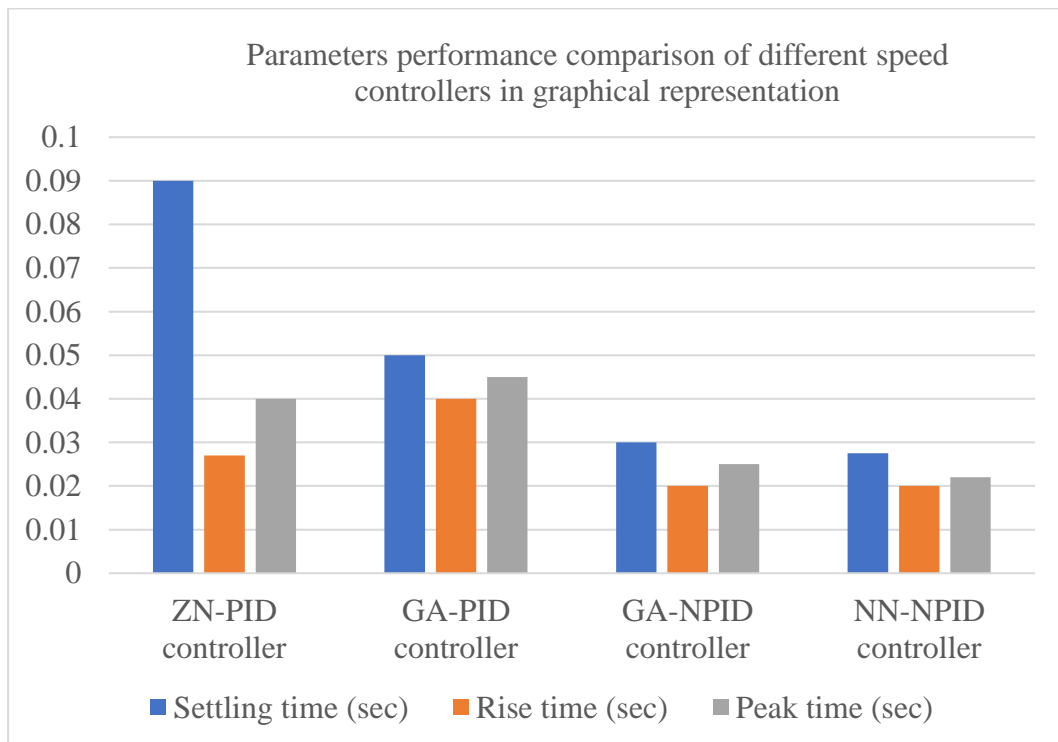


Figure 4.14 Graphical representation of speed dynamic performance parameters result

All the previous speed control system discussions were conducted at a constant load (20Nm) condition. The results of the speed dynamic performance parameters in the case of GA-NPID and NN-NPID controllers are almost similar and competent, just they have small differences in case of constant load condition.

In order to distinguish the two controllers, the system is simulated under the application of sudden load (30Nm) change and constant setpoint condition for all performed control systems. The ZN-PID controller has zero speed steady state error but the settling time is increased to 0.16sec which means it is a slow process. The GA-PID and GA-NPID speed controllers have 1% and 0.7% steady state error respectively but NN-NPID has 0.3% steady state error, which is half of the steady state error of GA-NPID controller result. Figure 4.15 depicts the result of the BLDC motor output speed for all performed control systems under sudden load change and constant speed setpoint conditions.

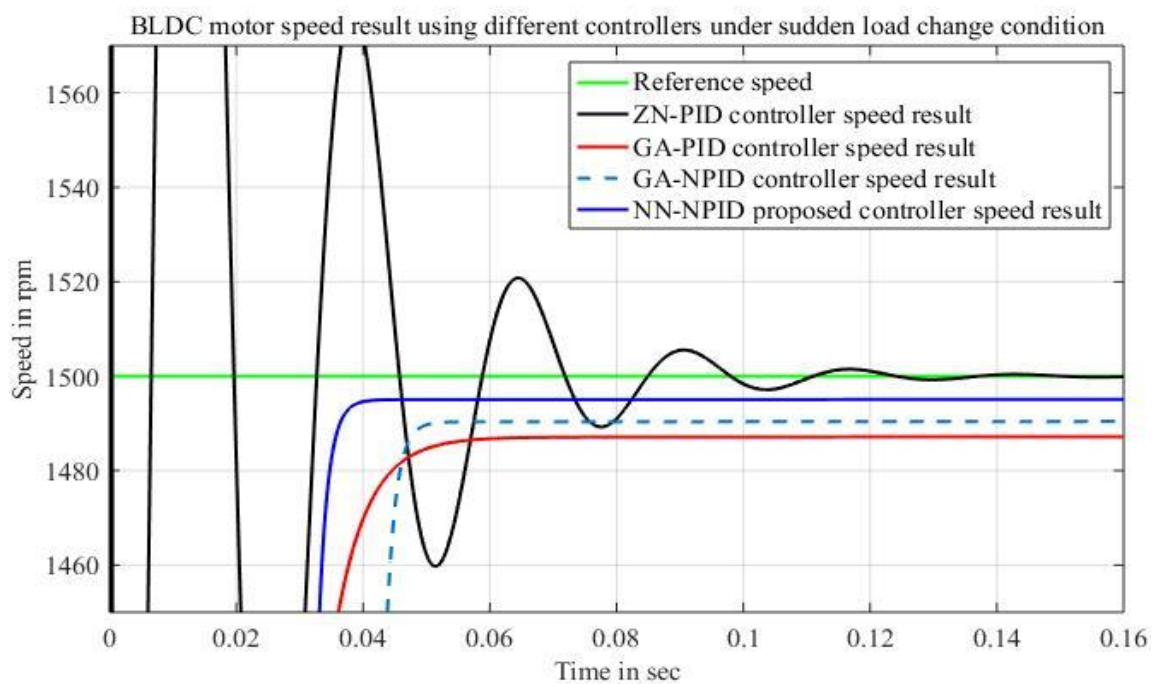


Figure 4.15 BLDC motor speed result using different controllers at 30Nm

The general performance parameters result for sudden load change condition is shown in Table 4.2. The result shows that when there is a sudden load change the speed dynamic performance is decreased. Specifically, the settling time, rise time, and peak time values are increased when compared to the system simulated under 20Nm condition. This shows that when the load is increased the system performance will be decreased. There is no variation in the case of overshoot result with the system simulated under 20Nm load.

Table 4.2 Speed controller performance parameter results under 30Nm load

Speed Controllers	Performance parameters result at constant 30Nm load condition				
	Settling in time sec	Rise time in sec	Peak time in sec	Steady state error in rpm	Percentage steady state error
ZN-PID controller	0.16	0.027	0.04	0	0%
GA-PID controller	0.06	0.04	0.05	15	1%
GA-NPID controller	0.05	0.04	0.05	10	0.7%
NN-NPID controller	0.04	0.036	0.04	4	0.3%

The percentage graphical representation of steady state speed error of the BLDC motor result is shown in Figure 4.16. ZN-PID and NN-NPID speed controllers have less steady state error than others. But, the ZN-PID speed controller has a large settling time which means it is slower than others. In general, the NN-NPID speed controller has better transient and steady state performance than the other speed controllers and it is recommended for the three phase BLDC motor speed controller for the propulsion of electric bajaj quite vehicle.

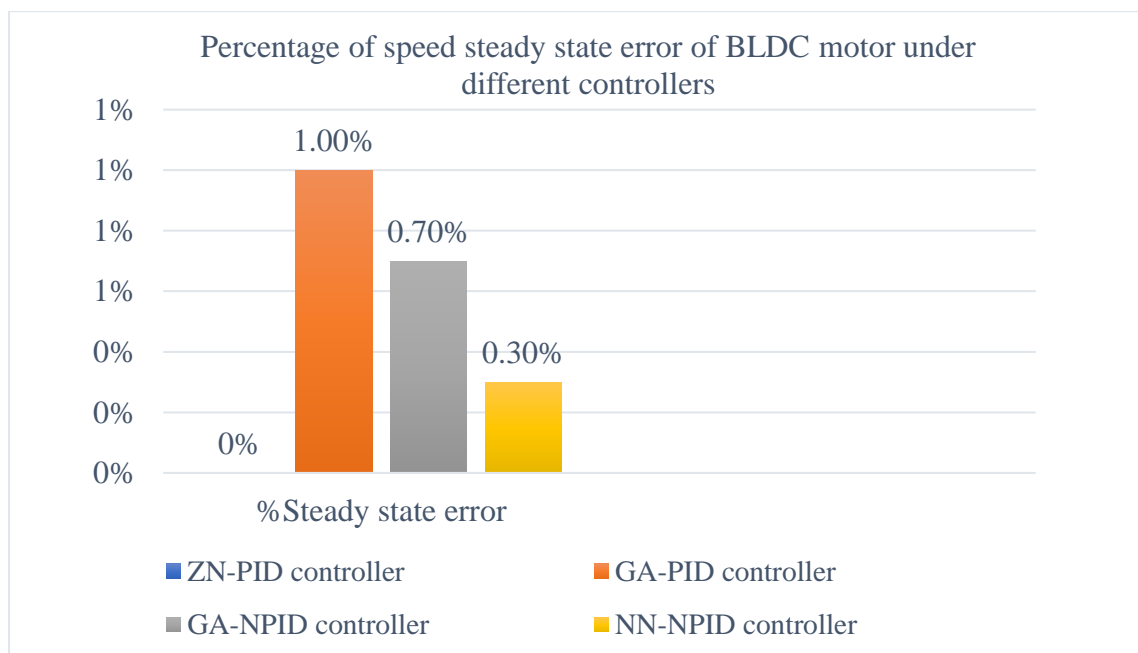


Figure 4.16 Steady state error graphical representations of speed controllers

4.2.1.2. Current Dynamic Performance of BLDCM

For the comparison purpose, two current regulators are implemented in this work. These are ZN-PI and GA-PI current controllers. ZN-PI current controller has a 0% overshoot and settling time of 0.09sec. However, the reference current by itself has large overshoot (i.e. greater than 77A or >50%) as shown in Figure 4.17.

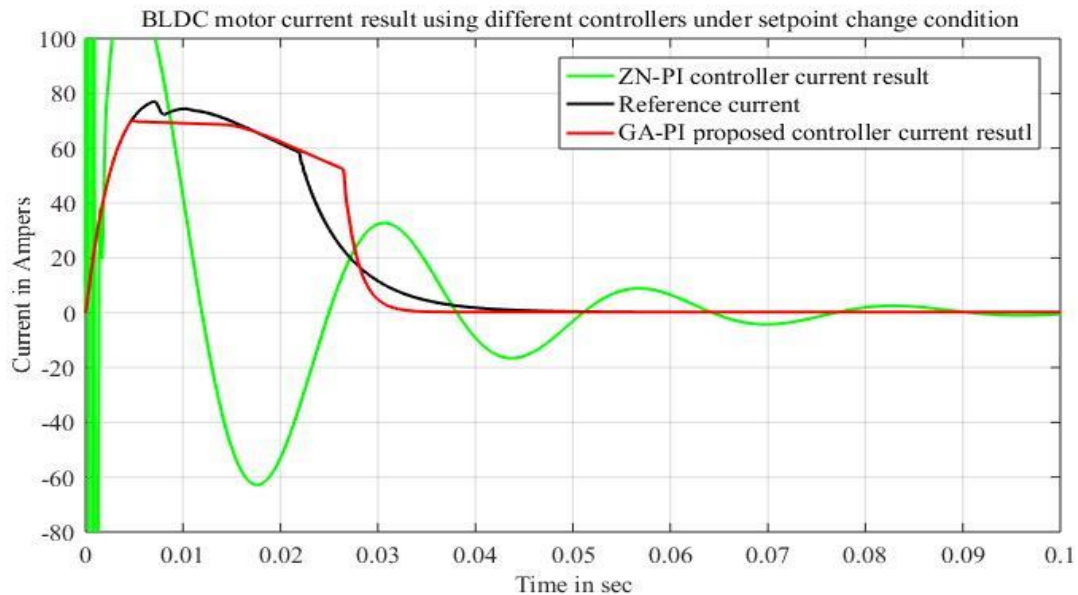


Figure 4.17 BLDC motor current zoomed result using different controllers

The GA-PI current controller has good dynamic performance with 0% overshoot and 0.02sec settling time. Hence the reference current from the NN-NPID speed controller has a maximum of 77A. The motor current follows the constant reference current as shown in Figure 4.17. For the comparison purpose, the simulation is performed in constant and variable setpoint conditions. The comparison result is taken from the modeling of linear BLDC motor drive. Table 4.3 shows the dynamic performance parameters of each controller result. ZN-PI current controller has poor performance than the GA-PI controller results.

Table 4.3 Current controller comparison of performance parameter results

Current Controllers	Performance parameters			
	Settling time in sec	Rise time in sec	Peak time in sec	Percentage overshoot
ZN-PI controller	0.09	0.0025	0.006	>50%
GA-PI controller	0.02	0.005	0.01	0%

The current control systems are simulated under setpoint change condition based on the reference current from the speed controller output and all have similar performance parameter results with Table 4.3. The result of all current control systems together is shown in Figure 4.18. The system simulated with similar parameters considered under study.

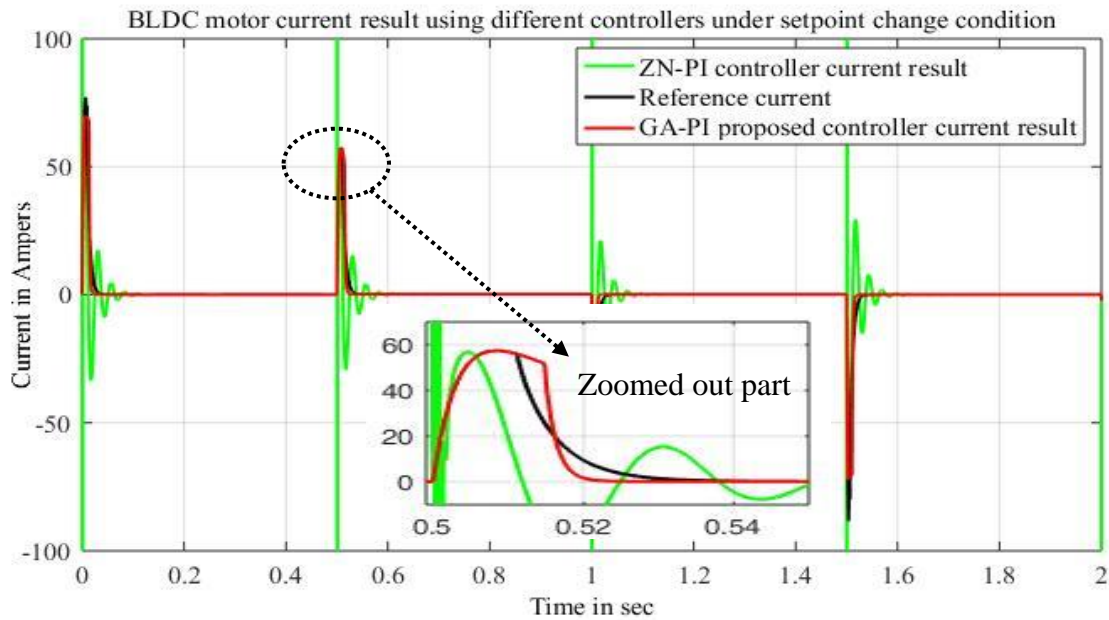


Figure 4.18 BLDC motor current result using different controllers for setpoint change

Figure 4.19 shown below demonstrates the current dynamic performance parameters (settling, rise, and peak times) graphical results of each current controllers. The GA-PI current controller has better performance parameters than ZN-PI current controller.

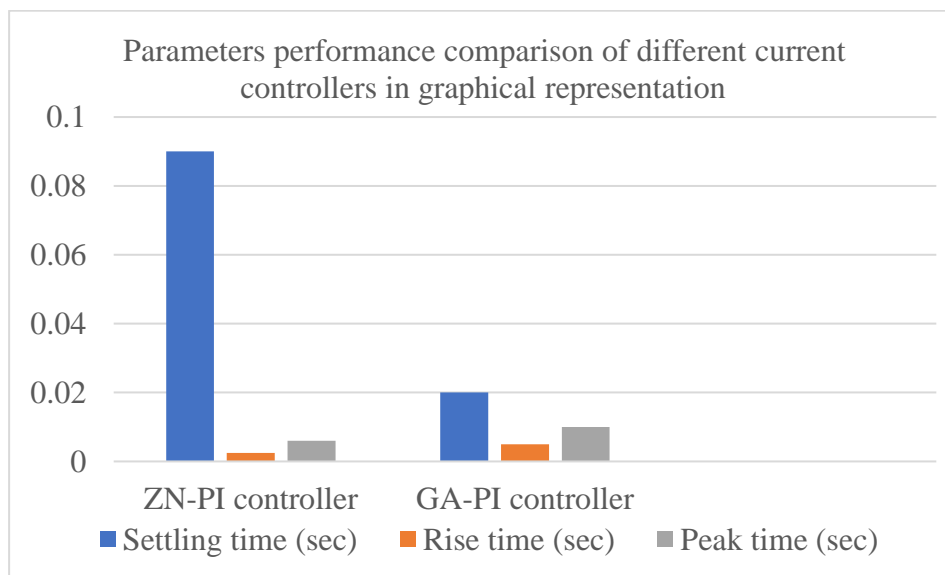


Figure 4.19 Graphical representation of current controllers parameter result

4.2.2. Discussion of BLDC Motor Drive Results

In this work, two BLDC motor drive schemes are considered for comparison purposes. The results of each drive techniques are compared and discussed in tabular and graphical forms.

4.2.2.1. PWM Based BLDCM Drive Results Discussion

The PWM based BLDC motor inverter switching scheme is performed. Figure 4.20 demonstrates the zoomed out result of stator current in phase-A and it follows the reference current with the harmonic distortion of 6%.

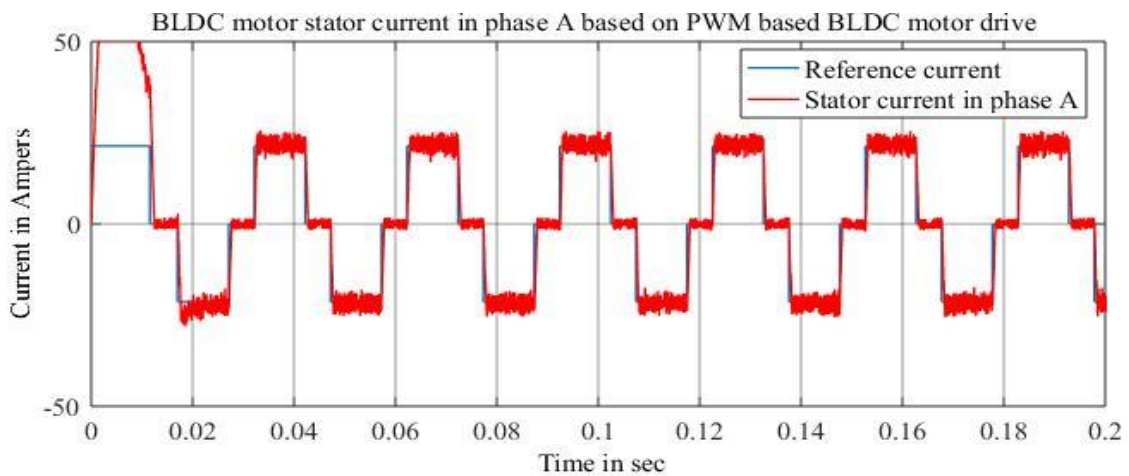


Figure 4.20 The zoomed out result of the stator current under PWM based drive

Hence the stator current is directly proportional to the electromagnetic torque of the BLDC motor. Figure 4.21 below depicts the electromagnetic torque result and its ripple is 6% as compared to the load torque.

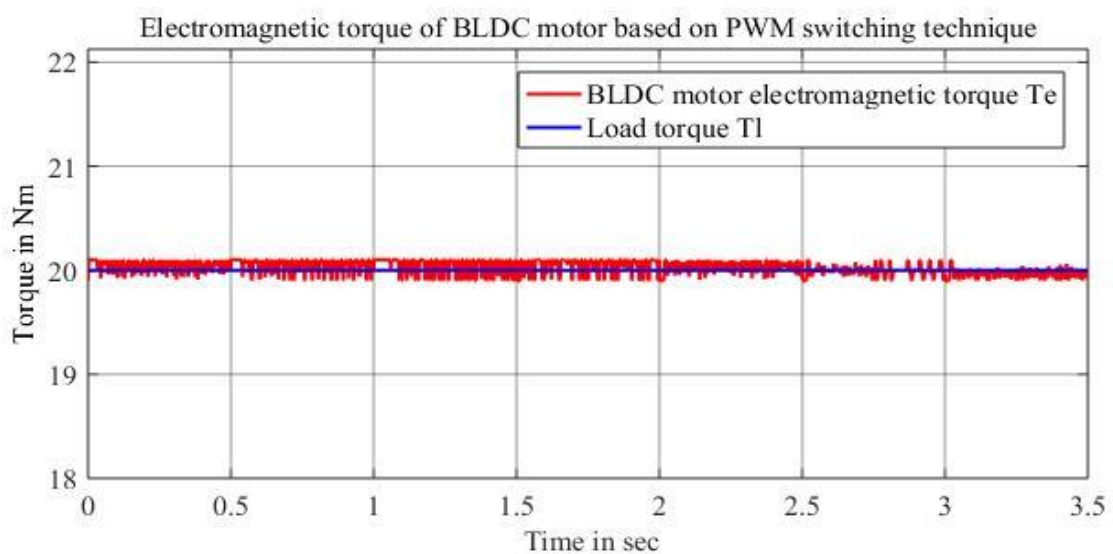


Figure 4.21 The result of electromagnetic torque under PWM based drive

4.2.2.2. Discussion of Relay Based BLDCM Drive Result

For the comparison purpose, the relay based BLC motor drive is performed. Its stator current result shows in Figure 4.22 below with 20% harmonics distortion. This shows that it has high current harmonics leads to high torque ripple.

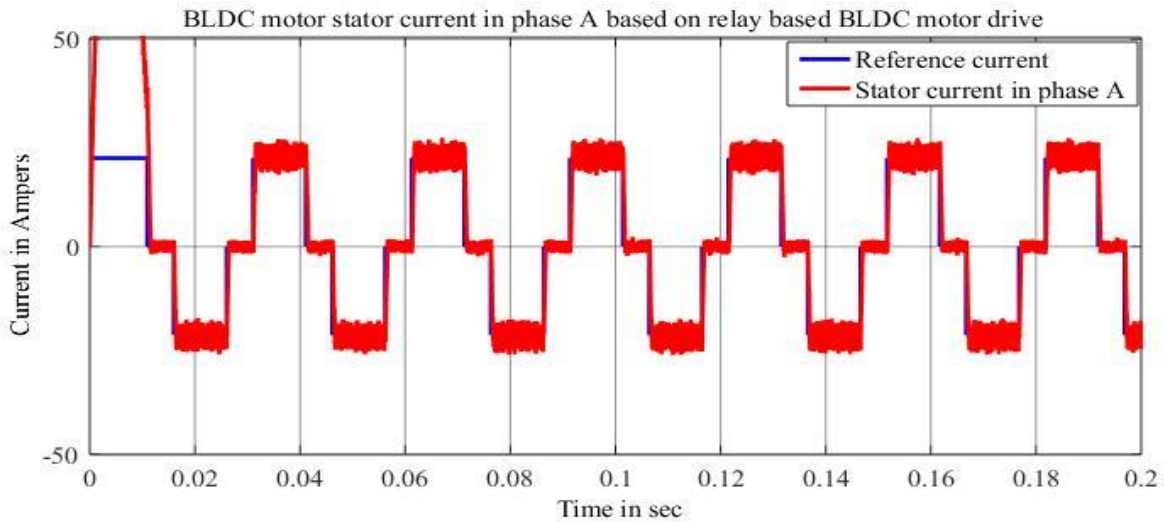


Figure 4.22 The result of the stator current under relay based drive

The electromagnetic torque zoomed out result based on relay based BLDC motor drive is shown in Figure 4.23. The result shows that the torque ripple is high due to the stator current harmonic and its value is 20%.

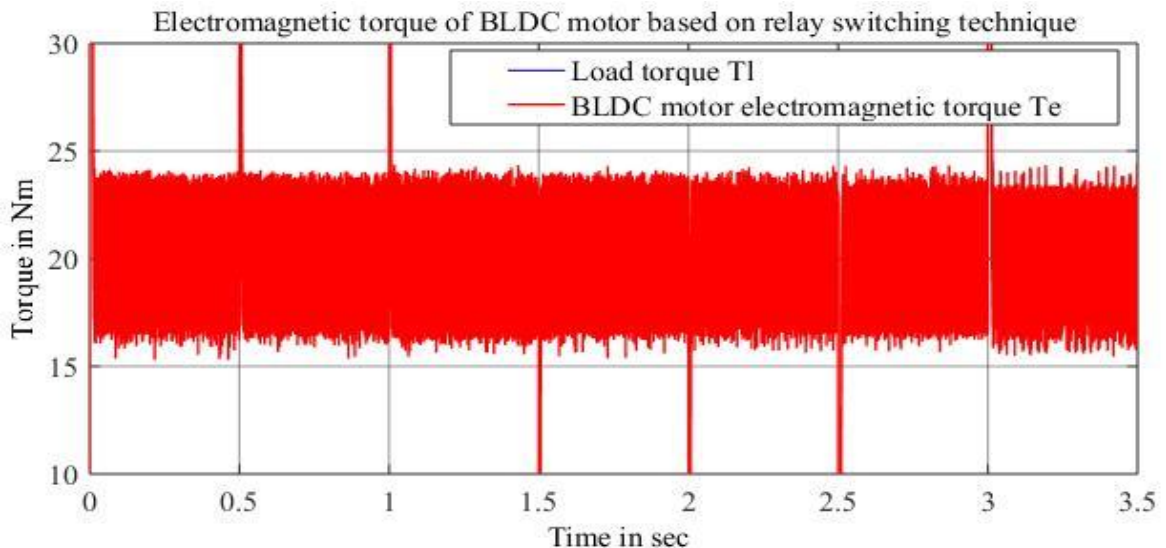


Figure 4.23 The result of electromagnetic torque under relay based drive

In general, the PWM based BLDC motor drive gives better current harmonics and torque ripple than relay based drive. Figure 4.24 depicts the percentage comparison graphical

representations of electromagnetic torque ripple of BLDC motor in both drive schemes. As a result, the PWM based drive is recommended for the three phase BLDC motor inverter switching for the propulsion of electric bajaj qute vehicle.

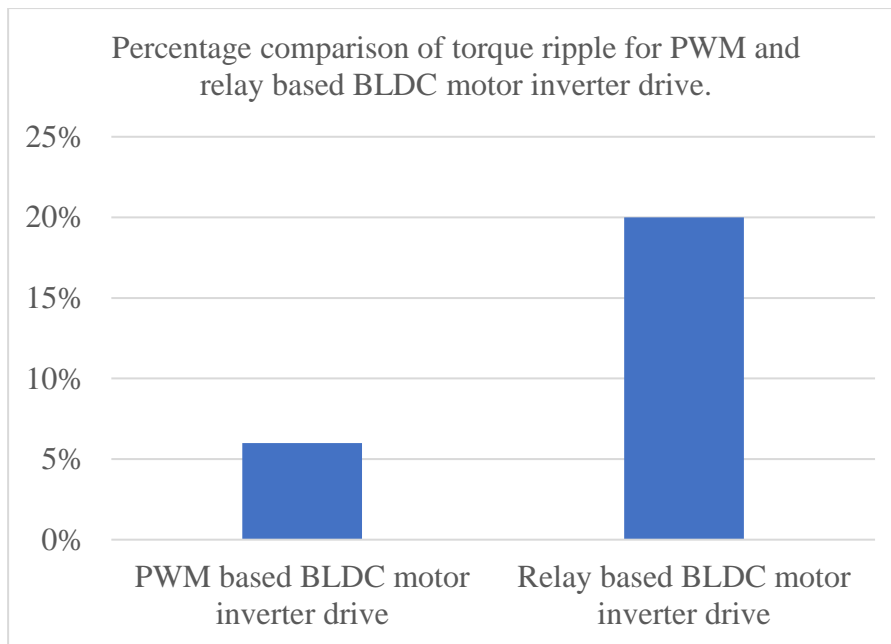


Figure 4.24 Percentage of torque ripple graphical representations

CHAPTER 5

5. CONCLUSIONS AND RECOMMENDATIONS

5.1. Conclusions

Fossil fuel cars are one of the sources of carbon dioxide emission to the environment and they take a high percentage of fossil fuels currently. Besides, the cost of fossil fuel is increasing and its amount is decreasing from year to year. To overcome this, one of the best first steps to start with prefers EVs over conventional internal combustion engines. By switching over to EVs the pollution levels can be controlled to a greater extent.

Over the years various electric drive systems like DC, PMSM, BLDC, IM, and SR motors were developed. Among them, IM and BLDC motors are the most popular drive trains used in EVs today. High power density, high torque at low speed, better efficiency and dynamic response, robustness, and low noise susceptibility are some of the important requirements of electric motors to use in EV propulsion. Since the characteristics of BLDCM can fulfill the requirements mentioned above and it was proposed as the Bajaj Qute EV traction motor.

BLDC motor needs an appropriate control algorithm to fulfill the above mentioned requirements. Over the years several types of BLDC motor inverter commutation or drive mechanisms have been proposed by researchers. Among them, Relay, VVS, and FOC based drives were discussed in the literatures. In addition to this, several speed control systems of BLDCM were reviewed and distinguished based on their dynamic performance. The major drawbacks of the result of literatures were, they have high torque ripple, less dynamic performance, and high starting current due to lack of current regulator.

In this thesis work, different cascade control systems along with inverter commutation schemes of BLDC motor were developed in both linear and nonlinear MATLAB/Simulink modeling. The cascade control system includes speed and current control systems were performed by using NN-NPID and GA-PI controllers respectively along with PWM based three phase inverter commutation scheme. In addition, for the comparison purpose, the system was simulated by using ZN-PID and PI, GA-PID and PI, and GA-NPID and PI cascade controllers. The speed dynamic performance of the BLDC motor drive by using the NN-NPID controller found to have the rise time of 0.02sec, settling time of 0.0275sec, the peak time of 0.0275sec, and 0% overshoot and steady state error per rated motor speed of

1500rpm and 20Nm applied load torque. GA-NPID speed controller has better performance than ZN-PID and GA-PID controllers, and it gives settling time of 0.03sec and 0% overshoot. But due to sudden load change (30Nm), it has a +0.7% steady state error which is twice that of the NN-NPID speed controller result (0.3%). On the other hand, the current dynamic performance of BLDC motor drive by using GA-PI controller results settling time of 0.02sec and 0% overshoot which is better than ZN-PI controller. The system also simulated under setpoint change conditions but the dynamic performance in both controllers is similar to the system results using constant setpoint condition.

Furthermore, the proposed PWM based inverter drive was compared with relay based inverter drive. The result shows PWM based inverter drive scheme results a 6% torque ripple which is better than when relay based inverter drive is used. As a result, NN-NPID speed and GA-PI current cascade controller with PWM based inverter drive was found to be focused because of its better performance response than others. After a few decades, the conventional internal combustion engine based vehicles will be replaced by electric vehicles because of environmental impact, incremental of the cost of fossil fuel, and the depletion of fossil fuels in the future. Because of these reasons, BLDC motor drives must be studied and improved further and further for EV propulsion.

5.2. Recommendations

The BLDC motor control and drive system can be further improved by adding the application of four quadrant DC-DC drive for fast dynamic braking operation. Besides, the percentage of torque ripple and current harmonics can be further improved by using multilevel inverters. But this will be costly and it needs very complex algorithms to generate inverter commutation signals. The hardware implementation of BLDC motor drive including NN-NPID speed and current cascade controller along with PWM inverter commutation using real time operating systems like digital signal processor (DSP) kit is recommended. Furthermore, it is also recommended the student to practice and implement the proposed control system in electric drives and control systems laboratory, the center of excellences in ASTU like the center of transportation and vehicle engineering (CTVE) and E-Bajaj center of excellences.

Acknowledgements: This research thesis was funded by Adama Science and Technology University under the grant number of **ASTU/SM-R/076/19**, Adama, Ethiopia.

References

- [1] K. G. Høyer, "The history of alternative fuels in transportation: The case of electric and hybrid cars," *ELSEVIER*, pp. 63-71, 2007.
- [2] C. C. Chan, "The Past, Present and Future of Electric Vehicle Development," in *International Conference on Power Electronics and Drive Systems*, Hong Kong, 1999.
- [3] J. Weinert, C. Ma and C. Cherry, "The transition to electric bikes in China: history and key reasons for rapid growth," *Springer*, vol. 34, pp. 301-308, 2007.
- [4] V. K. S. Patel and A.K.Pandey, "Modeling and Performance Analysis of PID Controlled BLDC Motor and Different schemes of PWM controlled BLDC Motor," *International Journal of Scientific and Research Publications*, vol. 3, no. 4, 2013.
- [5] A. A. R, "Control of Three Phase BLDC Motor using Fuzzy Logic Controller," *International Journal of Engineering Research & Technology (IJERT)*, vol. 2, no. 7, 2013.
- [6] A. Bello, I. M. Kilishi, M. M. Bari and U. Abubakar, "Comparative Review of PMSM and BLDCM based on Direct Torque Control Method," *International Journal of Scientific and Technology Research*, vol. 3, no. 3, 2014.
- [7] G. Luthra, "Comparison of Characteristics of Various Motor Drives Currently used in Electric Vehicle Propulsion System," *International Journal of Mechanical and Production Engineering*, vol. 5, no. 6, 2017.
- [8] N. Hashernnia and B. Asaei, "Comparative Study of Using Different Electric Motors in the Electric Vehicles," in *IEEE*, Tehran, 2008.
- [9] S. R. Jape, "Comparison of Electric Motors for Electric Vehicle Application," *IJRET: International Journal of Research in Engineering and Technology*, vol. 6, no. 9, p. 2, 2017.

- [10] M. Zeraouila, M. Benbouzid and D. Diallo, "Electric motor drive selection issues for HEV propulsion systems a comparative study, Vehicle Power and Propulsion," *IEEE*, vol. 7, no. 9, pp. 8 -15, 2005.
- [11] D. Liu, "Brushless DC Motors Made Easy," *Freescale*, 2008.
- [12] J. Gupta, "Theory and Performance of Electrical Machines," *S.K. Kataria and sons*, 2014.
- [13] A. J. Varghese, R. Roy and P. S. Thirunavukkarasu, "Optimized Speed Control for BLDC Motor," *International Journal of Innovative Research in Science, Engineering and Technology*, vol. 3, no. 1, 2014.
- [14] P. Yedamale, "Hands-on Workshop Motor Control Part 4 -Brushless DC (BLDC) Motor Fundamentals," *Microchip AN885*, 2003.
- [15] S. R. Jape and A. Thosar, "Comparison of Electric Motors for Electric Vehicle Application," *IJRET: International Journal of Research in Engineering and Technology*, vol. 6, no. 9, 2017.
- [16] S. Derammelaere, M. Haemers, J. D. Viaene and F. Verbelen, "A quantitative comparison between BLDC, PMSM, Brushed DC and Stepping Motor Technologies".
- [17] S. J. Anita and K. Boopathy, "Modeling of Motors for Electric Vehicles," *International Journal of Innovative Technology and Exploring Engineering (IJITEE)*, vol. 9, no. 2S4, 2019.
- [18] H. Jayetileke, W. d. Mel and H. Ratnayake, "Modelling and Simulation Analysis of the Genetic-Fuzzy Controller for Speed Regulation of a Sensored BLDC Motor Using MATLAB/Simulink," *IEEE*, 2017.
- [19] S. Swapna and K. S. Naidu, "Speed Characteristics of Brushless DC Motor Using Adaptive Neuro Fuzzy PID Controller under Different Load Condition," *International Journal of Recent Technology and Engineering (IJRTE)*, vol. 7, no. 5S3, 2019.

- [20] R. Nadolski, K. Ludwintk, J. Staszak and M. Jaskiewicz, "Utilization of BLDC Motor in Electrical Vehicles," *Przegląd Elektrotechniczny*, 2012.
- [21] A. K. Hassan, M. S. Saraya, M. S. Elksasy and F. F. Areed, "Brushless DC Motor Speed Control using PID Controller, Fuzzy Controller, and Neuro Fuzzy Controller," *International Journal of Computer Applications*, 2018.
- [22] L. Zheng-zhong and G. Guo-fang, "Study of Brushless DC Motor Control System with Current Hysteresis Loop," *Information Engineering and Applications, Springer*, 2012.
- [23] P. Mukherjee and M. Sengupta, "Closed loop speed control of a laboratory fabricated Brush-less DC Motor drive prototype using position sensor," in *National Power Electronics Conference (NPEC)*, Pune, India, 2017.
- [24] N. Veeramuthulingam, A. Ezhilarasi, M. Ramaswamy and P. Muthukumar, "Modeling of Brushless DC Motor Using Adaptive Control," *Springer Nature Singapore*, p. 764 –775, 2018.
- [25] G. Uma, "Research on Permanent Magnet BLDC for Small Electric Vehicle," in *Electrical and Electronic engineering*, Noida, 2017.
- [26] E. Klintberg, "Comparison of Control Approaches for Permanent Magnet Motors," Chalmers University of Technology, Göteborg, Sweden, 2013.
- [27] M. Żelechowski, "Space Vector Modulated – Direct Torque Controlled (DTC – SVM) Inverter – Fed Induction Motor Drive," Warsaw University of Technology, Warsaw – Poland, 2005.
- [28] R. Bhavina, N. Jamliya and K. Vashishtha, "Cascade Control of DC Motor With Advance Controller," *International Journal of Electrical, Electronics and Data Communication*, vol. 2, no. 3, 2014.
- [29] B. Rathod, "Reviews of Cascade Control of DC Motor with Advance Controller," *IJSRD - International Journal for Scientific Research & Development*, vol. 1, no. 5, 2013.

- [30] M. E. A. Mohamed and Y. Guo, "Design of Speed Control for Brushless DC Motor Used for Electric Vehicle Based on Adaptive Neuro-Fuzzy Inference System," in *IOP Conf. Series: Materials Science and Engineering*, 2019.
- [31] K. Premkumar and B.V.Manikandan, "Adaptive Neuro-Fuzzy Inference System based speed controller for brushless DC motor," *ELSEVIER: Neurocomputing*, pp. 260-270, 2014.
- [32] G. Tan, W. Shu, YifengGuo and M. Liu, "The Application of Fuzzy Control in Brushless DC Motor for Pure Electric Vehicle," *IEEE*, 2015.
- [33] "Design of PID-Fuzzy for Speed Control of Brushless DC Motor in Dynamic Electric Vehicle to Improve Steady-State Performance," *International Electronics Symposium on Engineering Technology and Applications (IES-ETA)*, 2017.
- [34] P. Mukherjee and M. Sengupta, "Closed Loop Speed Control of a Laboratory Fabricated Brushless DC Motor Drive Prototype using Position Sensor," *National Power Electronics Conference (NPEC)*, no. 6, 2017.
- [35] M. E. Blessy and M.Murugan, "Modeling and Controlling of BLDC Motor Based Fuzzy Logic," in *S.A. Engineering College*, Chennai, 2014.
- [36] A. M. Ahmed, "Brushless DC Motor Speed Control using both PI Controller," vol. 109, 2015.
- [37] K. Premkumar and B.V.Manikandan, "Fuzzy-PID Supervised Online ANFIS based Speed Controller for Brushless DC Motor," *ELSEVIER: Neurocomputing*, vol. 157, pp. 76-90, 2015.
- [38] X. Xin and C. Zhang, "Optimal Design of Electric Vehicle Power System with the Principle of Minimum Curb Mass," *ELSEVIER ScienceDirect*, vol. 105, p. 2629 – 2634, 2017.
- [39] M. Zhou, L. Zhao, Y. Zhang, Z. Gao and R. Pei, "Pure Electric Vehicle Power-train Parameters Matching Based on Vehicle Performance," *International Journal of Control and Automation*, vol. 8, no. 9, pp. 53-62, 2015.

- [40] A. Ranpariya, B. Shah, R. Salecha, V. Shah and P. Sharma, "Optimization of Required Power for an Electric Vehicle," *International Research Journal of Engineering and Technology (IRJET)*, vol. 6, no. 4, pp. 4605-4608, 2019.
- [41] A. Joy, A. Jose, J. Joseph, J. Fortel, R. V. P and A. E. Alias, "BLDC Motor Drive for Electric Vehicles," *International Journal of Advanced Research in Electrical, Electronics and Instrumentation Engineering*, vol. 7, no. 4, pp. 1679-1683, 2018.
- [42] M. J. Akhtar, R. K. Behera and S. K. Parida, "Propulsion System Design of Electric Vehicle," 2015.
- [43] E. A. Grunditz, "BEV Powertrain Component Sizing With Respect to Performance, Energy Consumption and Driving Patterns," Chalmers University of Technology, Göteborg, Sweden, 2014.
- [44] S. Borthakur and S. C. Subramanian, "Parameter Matching and Optimization of a Series Hybrid Electric Vehicle Powertrain System," In *Proceedings of the ASME 2016 International Mechanical Engineering Congress & Exposition*, Arizona, USA, 2016.
- [45] K. S. Amit, D. Ankit and K. Praveen, "Analysis of Induction Motor for Electric Vehicle Application Based on Drive Cycle Analysis," in *IEEE International Conference on Power Electronics, Drives and Energy Systems (PEDES)*, 2014.
- [46] Y. Indrajeet, "Variation of Gear Ratios of a Vehicle Gearbox Which Depends upon Its Type of Engine and Utility," *International Journal of Engineering Development and Research (IJEDR)*, vol. 5, no. 1, pp. 46-51, 2017.
- [47] M. B. Sheikh and P. S. Manware, "Brushless DC Motor Design for Electric Traction System," *Journal for Research*, vol. 2, no. 4, pp. 18-22, 2016.
- [48] P. Pillay and R. Krishnan, "Application Characteristics of Permanent Magnet Synchronous and Brushless dc Motors for Servo Drives," *IEEE Transactions on Industry Applications*, vol. 27, no. 5, pp. 986-996, 1991.
- [49] M. G. Geda, "Speed Control of BLDC Motor by Using PWM Current Controller Technique for Electric Vehicle Propulsion," Adama Science and Technology University, Adama, Ethiopia, 2018.

- [50] J. A. Mullick, "Fuzzy Controller for Speed Control of BLDC Motor using MATLAB," *International Research Journal of Engineering and Technology (IRJET)*, vol. 4, no. 2, pp. 1270-1274, 2017.
- [51] M.-H. Yang, B.-M. Lin, S.-F. Yeh and J.-S. Tsai, "Design of High Power Lithium Ion Battery for HEV Application," *The World Electric Vehicle Association Journal*, vol. 1, pp. 161 -164, 2017.
- [52] W. He, N. Williard, C. Chen and M. Pecht, "State of Charge Estimation for Electric Vehicle Batteries using Unscented Kalman Filtering," *ELSEVIER: Microelectronics Reliability*, pp. 1-8, 2012.
- [53] M. Murnane and A. Ghazel, "A Closer Look at State of Charge (SOC) and State of Health (SOH) Estimation Techniques for Batteries".*Technical Article*.
- [54] M.-K. Kim, H.-S. Bae and B.-S. Suh, "Comparison of IGBT and MOSFET Inverters in Low-Power BLDC Motor Drives," *Fairchild Semiconductor*.
- [55] M. H. Rashid, *Power Electronics Devices, Circuits, and Applications*, Florida: Electrical and Computer Engineering University of West Florida, 2014.
- [56] A. Tashakori, M. Ektesabi and N. Hosseinzadeh, "Modeling of BLDC Motor with Ideal Back-EMF for Automotive Applications," in *World Congress on Engineering (WCE)*, London, U.K, 2011.
- [57] M. Santanu, M. Arunabha and C. Madhurima, "Mathematical modeling and Simulation of Brushless DC motor with Ideal Back EMF for a Precision speed control".
- [58] V. G. Shirish and A. M. Jain, "Modeling and Simulation of Three Phase BLDC Motor for Electric Braking Using MATLAB/Simulink," *International Journal Of Electrical, Electronics And Data Communication*, vol. 5, no. 7, pp. 48-53, 2017.
- [59] P. Crnosija, T. Bjazic and R. Krishnan, "Optimization of PM Brushless DC Motor Drive".

- [60] P. Crnošija, R. Krishnan and T. Bjažić, "Performance Optimization of PM Brushless DC Motor," in *EDPE*, Dubrovnik, Croatia, 2005.
- [61] R. A. Gupta, R. Kumar and A. K. Bansal, "Artificial Intelligence Applications in Permanent Magnet Brushless DC motor Drives," *Springer*, no. 33, pp. 175-186, 2010.
- [62] A. S. A. Elhamid, "Cascade Control System of Direct Current Motor," *World Applied Sciences Journal*, vol. 18, no. 12, pp. 1680-1688, 2012.
- [63] Anagha, R. K., A. C.P., R. Das and A. A.S., "Cascade Speed Control of DC Motor," *International Journal of Electrical, Electronics and Data Communication*, vol. 2, no. 6, pp. 78-81, 2014.
- [64] G. G. Jin and Y. D. Son, "Design of a Nonlinear PID Controller and Tuning Rules for First-Order Plus Time Delay Models," *Studies in Informatics and Control*, vol. 28, no. 2, pp. 157-166, 2019.
- [65] G. B. So and G. G. Jin, "Temperature Control of a Regasification System for LNG-fuelled Marine Engines," in *Advances in Mechanical, Aeronautical and Production Techniques - MAPT*, 2018.
- [66] H. Espitia, J. Soriano, I. Machón and H. López, "Design Methodology for the Implementation of Fuzzy Inference Systems Based on Boolean Relations," *MDPI: electronics*, no. 8, pp. 1-28, 2019.
- [67] M. V. Ramesh, J. Amarnath, S. Kamakshaiyah and G. S. Rao, "Speed Control of Brushless DC Motor by Using Fuzzy Logic PI Controller," *ARPJ Journal of Engineering and Applied Sciences*, vol. 6, no. 9, pp. 55-62, 2011.
- [68] R. Arulmozhiyal and R.Kandiban, "Design of Fuzzy PID Controller for Brushless DC Motor," in *International Conference on Computer Communication and Informatics (ICCCI)*, Coimbatore, INDIA, 2012.
- [69] J. Manipatruni and N. S. Vedula, "Design and Implementation of PID Controller using Genetic Algorithm," *International Journal of Engineering Research & Technology (IJERT)*, vol. 7, no. 11, pp. 104-107, 2018.

- [70] A. Devanshu, "Genetic Algorithm Tuned PID Controller for Process Control," in *International Conference on Inventive Systems and Control (ICISC)*, 2017.
- [71] M. V. Sadasivarao and M. Chidambaram, "PID Controller tuning of cascade control systems using genetic algorithm," *Indian Institute of Science*, no. 86, p. 343–354, 2006.
- [72] K.Premkumar and B. Manikandan, "Speed control of Brushless DC motor using bat algorithm optimized Adaptive Neuro-Fuzzy Inference System," *ELSEVIER: Applied Soft Computing*, no. 32, pp. 403-415, 2015.
- [73] M. Dutt, V. Nunavath and M. Goodwin, "A Multi-Layer Feed Forward Neural Network Approach for Diagnosing Diabetes," in *International Conference on Developments in eSystems Engineering (DeSE)*, Grimstad, Norway, 2018.
- [74] A. Rubaai, R. Kotaru and M. D. Kankam, "A Continually Online-Trained Neural Network Controller for Brushless DC Motor Drives," *IEEE Transactions on Industry Applications*, vol. 36, no. 2, pp. 475-483, 2000.
- [75] V. Chopra, S. K. Singla and L. Dewan, "Comparative Analysis of Tuning a PID Controller using Intelligent Methods," *Acta Polytechnica Hungarica*, vol. 11, no. 8, pp. 235-249, 2014.
- [76] M. Zhang, C. Xia, Y. Tian, D. Liu and Z. Li, "Speed Control of Brushless DC Motor Based on Single Neuron PID and Wavelet Neural Network," in *IEEE International Conference on Control and Automation*, Guangzhou, CHINA, 2007.
- [77] D. H. Shah, "Design And Implementation Of PID Controller Using Relay Feedback On TRMS (Twin Rotor MIMO System)," 2016.
- [78] M. J. M, A. Iqbal and S. R. L, "PID Auto Tuning Using Relay Feedback," *International Journal of Engineering Research & Technology (IJERT)*, vol. 2, no. 4, pp. 1170-1175, 2013.

Reference Links

[L1] Reference links about the history of three and four wheeler Bajaj's, and the history of Bajaj's vehicles in Ethiopia [accessed on October 05, 2019]

1. <https://www.reuters.com/article/us-india-quadricycle/indias-bajaj-to-launch-four-wheel-vehicle-but-its-not-a-car-idUSBREA1M16320140223>
2. <https://addisfortune.net/articles/addiss-finest/>

[L2] Reference links of Table (2.1): Traction motors and electric vehicle models (accessed on December 12, 2019).

1. https://en.wikipedia.org/wiki/Electric_car
2. <https://www.tesla.com/>
3. www.mitsubishi-motors.com.au/vehicles/i-miev
4. www.morgan-motor.co.uk/mmc/researchanddev/pluse.html
5. <http://evworld.com>
6. www.buddyelectric.no
7. www.byd.com/na/auto/e6.html
8. www.theelectriccarcorporation.co.uk
9. www.smartaustralia.com.au
10. www.teslamotors.com
11. www.mahindrareva.com/

[L3] Reference link for Figure 3.8 (accessed on December 25, 2019)

1. https://www.google.com/search?client=firefoxbab&biw=1366&bih=596&tbm=isch&sa=1&ei=PWKfW4jQNq2XlwSF4LmIDA&q=3.4.3.%09Reducer+for+car+figure&oq=3.4.3.%09Reducer+for+car+figure&gs_l=img.3...19302.19302.0.20312.1.1.0.0.0.0.247.247.2-1.1.0....0...1c.1.64.img..0.0.0....0.35W_Pfyib-g

[L4] Link for Tables (Table 3.2 and 3.5) (accessed on January 07, 2020)

1. [http://www.xindaenergy.com/html_products/Electric-Vehicle-Brushless-Permanent-Magnet-DC-Motor-\(10-35kw\)-113.html](http://www.xindaenergy.com/html_products/Electric-Vehicle-Brushless-Permanent-Magnet-DC-Motor-(10-35kw)-113.html)

[L5] Link for figures (Figure 3.9 and 3.10) (accessed on February 7, 2020)

1. https://www.google.com/search?q=back+emf+control+in+bldc+motor&tbm=isch&hl=en&chips=q:hall+effect+back+emf+control+in+bldc+motor,online_chips:hall+effect,online_chips:sensor+signal&client=ms-android-samsung&prmd=ivn&hl=en

Appendixes

Appendix A: Appendixes related to analysis of data

MATLAB code for the analysis driving power vs speed of the bajaj vehicle

```
clear all; close all;
m=990; fric=0.01; g=9.81; a=1; r=0.25324; % Radius of the wheel in meter
K_friction=0.01; %Coefficient of friction by considering the asphalt road
F_tot=0; Tot_effcen.M=0.95; Cw=0.3; v=10; %speed of the rotor in m/se=51.444km/h
Adnsty=1.2; Af=2; vo=0; %Kd/m3 , %area in m2 , and %air velocity in m/s respectively
Vkph=0; Vkph1=0; d_Vkph=1e-2; %Initial conditions and unit step increment
Vkph_final=90; x=1; n=1; %final value in km/hr. and initial conditions
while(Vkph<Vkph_final),
    Vmps=Vkph*(1000/3600);
    Fadya=0.5*Adnsty*Cw*Af*(Vmps+vo)^2;
    if Vkph<=100*d_Vkph;
        statfric=0.1;
    else
        statfric=0;
    end
    F_tot=m*g*(K_friction+statfric)+Fadya+m*a; % Total force(Nm)
    Power=F_tot*Vmps/0.95; % Required input power (Watt)
    Vkph=Vkph+d_Vkph;
    if x>16,
        Powern(n)=Power/1000; %Power in KW
        Vkphn(n)=Vkph; n=n+1; x=1;
    end
    x=x+1;
end
plot(Vkphn,Powern,'r','LineWidth',2);
set(gca,'FontSize',12)
axis([0 90 0 40]);
grid
xlabel('Speed of the of the car(Km/hr)')
ylabel('Power (KW)')
```

MATLAB code for torque versus speed characteristics curve

```
clear
Ratedpower=10000; %Rated power in Watt
wrpm=0; x=1; n=1; wb=157.17; d_wrpm=1e-2; wrpm_final=6000; %initial condition, base
speed in rad/sec, unit step increment, and final value in RPM respectively
while(wrpm<wrpm_final),
wm=wrpm*(2*pi)/60; Torque= Ratedpower/wm;
if Torque>=127/2,
Torque=127/2;
end
if Torque<127/2,
Torque= Torque;
end
Power=Torque*wm; wrpm=wrpm+d_wrpm;
if x>16,
wrpmn(n)=wrpm; Torquen(n)=Torque; Powern(n)=Power/1000; n=n+1; x=1;
end
x=x+1;
endc
figure(1);
[AX,Torque,Power]=plotyy(wrpmn,Torquen, wrpmn,Powern);
axis([0 6000 0 70]);
set(get(AX(1),'ylabel'), 'string','Motor torque in Nm')
set(get(AX(2),'ylabel'), 'string','Motor power kW')
set(Torque,'LineStyle','--')
set(Power,'LineStyle','-')
set(gca, 'FontName','TimesNewRoman')
set(gca, 'FontSize',12)
set([Torque,Power],'LineWidth',1)
xlabel('Motor speed in rpm')
grid on
```

MATLAB code for analysis of the effect of the gradient angle in the power of the vehicle

```
m=990; fric=0.01; g=9.81; a=0; r=0.25324; % Radius of the wheel in meter
c_ofriction=0.01; %Coefficient of friction by considering the asphalt road
```

```

d=0.25324; Cw=0.5; Tot_effcen.M=0.95; v=11.722; %speed of the rotor in m/se=35km/h
Adnsty=1.2; Af=2; vo=0; %Kd/m3, %area in m2, and %air velocity in m/s respectively
angleR=0; angleR1=0; d_angleR=1e-6; %Initial condition and %unit step increment
angleR_final=20; x=1; n=1; %final value in degree and initial conditions
while(angleR<angleR_final),
Fadyna=0.5*Adnsty*Cw*Af*(v+vo)^2;
theta=angleR*2*pi/360; %Degree to radian conversion
F_tot=m*g*(sin(theta)+c_ofriction*cos(theta))+Fadyna+m*a; % Total force(Nm)
Power=F_tot*v; angleR=angleR+d_angleR; %W
if x>16,
Powern(n)=Power/1000+1.5; thetan(n)=angleR; n=n+1; x=1;%Power in KW
end
x=x+1;
end
plot(thetan,Powern,'b','LineWidth',2);
axis([0 20 0 35]);
grid
xlabel('The approaching angle in degree')
ylabel('Power (kW)')

```

Appendix B: Appendixes related to system modeling

Appendix B1: The GA-NPID speed and PI current controller MATLAB code

```

function Sim_FNPID_PI_DCMotor
t= 0; xi= 0; xa= 0; xd= 0; xf= 0; h= 0.0001; loop= 20000; wr= 800*pi/30; objfunc= 0;
ui_sat=0; us_sat=0; Ke= 0.8268; Kt= 0.8268; ilimit= 28; slimit= 77; Tl=20; % parameters
% Setting the gains of the speed and current controllers
Kps= 23.8933; Kis= 1.4326; Kds= 0.0237; c1=0.8575; Kpi= 4.3912; Kii= 0.4587; alpha=
1; %IAEU Obj=30.3444; zs= 0; zi= 0; ees= 0; eei= 0; eeke= 0; dwr= wr; es=0; ke=0;
b= [t xd xa wr ui_sat us_sat es ke dwr 0]; % Initializes a buffer for graphics
for i= 1:loop
    if i== loop/4
        wr= 1500*pi/30; dwr=700*pi/30;
    end
    if i== loop/2

```

```

wr= 1000*pi/30;   dwr=500*pi/30;
end
if i== 15000
wr= 300*pi/30;   dwr=700*pi/30;
end
if i== 20000
wr= 0;   dwr=300*pi/30;
end
xdm= xd+(0*pi/30)*randn;   % Adds Gaussian random noises, N(0,0.1^2)
es= wr-xdm;
se= abs(es)+alpha*abs(ui_sat); % Measures the performance index
if i==1 || i==loop
    objfunc= objfunc+0.5*h*se;
else
    objfunc= objfunc+h*se;
end
    % Calculates the NPID controller for speed control
ke= nonlfun(es,dwr,c1); % calling the nonlinear gain function
eke=es*ke;
zs= zs+0.5*h*(eke+eeke);   eeke= eke;
cs= (es-ees)/h; ees= es;
us= Kps*es+Kis*zs+Kds*cs;   us_sat= Saturation(us, [-slimit,slimit]); % Limits us
    % Calculates the PI controller for current control
ei= us_sat-xf;
zi= zi+0.5*h*(ei+eei);   eei= ei;
ui= Kpi*ei+Kii*zi;   ui_sat= Saturation(ui, [-ilimit,ilimit]);
.....
% calls RK4
    % Calls the Inverter function
xi= RK4(@Inverter,t,xi,ui_sat,h);
va= xi-Ke*xd;
    % Calls the Armature function
xa= RK4(@Armature,t,xa,va,h);
    % Calls the Filter function

```

```

xf= RK4(@Filter,t,xf,xa,h);
% Calculates the driving torque
Tm= Kt*xa-Tl;
% Calls the Dynamics function
xd= RK4(@Dynamics,t,xd,Tm,h);

.....

t= t+h;
b= [b;t xd xa wr ui_sat us_sat es ke dwr 0];
end
save 'GA_FNPID_PI' 'b'
objfunc
subplot 211
plot(b(:,1),b(:,4)*30/pi,'r',b(:,1),b(:,2)*30/pi,'b','linewidth',1.5)
axis([0 h*loop -100 2000])
grid on
subplot 212
plot(b(:,1),b(:,6),r',b(:,1),b(:,3),'b','linewidth',1)
axis([0 h*loop -100 100])
grid on
%calls the BLDC motor modeling
Implementation of the BLDC motor modeling
function xdot= Inverter(t,x,u) % Implements an inverter
Kr= 9.36; Tr= 8.333e-5;
xdot= (-x+Kr*u)/Tr;
function xdot= Armature(t,x,u) % Implements the armature circuit
L= 8.5e-3; R= 2.875;
xdot= (-R*x+u)/L;
function xdot= Dynamics(t,x,u) % Implements the mechanical dynamics
J= 0.0089; B= 0.001;
xdot= (-B*x+u)/J;
function xdot= Filter(t,x,u) % Implements a filter for measurement
Kf= 1; Tf= 0.0001;
xdot= (-x+Kf*u)/Tf;
Implementation of the nonlinear gain function using fuzzy logic controller

```

```

function [ke]= nonlfun(e,ddyr,c1)
dyr=abs(ddyr); m= 3; g= 1/dyr;
N= sigmf(e,[-g, -m*dyr]);
Z= trimf(e,[-m*dyr, 0, m*dyr]);
P= sigmf(e,[g, m*dyr]);
ke= (c1*N+1*Z+c1*P)./(N+Z+P);

```

Implementing the object function for GA optimization

```

function objfunc= EvalObj_FNPID_PI_DCMotor(pop)
popsize= size(pop,1); objfunc= zeros(popsize,1);
for k= 1:popsize
t= 0; xi= 0; xa= 0; xd= 0; xf= 0; h= 0.0001; loop= 20000; wr= 1500*pi/30; % Parameters
ui_sat= 0; us_sat=0; Ke= 0.8268; Kt= 0.8268; Tl= 20; ilimit= 28; slimit=77;
% Setting the gains of the speed and current controllers
Kps= pop(k,1); Kis= pop(k,2); Kds= pop(k,3); c1= pop(k,4); Kpi= pop(k,5); Kii= pop(k,6);
alpha= 1; zs= 0; zi= 0; ees= 0; eei= 0; eeke= 0; dwr= wr;
    for i= 1:loop
        xdm= xd+(0*pi/30)*randn;    % Measures the error
        es= wr-xdm;
        se= abs(es)+alpha*abs(ui_sat);    % Measures the performance index
        if i==1 || i==loop
            objfunc(k)= objfunc(k)+0.5*h*se;
        else
            objfunc(k)= objfunc(k)+h*se;
        end
        if objfunc(k) > 1e+10
            objfunc(k)= 1e+10;
            break;
        end
        % Calculates the FNPID controller for speed control
        eke= nonlfun(es,dwr,c1);
        zs= zs+0.5*h*(eke+eeke); eeke= eke;
        cs= (es-ees)/h; ees= es;
        us= Kps*es+Kis*zs+Kds*cs;    us_sat= Saturation(us,[-slimit,slimit]); % Limits us
        % Calculates the PI controller for current control

```

```

ei= us_sat-xf;
zi= zi+0.5*h*(ei+eei); eei= ei;
ui= Kpi*ei+Kii*zi;  ui_sat= Saturation(ui,[-ilimit,ilimit]);    % Limits ui
% calls RK4
t= t+h;
end

```

```
end
```

%calls the BLDC motor modeling

GA optimization of NPID speed and PI cascade current controller

% FNPID controller tuning by using the MATLAB ga function

```
function MATLABGA_FNPID_PI
```

```
options= optimoptions('ga','PlotFcn',@gaplotbestf);
```

```
options.PopulationSize= 30;
```

```
options.MaxGenerations= 30; n= 6;
```

```
LB= [0 0 0 0 0 0]; UB= [50 20 1 1 100 10];
```

% calls the objfunc function using the MATLAB built in GA syntax

```
[x,fval]= ga(@EvalObj_FNPID_PI_DCMotor,n,[],[],[],[],LB,UB,[],options)
```

Appendix B2: The proposed NN based NPID speed controller MATLAB code

x = inputs'; y = output'; % input - input data and % out - target data.

% For choosing from a list of all training functions type: help nntrain

% 'trainlm' is usually fastest.

% 'trainbr' takes longer but may be better for challenging problems.

% 'trainscg' uses less memory. Suitable in low memory situations.

trainFcn = 'trainlm'; % Levenberg-Marquardt backpropagation.

hiddenLayerSize =[6 4]; % Create a Fitting Network

```
net = fitnet(hiddenLayerSize,trainFcn);
```

% Setup Division of Data for Training, Validation, Testing

```
net.divideParam.trainRatio = 80/100;
```

```
net.divideParam.valRatio = 10/100;
```

```
net.divideParam.testRatio = 10/100;
```

```
net.trainParam.epochs= 1000;
```

```
[net,tr] = train(net,x,y); % Train the Network
```

```
y = net(x); % Test the Network
```

```

e = gsubtract(x,y);
performance = perform(net,x,y)
gensim(net) %To generate the NN on simulink block

```

Appendix B3: The GA-PID speed and PI current controller MATLAB code

```

function Sim_PID_PI_DCMotor
t= 0; xi= 0; xa= 0; xd= 0; xf= 0; h= 0.0001; loop= 20000; wr= 800*pi/30; % parameters
objfunc= 0; ui_sat=0; Ke= 0.8268; Kt= 0.8268; Tl= 20; limit= 28; us_sat=0;
Kps= 9.8296; Kis= 0.3190; Kds= 0.0364; Kpi= 9.3062; Kii= 0.7038; %IAEU Obj= 3.1713;
zs= 0; zi= 0; ees= 0; eei= 0; % Setting the gains of the speed and current controllers
b= [t xd xa wr 0]; % Initializes a buffer for graphics
for i= 1:loop
    if i== loop/4
        wr= 1500*pi/30;
    end
    if i== loop/2
        wr= 1000*pi/30;
    end
    if i== 15000
        wr= 300*pi/30;
    end
    if i== 20000
        wr= 0;
    end
    xdm= xd+(0*pi/30)*randn; % Adds Gaussian random noises, N(0,0.1^2)
    es= wr-xdm;
    se= abs(es)+alpha*abs(ui_sat); % Measures the performance index
    if i==1 || i==loop
        objfunc= objfunc+0.5*h*se;
    else
        objfunc= objfunc+h*se;
    end
    % Calculates the PID controller for speed control
    zs= zs+0.5*h*(es+ees);

```

```

cs= (es-ees)/h; ees= es;
us= Kps*es+Kis*zs+Kds*cs; us_sat= Saturation(us,[-77,77]); % Limits us
% Calculates the PI controller for current control
ei= us_sat-xf;
zi= zi+0.5*h*(ei+eei); eei= ei;
ui= Kpi*ei+Kii*zi; ui_sat= Saturation(ui,[-limit,limit]); % Limits ui
% calls RK4
t= t+h;
b= [b;t xd xa wr us_sat];
end
save 'GA_PID_PI' 'b'
objfunc
subplot 211
plot(b(:,1),b(:,4)*30/pi,'r',b(:,1),b(:,2)*30/pi,'b','linewidth',1.5)
axis([0 h*loop -200 2000])
grid on
subplot 212
plot(b(:,1),b(:,3),'k',b(:,1),b(:,5),'r','linewidth',1)
axis([0 h*loop -100 100])
grid on
%calls the BLDC motor modeling
Implementation of the object function for GA optimization
function objfunc= EvalObj_PID_PI_DCMotor(pop)
popsize= size(pop,1);
objfunc= zeros(popsize,1);
for k= 1:popsize
clear PID PID1
Kps= pop(k,1); Kis= pop(k,2); Kds= pop(k,3); Kpi= pop(k,4); Kii= pop(k,5); alpha= 1;
gains_speed= [Kps Kis Kds -1]; gains_current= [Kpi Kii 0 -1]; % PID and % PI
t= 0; xi= 0; xa= 0; xd= 0; xf= 0; h= 0.0001; loop= 2000; wr= 1000*pi/30; % Parameters
ui_sat= 0; Ke= 0.8268; Kt= 0.8268; Tl= 0; limit= 28;
for i= 1:loop
% Measures the error
xdm= xd+(0*pi/30)*randn;

```

```

es= wr-xdm;
% Measures the performance index
se= abs(es)+alpha*abs(ui_sat);
if i==1 || i==loop
    objfunc(k)= objfunc(k)+0.5*h*se;
else
    objfunc(k)= objfunc(k)+h*se;
end
if objfunc(k) > 1e+10
    objfunc(k)= 1e+10;
    break;
end
% Calculates the NPID controller for speed control
us= PID(wr,xdm,h,gains_speed);
% Calculates the PI controller for current control
ui= PID1(us,xf,h,gains_current);
ui_sat= Saturation(ui,[-limit,limit]); % Limits us
% calls RK4
t= t+h;
end
end
%calls the BLDC motor modeling
GA optimization of PID speed and PI cascade current controller
% PID controller tuning by using the MATLAB ga function
function MATLABGA_PID_PI
options= optimoptions('ga','PlotFcn',@gaplotbestf);
options.PopulationSize= 30;
options.MaxGenerations= 30; n= 5;
LB= [0 0 0 0 0]; UB= [10 10 1 10 10];
[x,fval]= ga(@EvalObj_PID_PI_DCMotor,n,[],[],[],[],LB,UB,[],options)

```

Appendix B4: MATLAB code related to discussion of results

```

clf
load 'ZN_PID_PI'

```

```

y0= b(:,2)*30/pi; y0c=b(:,3);
load 'GA_PID_PI'
t= b(:,1); y1= b(:,2)*30/pi; y1c=b(:,3);
load 'GA_FNPID_PI'
y2= b(:,2)*30/pi; y3=b(:,4)*30/pi; y2c=b(:,3);
% load tout and NN_NPID data from workspace
gh= plot(t,y3,'g',t,y0,'k',t,y1,'r',tout,NN_NPID,'--',t,y2,'b');
gh= plot(t,y0c,'g',t,y1c,'k',t,y2c,'r');
set(gh,'linewidth',1.5)
grid on
set(gca,'xlim',[0,2]);

```

Appendix B4: MATLAB code related to battery SOC versus bajaj speed in km/hr

```

V1=70; %Km/hr
Wrated=16; %KW hr
Pm=12; %KW
S=0; d_S=1e-4; S_final=100; %unit step increment and % Km final value
x=1; n=1;
while(S<=S_final),
W=Pm*S/V1;
SOC=(Wrated-W)*100/Wrated;
S=S+d_S;
if x>16,
SOCn(n)=SOC; Sn(n)=S; n=n+1; x=1;
end
x=x+1;
end
figure(1);
plot(Sn,SOCn,'r','LineWidth',2);
axis([0 90 0 100]); set(gca,'xticklabel')
xlabel('Distance in Km')
ylabel('SOC (%)')
title('State of charge vs distance in KM')
grid

```

Appendix C: Related to the linear BLDC motor MATLAB/Simulink model

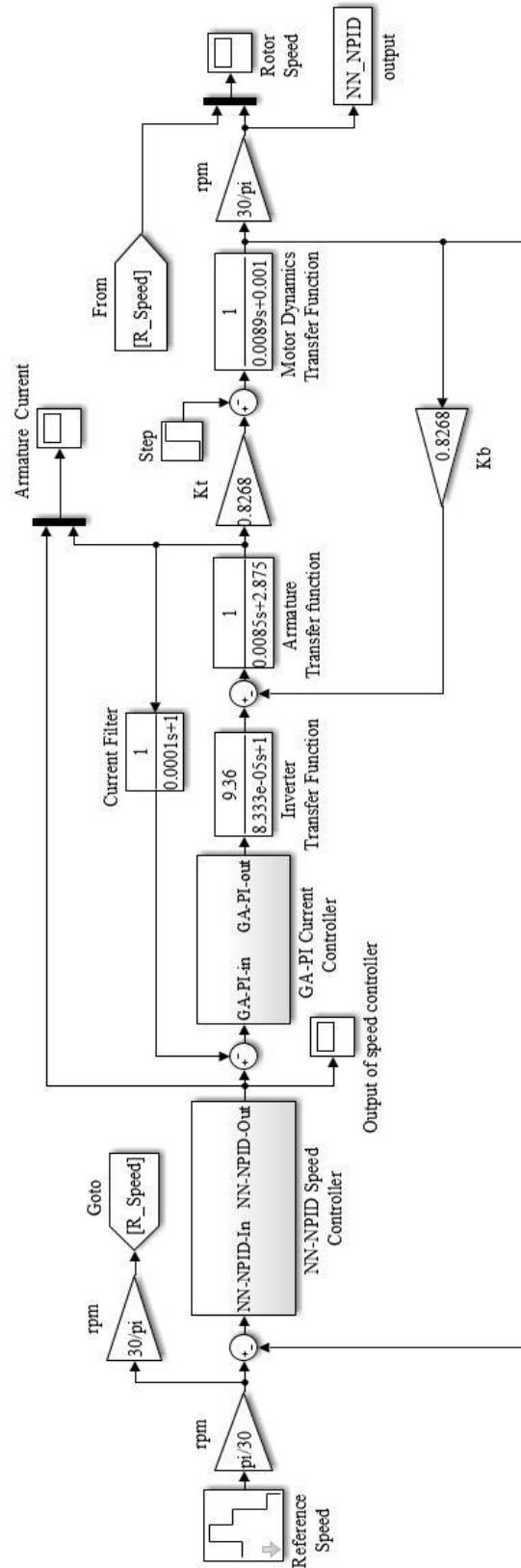


Figure C.1 MATLAB Linear Simulink model of the proposed cascade control system

Appendix D: Related to the nonlinear BLDC motor Simulink model

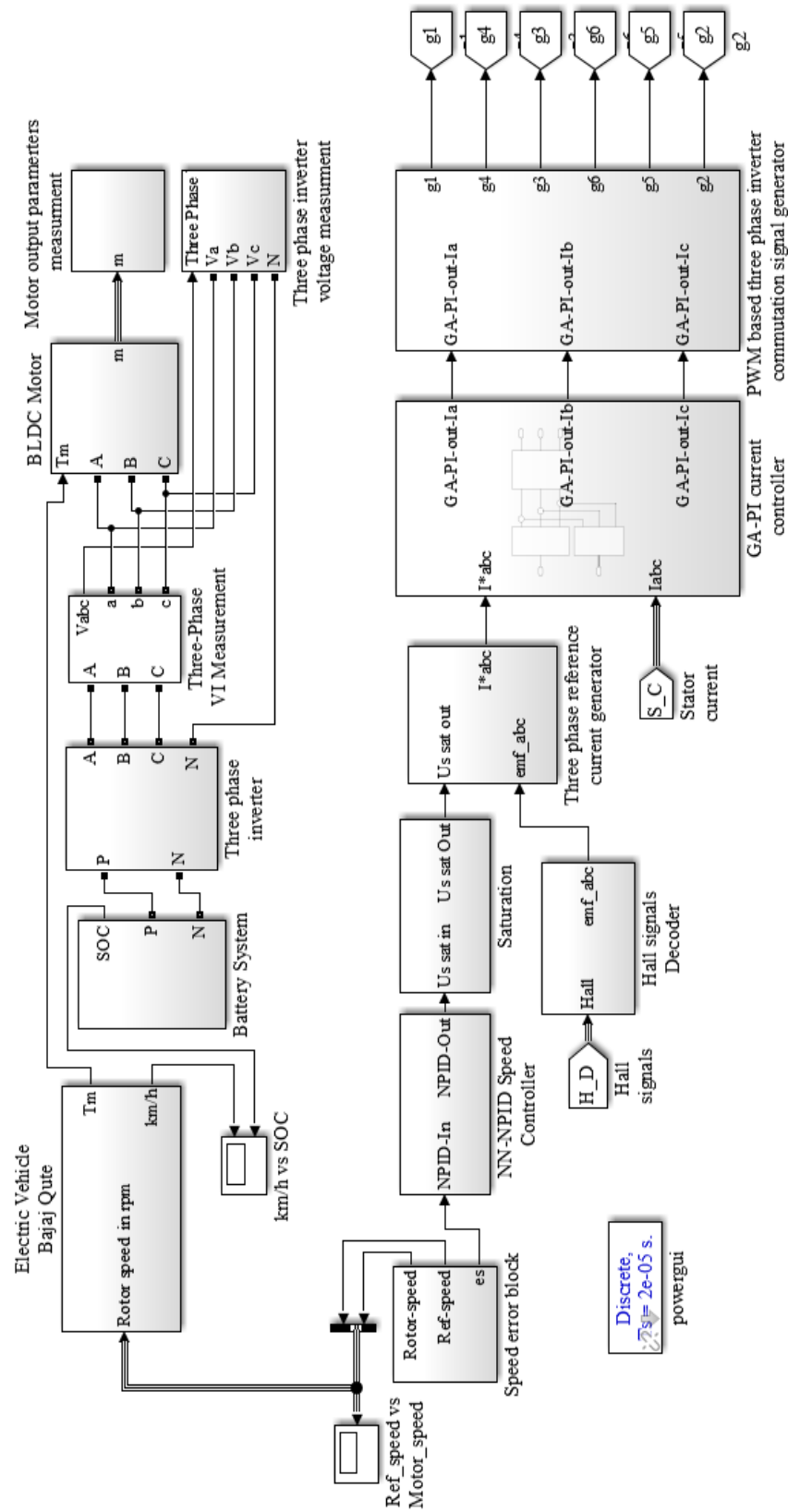


Figure D.1 MATLAB/Simulink nonlinear model of the proposed drive control system

NN-NPID speed controller Simulink block for both BLDC motor

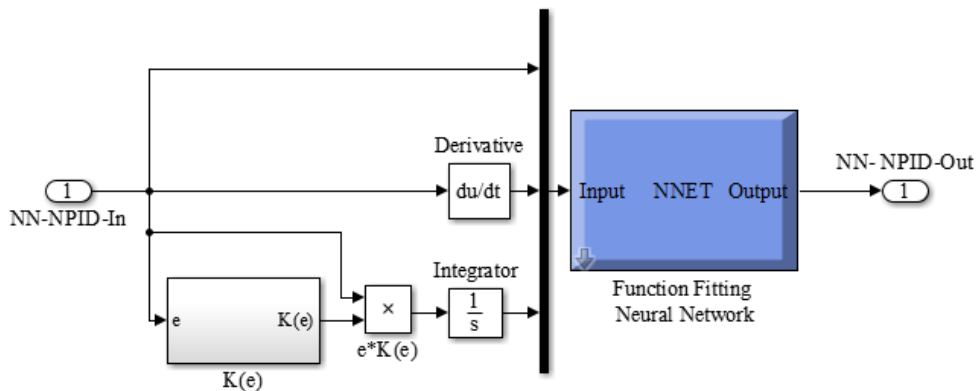


Figure D.2 NN-NPID speed controller Simulink block

Implementation of nonlinear gain using MATLAB function in Simulink

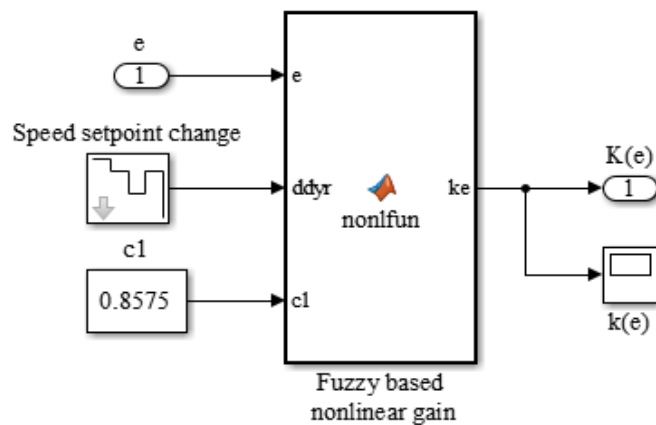


Figure D.3 Nonlinear gain function Simulink block

Implementation of nonlinear gain using MATLAB code

```
function ke = nonfun(e,ddyr,c1)
dyr=abs(ddyr);
m= 3; g= 1/dyr;
N= mysigmf(e,[-g, -m*dyr]);
Z= mytrimf(e,[-m*dyr, 0, m*dyr]);
P= mysigmf(e,[g, m*dyr]);
ke= (c1*N+1*Z+c1*P)./(N+Z+P);
function mg= mysigmf(x,par)
a=par(1); c= par(2);
mg=1./(1+exp(-a*(x-c)));
function mg= mytrimf(x,par)
a=par(1); b= par(2); c=par(3);
```

```

if x>=a && x<=b
    mg= (x-a)/(b-a);
elseif x>b && x<=c
    mg= (c-x)/(c-b);
else
    mg=0;
end

```

NPID speed controller Neural Network training tool



Figure D.4 Neural network training tool

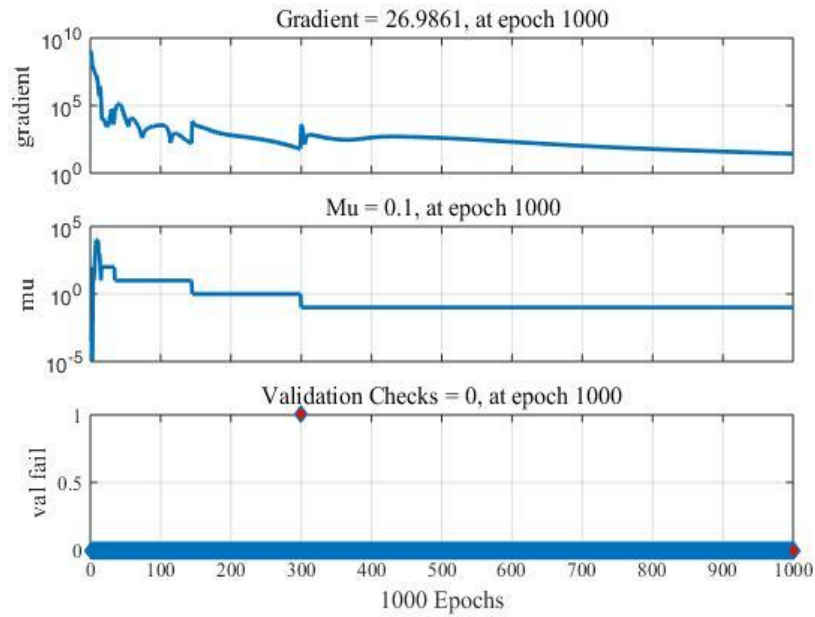


Figure D.5 Gradient and validation vs epochs result

Implementation of speed controller limiter using MATLAB function

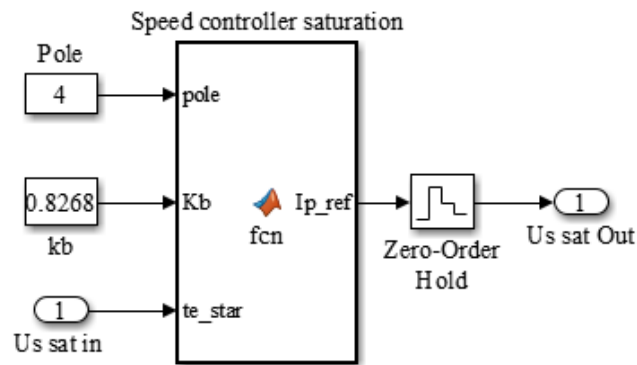


Figure D.6 Speed controller limiter Simulink block

Implementation of speed controller limiter using MATLAB code

```
function Ip_ref = fcn(pole, Kb, te_star)
te_rate = 63.23;
lamda_p = Kb*(pole/2);
% torque limit => up to 2 [p.u.]
te_lim_p = 2*te_rate; te_lim_n = -2*te_rate;
if (te_star >= te_lim_p)
te_cmd = te_lim_p;
elseif (te_star <= te_lim_n)
te_cmd = te_lim_n;

```

```

else
te_cmd = te_star;
end
Ip_ref = te_cmd/(2*lamda_p);
End

```

Hall position sensor decoder implementation using MATLAB function in Simulink

```

function [H1T, H2T, H3T] = fcn(H1, H2, H3)
H1T=0; H2T=0; H3T=0;
if ((H1==0) && (H2==0) && (H3==0)) %TH1
H1T=0; H2T=0; H3T=0;
end;
if ((H1==0) && (H2==0) && (H3==1)) %TH2
H1T=0; H2T=-1; H3T=+1;
end;
if ((H1==0) && (H2==1) && (H3==0)) %TH3
H1T=-1; H2T=+1; H3T=0;
end;
if ((H1==0) && (H2==1) && (H3==1)) %TH4
H1T=-1; H2T=0; H3T=+1;
end;
if ((H1==1) && (H2==0) && (H3==0)) %TH5
H1T=+1; H2T=0; H3T=-1;
end;
if ((H1==1) && (H2==0) && (H3==1)) %TH6
H1T=+1; H2T=-1; H3T=0;
end;
if ((H1==1) && (H2==1) && (H3==0)) %TH7
H1T=0; H2T=+1; H3T=-1;
end;
if ((H1==1) && (H2==1) && (H3==1)) %TH8
H1T=0; H2T=0; H3T=0;
end;

```

Three phase reference current generation

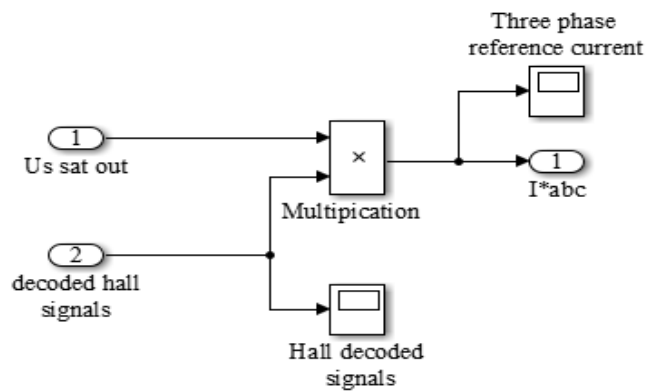


Figure D.7 Three phase reference current generation Simulink block

GA-PI current controller Simulink block for nonlinear BLDC motor model

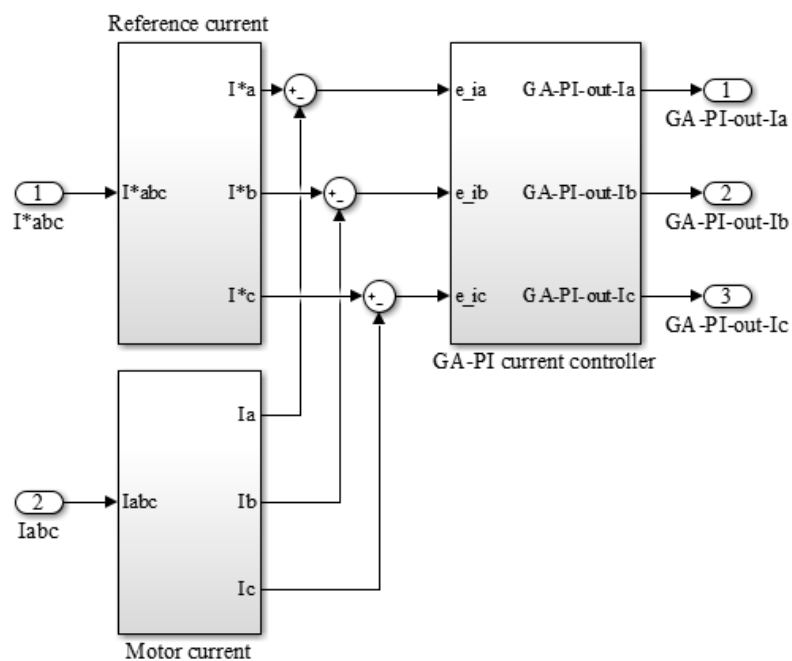


Figure D.8 GA-PI current controller Simulink block

The lithium ion battery Simulink block for nonlinear BLDC motor drive

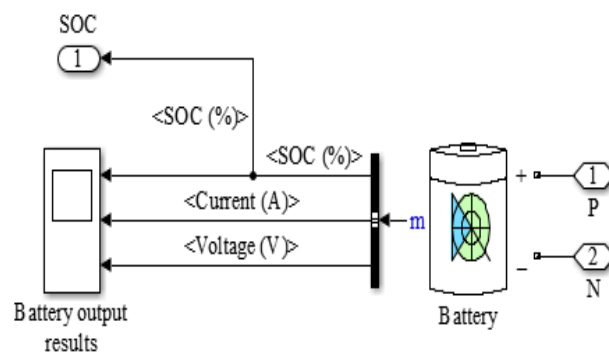


Figure D.9 Lithium ion battery Simulink block

PWM inverter switching implementation for the nonlinear BLDC motor drive

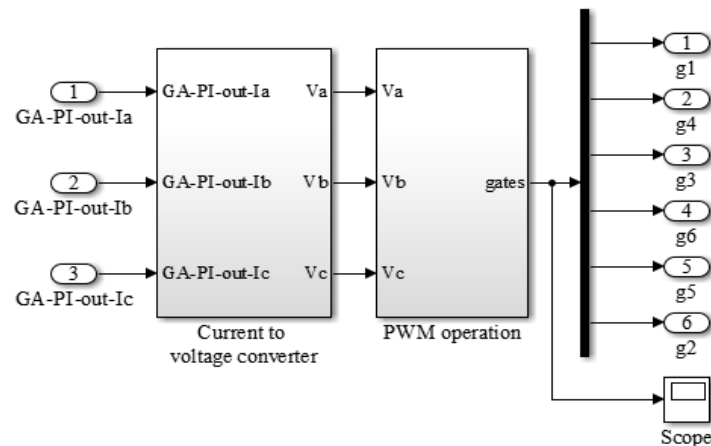


Figure D.10 Inverter switching signal generation using PWM operation

Electric bajaj vehicle dynamics and generation of speed in km/hr Simulink block

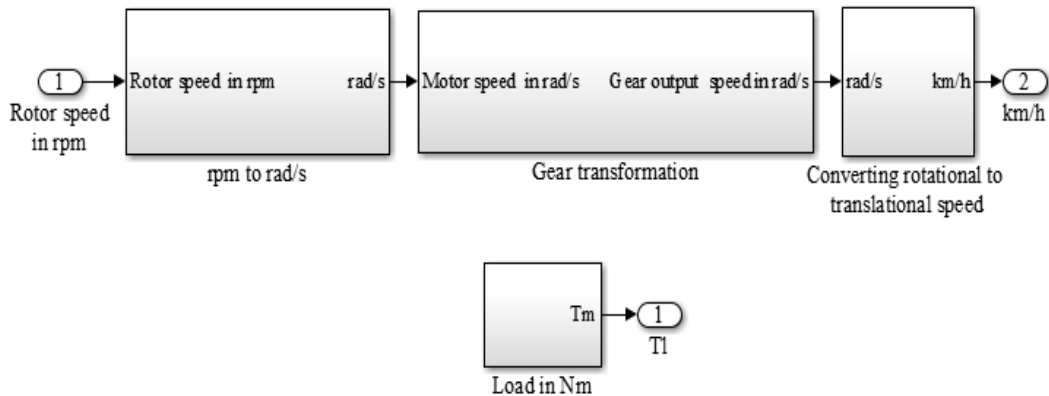


Figure D.11 Electric bajaj vehicle dynamics modeling and speed in km/hr Simulink block

Implementation of the three phase inverter using MOSFET and freewheeling diode

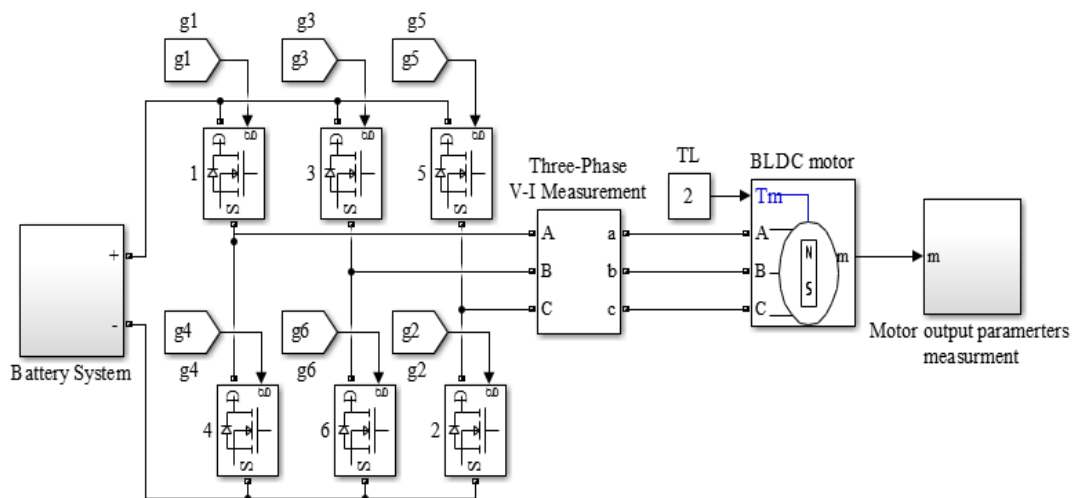


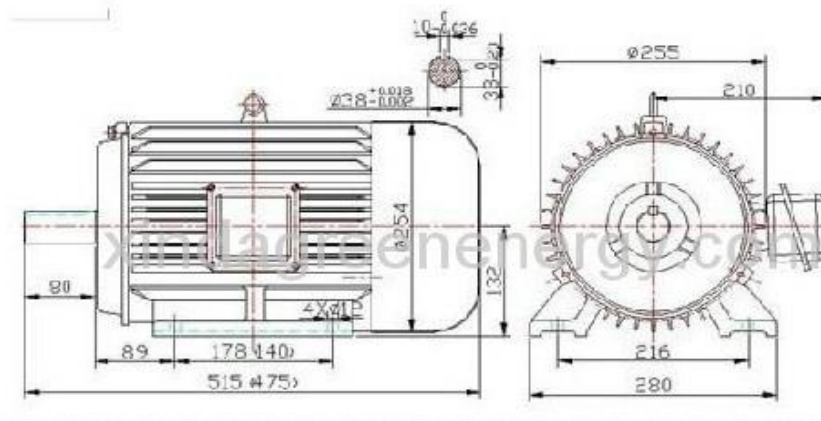
Figure D.12 Three phase inverter and BLDC motor Simulink block

Appendix E: Appendixes related to data collection

Data from internet: Data of similar size but engine based (accessed on October 05, 2019).



Data from internet: Data of similar size motor used for EV (accessed on 07/01/2020)



Power	The battery voltage	Speed	Rated torque	Peak torque	Peak power	current	Peak current	Efficiency	Weight
10kw	72V	1500rpm	63.7Nm	130Nm	25KW	154A	260A	93.6%	62kg
10kw	144V	1500rpm	63.7Nm	130Nm	25KW	77A	160A	93.6%	62kg
12kw	144V	3500rpm	32.7Nm	70Nm	30KW	91.3A	180A	93.7%	46kg
15kw	144V	3500rpm	40.1Nm	90Nm	40KW	114.4A	220A	93.8%	48kg
18 kw	144V	3500rpm	49Nm	120Nm	40KW	137.5A	270A	94.5%	55kg
25 kw	144V	4000rpm	60Nm	130Nm	60KW	191.4A	380A	94.8%	58kg
27 kw	144V	4500rpm	57Nm	130Nm	65KW	206.8A	380A	94.8%	62kg
30 kw	333V	6000rpm	47Nm	100Nm	65KW	100.1A	180A	94.8%	58kg
35kw	333V	6000rpm	55Nm	120Nm	70KW	116.6A	210A	94.9%	62kg